ISSN: 1443 9255
Volume 23 (2) - 2023

Electronic Journal
of

STRUCTURAL ENGINEERING

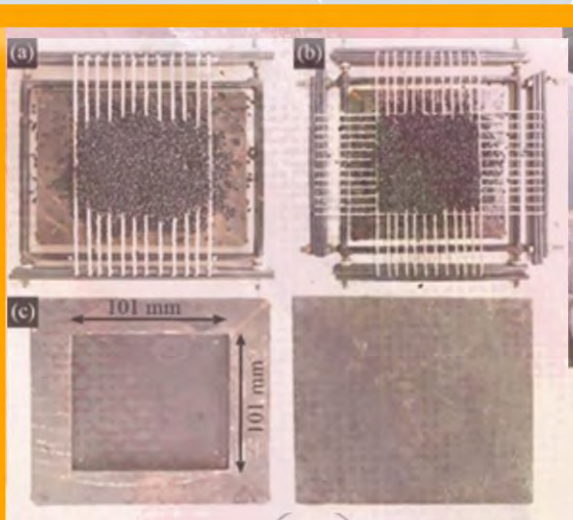

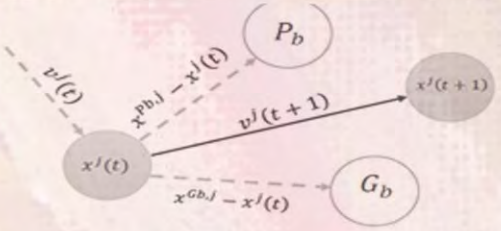

PSO

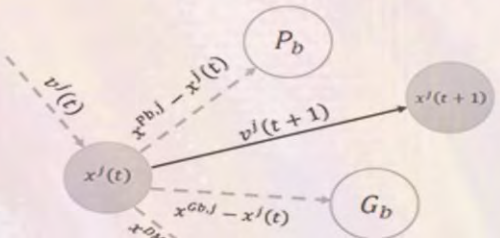

eJSE
INTERNATIONAL

Electronic Journal of Structural Engineering

Original Article

Cite this: DOI:10.56748/ejse.233642

Received Date: 22 September 2022
Accepted Date: 30 January 2023

1443-9255
https://ejsei.com/ejse

Machine learning-based optimum reinforced concrete design for progressive collapse

Mohammad Javad Esfandiari [a]*, Homa Haghighi [a] and Girum Urgessa [a]
[a] Department of Civil Engineering, George Mason University, VA, USA
* Corresponding Author: Mesfandi@gmu.edu

Abstract

This paper investigated progressive collapse analysis of three-dimensional (3D) reinforced concrete (RC) frames that are optimized for carrying structural loads by introducing a unique simultaneous multi-column removal using Machine Learning. The various load paths resulting from multiple-column removal are incorporated in the optimization automatically. The investigation includes formulating an integrated computational framework that incorporates a self-training machine learning algorithm. The efficiency of the algorithm is tested by using several hundreds of optimized structures. The efficiency of the computational framework was shown by conducting a comprehensive study on the optimization and behavior of structures considering seismic loading, alternative load path due to progressive collapse, and second order (P–delta) effects. The results show that the proposed framework ensures that system solutions meet both structural integrity and constructability requirements of the ACI and the Unified Facilities Criteria.

Keywords

Machine Learning, Structural Optimization, Progressive Collapse, Reinforced Concrete, Artificial intelligence

1. Introduction

Local failure of structural members will result in increased internal forces and overloading and may cause a progressive collapse of the entire or a part of a given structures. A few examples of progressive collapse (PC) include the Murrah Building in Oklahoma City in 1995, the Twin Towers in New York City in 2001, and the Plasco Building in Tehran in 2017, and the Hard Rock Hotel in New Orleans in 2019. PC results in economic losses and death of occupants. Hence, structures must be designed to better withstand progressive collapse.

The number of PC studies consisting of experimental programs and numerical studies have increased significantly since 2001. Byfield et al (Byfield et al., 2014), Wang et al (Wang et al., 2014) and Qian and Li (Qian and Li, 2015) provided detailed reviews on this topic.

As far as numerical studies are concerned, various representative models are found in literature (Bao et al., 2008; Talaat and Mosalam, 2007; Buscemi and Marjanishvili, 2005) including computational FEM models for determining the response of structures before failure with a reasonable accuracy and DEM models that are more effective for moving and collision between rigid bodies after failure. Marchand et al (Marchand and Stevens, 2015) argued that common structural design software (e.g., SAP2000 and ETABS) can provide reasonable results than those determined with high-fidelity physics-based software. Esfandiari et al (Esfandiari and Urgessa, 2018) presented a non-linear time history pull-down of a two-span steel frame in ETABS and showed that the numerical results were in excellent agreement with experimental results.

Machine Learning (ML) and Artificial Intelligence (AI) applications in recent years have opened new opportunities for use in traditional engineering problems. Machine learning mostly deals with problems where paired examples, X → Y, exist. For this paper, X and Y can be interpreted as features of the structure and the optimum solution, respectively. As such, the machine learning technique attempts to map G: X → Y` with the translated domain Y` distributed identically to Y. However, in the field structural engineering, the main challenge is the lack of adequate optimum data that is needed to train the algorithm. Therefore, seeking an algorithm that could learn to map between domains without paired input-output scenarios is crucial.

Zue et al. (Zhu et al., 2017) used Cycle-Consistent Adversarial Networks in image-to-image transformation for learning to map between an input and output image when paired examples are absent. They simultaneously trained G: X → Y and another translator F: Y→ X with a cycle consistency loss such that F(G(x)) ≈ x and G(F(y)) ≈ y. However, in structural analysis, it is important to create an alternative algorithm for capturing the complex system behavior where few training paired data are available.

Sra et al. (Sra et al., 2012) showed that learning from available dataset combined with optimization is applicable to a myriad of complex, dynamic, and stochastic problems. Mosavi et al. (Mosavi and Varkonyi-Koczy, 2017) combined machine learning with optimization to increase the learning ability of robots. They concluded that integrating ML and optimization significantly increases the quality of decision making and learning capability in decision systems.

As far as machine learning techniques, Jong-Su Jeon et al. (Jeon et al., 2014) proposed probabilistic joint shear strength models by implementing ML. They used the prediction model as joint response models for evaluation of seismic performance and inelastic responses of frames. (Nick et al., 2015) have used different machine learning techniques for identifying the existence and location of damage, and the type and severity of damage. Ni Hong-Guang and Wang Ji-Zong (Ni and Wang, 2000) used a multi-layer feed-forward neural network and presented a method for predicting 28-day compressive strength of concrete. Dac-Khuong Bui et al. (Bui et al., 2018) developed a model for determining the tensile strength of High-Strength Concrete. They selected neural network for their research due to the nonlinear relation between concrete strength and its components.

In this paper, classification techniques are used because the algorithm needs to correctly determine the class labels for unseen instances on the basis of previously observed optimum structural system data and suggests a specific class to the optimization for further constraints handlings. The algorithm starts to run with a few training data and as it is applied on different structures, it can consider the result for its future training data. As the training data becomes more available, the performance improves dramatically over time. Different classification techniques such as decision tree, SoftMax, and nearest neighbors are presented.

2. Structural optimization problem for reinforced concrete frames

Esfandiari et al (Esfandiari et al., 2018b) presented a general structural optimization problem as shown in Equation 1.

$$\begin{aligned} & x = [x_1, \dots, x_n]^T \\ & g(x) \le 0, \qquad k = 1, \dots, m \\ & x^L \le x \le x^U \end{aligned} \tag{1}$$

where x is a vector of n structural system variables, $f(x)$: $R^n \rightarrow R$ is the objective function which returns a scalar value to be minimized, the vector function $g(x)$: $R^n \rightarrow R^m$ returns a vector of length m containing the values of the inequality constraints evaluated at x, and x^L, $x^U$are two vectors of length n containing the lower and upper bounds of the structural system variables, respectively. The above equation contains only inequality constraints because equality constraints are usually not found in structural optimizations.

Equation 2 shows a common constraint k in a structural optimization problem.

$$g_k(x) = |q_k(x)| - q_{allow,k} \tag{2}$$

where $q_k(x)$ is a response measure for analysis and design x; and $q_{allow,k}$ is its maximum allowable absolute value.

The objective function in structural optimization problems is generally defined by the weight or total cost of the structure (Tahmouresi et al., 2021). When considering total cost, the concrete, steel and labor costs are included. However, when the objective function is the total weight, only the weight of concrete and steel are included. Equation 3 shows the resulting objective function.

$$f_{Obj} = Obj_c + Obj_s + Obj_f \tag{3}$$

where $Obj_c, Obj_s, and\ Obj_f$ are the costs of concrete, reinforcing steel bars, and labor, respectively.

Equations 4-6 show the costs of each component when the objective function is the total cost of a structural frame.

$$Obj_c = C_C\left(\sum_{i=1}^{N_{col}} b_i.d_i.L_{n\ column,i} + \sum_{j=1}^{N_{beam}} b_{w\ j}.h_j.L_{beam\ j}\right) \tag{4}$$

$$Obj_s = C_s.\gamma_s.\left(\sum_{i=1}^{N_{col}}\sum_{j=1}^{N_{bar,i}} A_{St\ j}.L_{bar\ j} + \sum_{i=1}^{N_{col}}\sum_{k=1}^{N_{tie,i}} A_{Sh\ k}.L_{tie\ k} + \sum_{m=1}^{N_{beam}}\sum_{l=1}^{N_{bar,m}} A_{St\ l}.L_{bar\ l} + \sum_{m=1}^{N_{col}}\sum_{n=1}^{N_{tie,m}} A_{Sh\ n}.L_{bar\ n}\right) \tag{5}$$

$$Obj_f = C_f\left(\sum_{i=1}^{N_{col}}\left[2(b_i + h_i).L_{n\ column,i}\right] + \sum_{j=1}^{N_{beam}}\left[\left(b_{w\ j} + 2h_j\right).L_{beam\ j}\right] - \sum_{k=1}^{N_{col}} b_k + d_k\right) \tag{6}$$

where N_{col} , N_{beam} , b, d, b_w , h, L, and L_n are the number of columns, the number of beams, the width of column, the depth of column, the width of beam, the height of beam, the length of the members, and the length of clear span between supports, respectively; C_C, C_f and C_s are unit cost of the concrete, the labor and the steel, respectively; A_{st} , L_{bar} , and N_{bar} are the area, the length and the number of main rebars placed in the member while A_{sh} , L_{tie}, and N_{tie} are the area, the length and the number of shear reinforcement used in the member respectively; and γ_s is the density of rebars (kg/m3).

3. Proposed DMPSO-ML algorithm

3.1 Overview

Figure 1 shows the basic concept of the particle movement in the traditional Particle Swarm Optimization method (PSO) versus the proposed Decision-Making Particle Swarm Optimization method (DMPSO). As shown in the figure, each particle in PSO only searches for the best solution according to its own best experience, and the best solution is determined by all particles (Kennedy and Eberhart, 1995). However, in structural optimization, it is important to ensure that the structure is stable and safe. An experienced structural engineer can decide the sort of alterations in the system variables that could lead to a preferable solution. As an example, if the demand to capacity ratio of a member is greater than one, the acceptable solution for addressing this issue may be changing the cross-sectional sections of the member or the rebar reinforcement ratio of the section. However, a human decision maker cannot be available and actively participate in the solution process and direct it according to the preferences in the entire process of an optimization. The decision maker (DM) algorithm acts similar to an experienced structural engineer.

More details regarding how the DM is formulated and operates, and how it is fused with PSO, are discussed in the following subsections.

3.2 DMPSO Algorithm Enhanced with ML

DMPSO uses an informed strategy and the knowledge beyond the definition of the problem itself, to empower PSO optimization algorithm and accelerate convergence toward the optimum solution. The DM formulation in this paper, which is inspired by Bayes' theorem, seeks the probability of a member not failing given the geometry and loading application. Bayes' theorem is stated mathematically by Equation 7.

$$P(B) = \frac{P(A)P(A)}{P(B)} \tag{7}$$

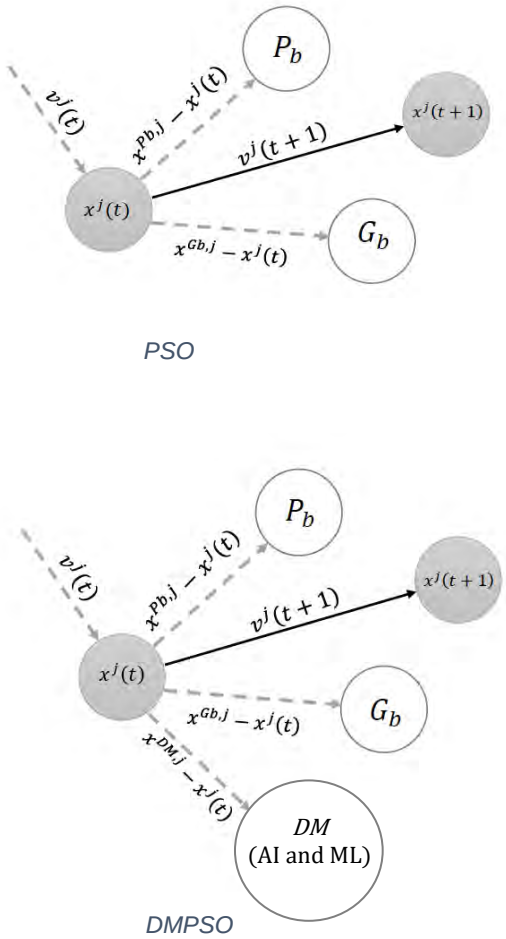

Fig 1. PSO versus DMPSO

The probability of geometry and loading for a given member specification can be determined from previously analyzed optimum structures. Accordingly, DM implements machine learning to find the most probable structural member according to the geometry, loading condition and location of the member. However, for incorporating dependencies, Bayes' theorem needs fundamental assumptions about dependence and independence between system variables, and determining the marginal in the Bayes' theorem is computationally expensive. For that reason, alternative machine learning methods can be cost effective and are investigated in this paper.

The decision maker algorithm can also disregard a solution at any given time of the computation process when it determines that a better fitness cannot be obtained. The principle of pruning from AI was adopted in this paper, which allows the DM algorithm to ignore portions of the search space or analysis that make no difference to the final choice. The heuristic evaluation function allows us to estimate the objective function without doing a complete analysis. When pruning is applied to a standard search tree, it returns the same move as a search would, but it prunes away branches that cannot possibly influence the final decision. This requires examining first the successors that are likely to be the optimum solution.

To equip the DM with machine learning power, different ML methods were investigated in this paper.

The first step was the collection and preparation of the training data set. Since there was no training data available at the beginning, a small sub-set of structures was selected, and the optimization algorithm was used for producing the training set. The small sub-set of structures was later used to produce more complex training sets. Then, the behavior of 640 more complex structures were considered as the training data. For each structure, the structure was separately optimized for 10 random column removal scenarios for progressive collapse analysis. The goal was to classify the best cross section for the elements under different loading conditions. For this purpose, three separate machine learning (ML) models were trained. Table 1 provides the specifics of these ML models.

Table 1. Detail of the ML models

	Model 1	Model 2
Features	Number of bays in each direction Maximum bay span in each direction Number of stories Dead load Live load Seismic parameters	Element type Maximum adjacent bays length at the element Moment and shear of the element Top and bottom connected beams, The number of stories above the element The number of stories below the element.
Usage	Initial randomized section at the beginning	Optimum separate elements based on conventional loading

Model 1 related the final result of the average size of optimum elements in each story to the overall geometric feature of the structure, including number of bays in each direction, maximum bay span in each direction, number of stories, dead load, live load and seismic parameters. This model was only used in the first iteration to generate initial randomized sections.

The second and third models connected the output of the optimum separate elements to its learning feature for the whole structure and progressive collapse removal scenario cases, respectively. The learning features considered include element type, actual bay length, moment and shear of the element before and after removal scenarios, bottom and top connected beams, and the number of stories above and below the removed element.

To streamline the problem for ML and to avoid overfitting, the class of the sections for columns and beams were restricted to 8 and 6 sections, respectively as shown in Fig. 2 and Fig. 3. Rectangular cross-sections were deliberately considered with 100mm difference in width and height to have the best arrangement of the classes covering most of the practical results.

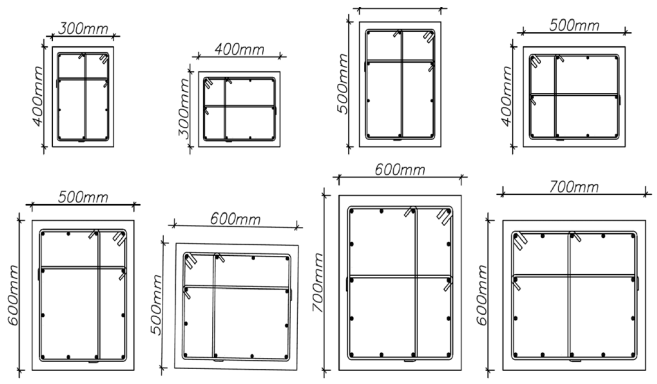

Fig 2. Different section classes for columns in the ML classification problem

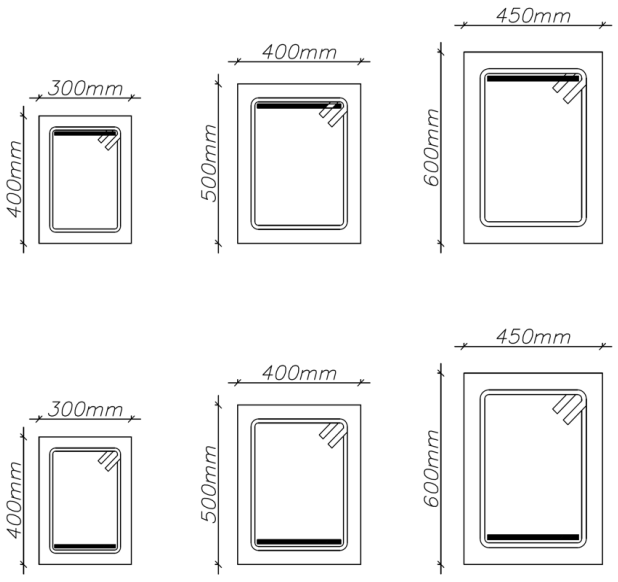

Fig 3. Different section classes for beams in the ML classification problem

For the beams, cross sectional dimensions and the location of the rebar were considered as variables. The corresponding reinforcement amount was calculated and placed later based on strength requirements.

The section restrictions did not affect the final results because the initial guess from ML is fed to the optimization algorithm with no restriction on its variable. In other words, these initial guesses show the preference of the DM to the optimization algorithm and guide it to find a better solution.

For identifying the best ML technique that will be integrated with the optimization algorithm, the following classifiers were investigated.

3.3 K-Nearest Neighbor (KNN)

The K-nearest-neighbor (KNN) density estimation method (Paya et al., 2008) was applied to each class followed by employing Bayes' theorem. Consider a data set comprising Nk members' cross section in class Ck with a total of N points. To classify a new structural element x, a sphere centered on x can be drawn in the feature space, precisely holding K elements' cross section regardless of their class. Suppose this sphere contains Kk member from class Ck. The posterior probability of selecting a structural element's cross section can be obtained by applying the Bayes' theorem as shown in Equation 8.

$$p(C_k) = \frac{P(C_k)p(C_k)}{p(x)} = \frac{K_k}{K} \tag{8}$$

In the KNN formulation, the cross section with the largest posterior probability should be assigned to element x to minimize the probability of misclassification. When the algorithm needs to find an appropriate cross section for a new element, it can identify the K nearest similar members from the training data set of optimum structures and then assign a cross section with the average of variables from the KNN. It is important to find the best K for the problem. Small Ks result in many small regions of each class and make the model more biased. On the other hand, large Ks led to fewer larger regions which may affect the final result.

3.4 SoftMax Classifier

SoftMax classifier (Duan et al., 2003) is the generalization of binary Logistic Regression classifier to multiple classes. Softmax classifier uses a linear classifier for mapping and generating scores as the unnormalized log probabilities with cross-entropy loss having the form shown in Equation 9.

$$L_i = \log\left(\frac{e^{f_{yi}}}{\sum_j e^{f_j}}\right) \tag{9}$$

Where fj is the j-th element of the vector of class scores f. The use of the exponential scores gives the unnormalized probabilities, and the division for normalization purpose. This will ensure that the sum of the probabilities is one. The stochastic gradient descent was used for training. Here the best section that has the highest probability for the corresponding element was sought. The data was trained in 16 mini batches.

3.5 Decision Tree Classifier

Decision tree classification algorithms (Safavian and Landgrebe, 1991) have a significant potential for a variety of problems and have been used in civil engineering applications. There are different measures that can be utilized to determine the best way to split between classes. Gini index and entropy were used for selecting the best split based on the degree of impurity of the child nodes. Binary decision tree with 5 and 6 depths were tested.

4. Metrics and performance evaluation

The data set used here was divided into 3 different groups: training, validation, and testing. The training dataset was used to train models with various hyper parameter values. Then the validation dataset was used to identify the best working parameters. To validate the model, a 5-fold cross validation was used. After that, the training and validation datasets were used to train the final model.

Evaluation presented a major challenge. Consider a single column under pure compression loading. This column can be designed with different cross sections that can satisfy the stability requirements of the structure. Since the optimization does not warrant the global optimum in a complex system, it accepted near-optimum solutions in the evaluation. Moreover, the element classes of the final result did not exactly match the output of the machine learning classes. For the machine learning outputs, only 8 classes were considered for the columns and 6 classes for the beams, while the final result of the optimum structure does not have any restriction and the dimensions of the elements might change through the optimization process. Therefore, if the structural requirements were only checked, all

over designed solutions would pass the evaluation criteria. On the other hand, if the optimum solution was only checked, the accuracy would be very low. This issue was addressed by finding the nearest neighbor of the actual sections of the structure with class samples of one increment threshold for accepting the result.

Finding the final optimum solution was not the goal of this initial step but rather keeping the variables within an acceptable range of initial guesses. Later the algorithm would find the best optimum solution. Therefore, different hyperparameters and methods were investigated, and the best parameters were selected for integrating it with the optimization algorithm. The comparison of the results is shown in Fig. 4.

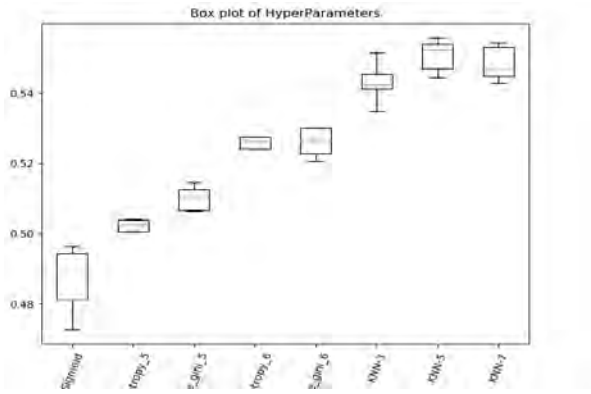

Fig 4. Box plot of different hyper parameters

The number and size of rebars in each direction of the concrete section presented a challenge because specific required rebar area could be placed in several arrangements. As an example, 450 mm2 of required rebar area can be satisfied by using 6-D10, 4-D12, or 2-D25 bars. The results can be improved by only considering the cross-sectional dimension parameters and the overall required area of the rebar for the section with 10 percent threshold for the columns and the beams. Later, when this section is ready to be fed to the optimization algorithm, the overall required area would be converted to the best arrangement for the rebars size and numbers in each direction, for that specific section. This approach dramatically improved the findings obtained as shown in Fig. 5.

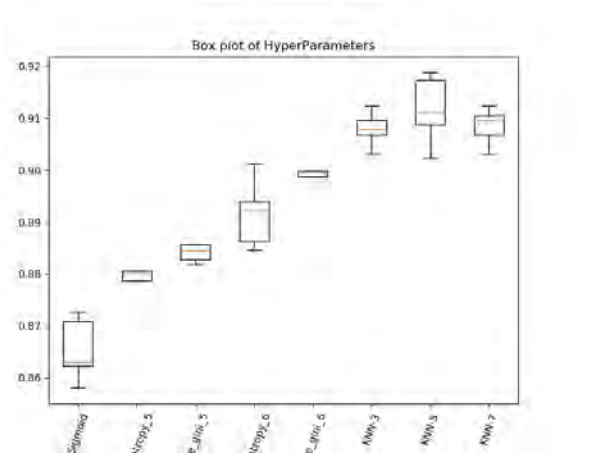

Fig 5. Box plot when only cross-sectional dimensions were considered as variables

The KNN-5 method resulted in the highest accuracy compared to all the techniques investigated. The DMPSO then modifies its velocity and position according to its experience, neighboring particles' experience, and the preference of the decision maker (DM) by employing Equation 10 and Equation 11 (Esfandiari et al., 2018a).

$$v^j(t+1) = wv^j(t) + c_1 r_1 \odot \left(x^{Pb,j} - x^j(t)\right) + c_2 r_2 \odot \left(x^{Gb,j} - x^j(t)\right) + c_3 r_3 \odot \left(x^{DM,j} - x^j(t)\right) \quad (10)$$

$$x^j(t+1) = x^j(t) + v^j(t+1) \quad (11)$$

Where $v^j(t)$ *and* $x^j(t)$ represent the velocity and the position vectors of particle j at time t, respectively. The term w is a modifier employed to control the exploration capabilities of the swarm. Vector $x^{Pb,j}$ denotes the personal best position which is registered by particle j, vector $x^{Gb,j}$ is the global best position attained by the entire swarm up to the current iteration, and vector $x^{DM,j}$ indicates the position of preference of the decision maker in the search space. The acceleration coefficients c_1 and c_2, and c_3 rule the impact of the particle's own experiences, the other particles' experiences, and the decision maker's preference on the trajectory of each particle, respectively. r_1, r_2, r_3 are three random vectors with uniformly distributed numbers in the interval [0, 1]. The symbol "⊙" is the element-wise product of two vectors. The two acceleration coefficients (c1 and c2) and the smallest and largest value of inertial factor (wmin and wmax) were taken as 2.025, 2.025 and 0.4, 0.9, respectively (Alam et al., 2015; Eberhart and Shi, 2000). The acceleration coefficient for DM, c_3, was initially taken as 2.025 (the same as c_1 and c_2) and decreased over iterations. Therefore, for the first few iterations, the algorithm mostly relies on the DM. To ensure the functionality, if the demand to capacity ratio of a member is not within 50% in the optimization process, the DM algorithm suggests its preference, such as increasing or decreasing a relevant parameter, to the DMPSO algorithm.

The DM algorithm gathers statistics from a database of previously analyzed structures to determine members most often lead to an optimum structure. In the early iterations, there were a few choices among the large number of possible variables. Thus, the DM commentary based on past structures has a higher impact on DMPSO. Usually after the first 100 iterations, the DMPSO algorithm mostly relies on optimization rather than the DM preference.

5. Incorporating progressive collapse in DMPSO-ML

In progressive collapse analysis, multiple scenarios of removing critical members should be considered, which drives the structural system and cross-section selection to be tedious and costly. Therefore, investigating the formulation of a computational framework is important for producing d cost-effective solutions. This was achieved by a series of steps. First, a finite element model capable of accurately modeling new load paths to progressive collapse analysis was developed. Then, the finite element model was integrated with DMPSO to automatically evaluate structural response for progressive collapse.

There are two groups of constraints needed for expanding the optimization problem and incorporating progressive collapse. These include general concrete structural system constraints and progressive collapse (UFC) constraints. The first group includes parameters typical of structural systems subjected to traditional lateral loads such as plastic rotations.

The second group includes those related to progressive collapse as defined in UFC (Gsa, 2003; Defense, 2005) and GSA. These constraints ensure that the structure is capable of bridging over critical vertical load-carrying elements that are eliminated during a progressive collapse scenario such as redundancy requirements.

The integrated framework of the DMPSO algorithm that is empowered by ML is shown schematically in Fig. 6 and Fig. 7.

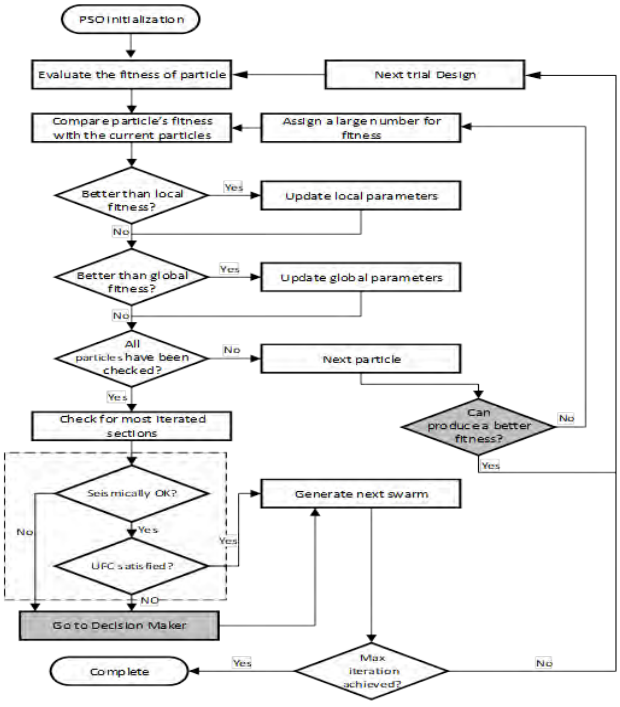

Fig 6. Modified DMPSO for Progressive Collapse

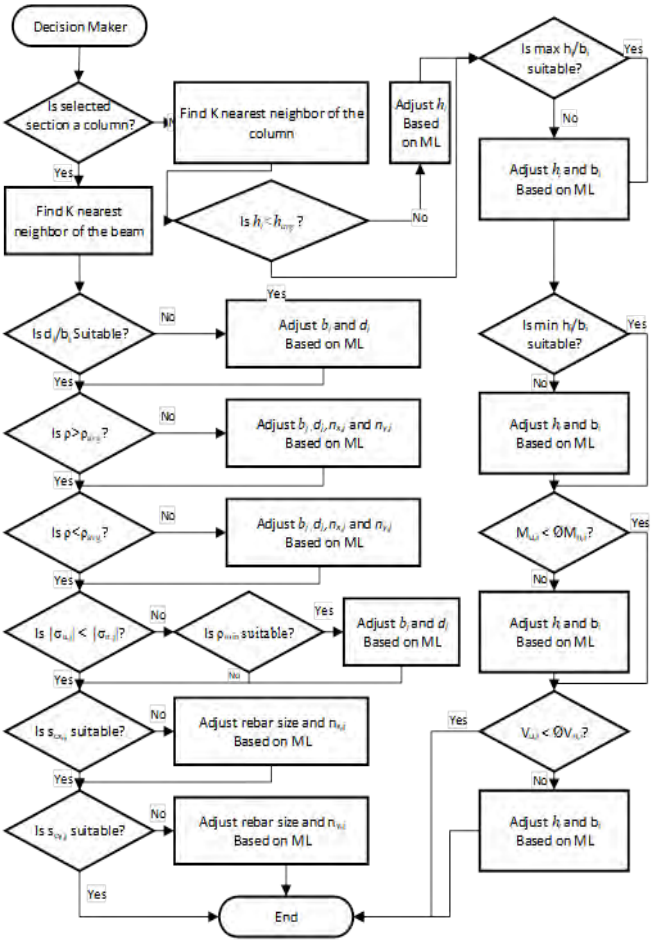

Fig 7. Flowchart of decision maker empowered by Machine Learning (ML)

6. Practical example on progressive collapse analysis of 3D optimized RC frames.

The proposed DMPSO-ML framework was used to analyze a given 7-story RC frame with three spans whose geometry, grouping details, and removal scenarios are shown in Fig. 8. A total of sixteen unique column removal scenarios were implemented in the alternate path investigation of this example frame. Although a symmetric plan was used, sections A and C differ in size. This implies that one set of eight removal scenarios, as shown in Fig. 8, is considered in each of these sections. These columns eliminated are located at the corner and middle of each direction of the members in the first story above the grade, the story directly below the roof, and the story above the location of a column splice at every other floor. The objective function here is the construction weight similar to a baseline optimized structure for conventional loadings without considering progressive collapse (Esfandiari et al., 2018b). The frame includes 180 members, 84 beams and 96 columns, which were arranged into 42 groups: 28 groups for beams and 14 groups for columns. It contains 574 system variables, 504 were for beams and 70 were for columns. Beams and columns were grouped to satisfy the uniformity of members and having similar behaviors according to their place in the frame and loading conditions. To ensure best results for the stochastic decline, a population size of 150 was selected.

Table 2 shows the optimal frame systems from the present progressive collapse optimization, considering all of the given removal scenarios Both linear static (LS) and nonlinear dynamic (ND) methods were considered. Furthermore, the result of the optimal frame analysis without including progressive collapse is also presented as the baseline to depict the changes made in the structural member and reinforcing steel sizes of optimal results when compared to current integrated progressive collapse analysis.

Fig. 9 shows DMPSO-ML algorithm evolutions for obtaining the solutions. DMPSO did not confine local values and carried on converging. As validated, the baseline structure without considering the progressive collapse requirements converged to the optimum results in smaller number of structural analysis and flatten out within less generations. This is expected because for progressive collapse analysis DMPSO has to confirm the constraints in two steps. In the first step, constraints related to traditional lateral systems (e.g., seismic) requirements were checked (Randall W. Poston and Basile G. Rabbat, 2011). If the criteria are not met here, it proceeds to the Decision Maker (DM) portion of the algorithm for adjusting parameters. Otherwise, it proceeds to the second step for checking progressive collapse requirements. The results are not registered until every constraint consisting of both lateral and progressive collapse requirements are met.

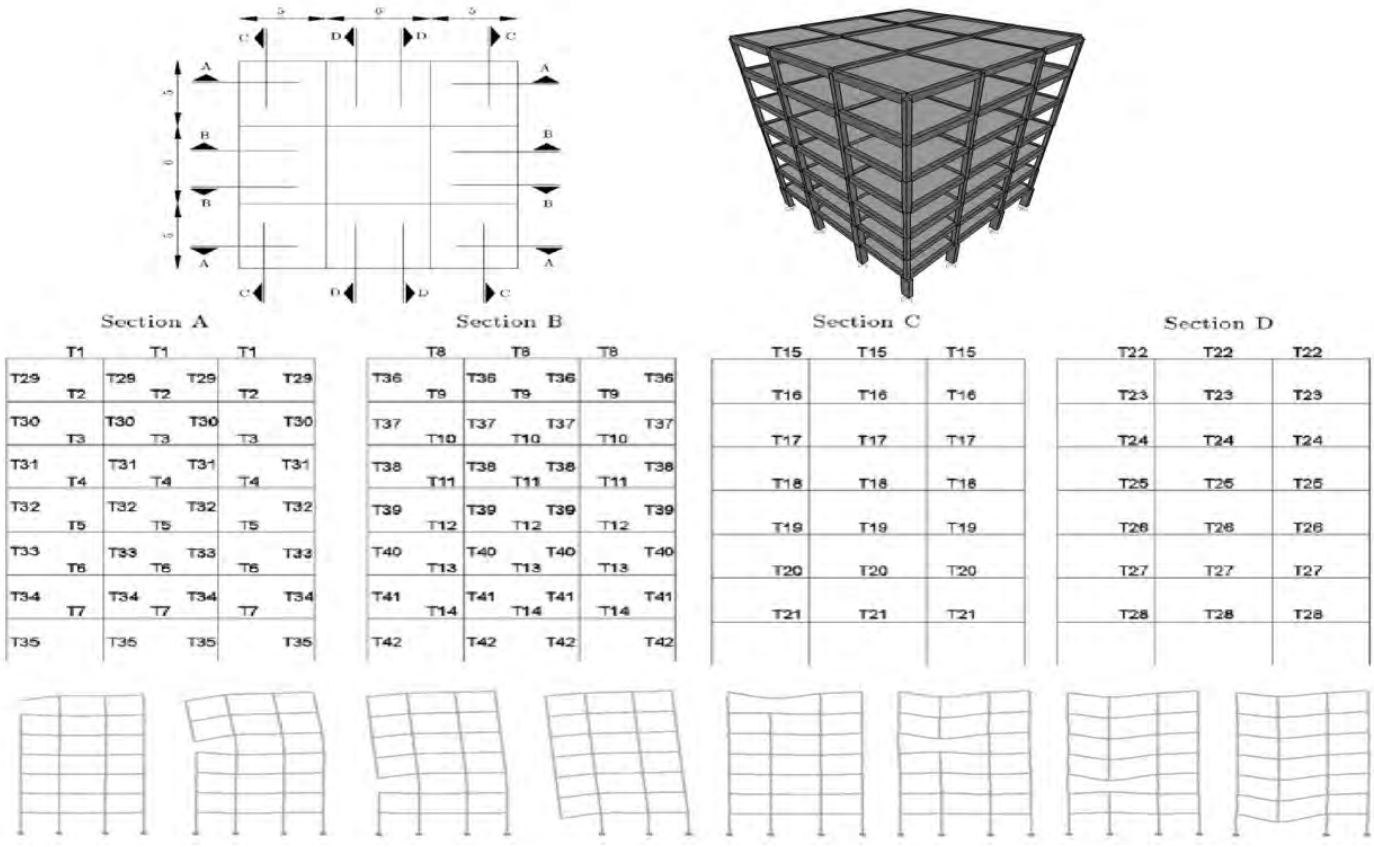

Fig 8. Geometry, member classification, and removal scenarios

Thus, the need for evolutionary generation to handle these two types of constraints is evident in the progressive analysis case.

Fig. 10 illustrates the demand to capacity ratio (DCR). The demand capacities for LS and ND were calculated for regular loading after the structure was totally designed for progressive collapse. This implies that after the process of removing elements are completed and the optimum result was obtained, the DCR is calculated using those sections. Bigger sections were used in LS and ND when compared to the structure considered without progressive collapse. As a result, the DCR of elements in LS is the least among all the methods. Nevertheless, all the DCRs obtained were above 0.61, which shows that the algorithm can obtain acceptable results.

Note that in the ML algorithm, the results are obtained instantaneously given data is used to train the algorithm and the pretrained model is used for prediction. The optimization piece requires close to 12 hours to run because each iteration takes around 10 seconds.

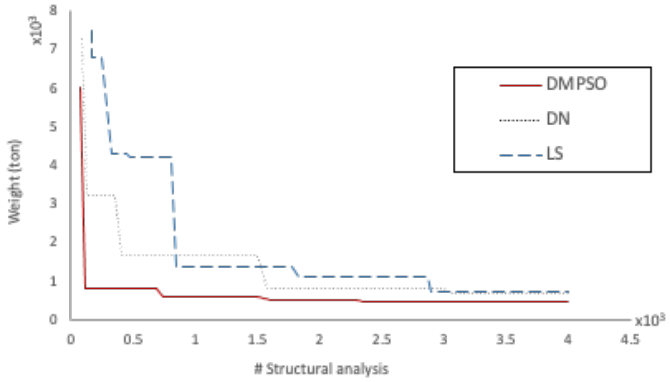

Fig 9. Convergence rate from DMPSO, based on LS, ND compared to the system without considering progressive collapse.

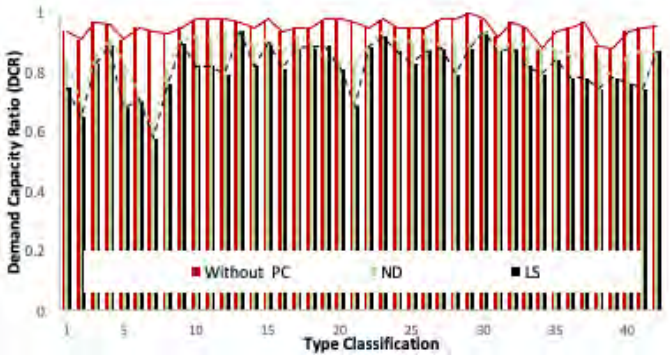

Fig 10. Maximum DCR of members for each analysis method

7. Conclusion

This paper presented the integration of optimization and progressive collapse analysis computational framework empowered by machine learning. The main objective was to evaluate the behavior of reinforced concrete structures while satisfying the limitations and specifications of the American Concrete Institute 318 code and Unified Facilities Criteria progressive collapse requirements. Three machine learning algorithms, K nearest neighbor, SoftMax, and decision tree classifiers were evaluated. The KNN machine learning algorithm provided better performance to alleviate the computational challenge for the structural optimization problem involving progressive collapse.

Using a case study, the analysis was shown to enhance load redistribution capability of the structure by considering the alternate path criteria through finding appropriate structural member sizes. Meanwhile, the cost of the example frame analyzed reduced substantially through the optimization process. The case study showed the capability of the DMPSO-ML algorithm to accelerate convergence toward the optimum system solutions while reducing computational effort.

References

Alam MN, Das B and Pant V. (2015) A comparative study of metaheuristic optimization approaches for directional overcurrent relays coordination. *Electric Power Systems Research* 128: 39-52.

Bao Y, Kunnath SK, El-Tawil S, et al. (2008) Macromodel-Based Simulation of Progressive Collapse: RC Frame Structures. *Journal of Structural Engineering* 134: 1079-1091.

Bui D-K, Nguyen T, Chou J-S, et al. (2018) A modified firefly algorithm-artificial neural network expert system for predicting compressive and tensile strength of high-performance concrete. *Construction and Building Materials* 180: 320-333.

Buscemi N and Marjanishvili S. (2005) SDOF Model for Progressive Collapse Analysis. *Structures Congress 2005.* 1-12.

Byfield M, Mudalige W, Morison C, et al. (2014) A review of progressive collapse research and regulations. *Proceedings of the Institution of Civil Engineers - Structures and Buildings* 167: 447-456.

Defense Do. (2005) Unified Facilities Criteria: Design of Buildings to Resist Progressive Collapse (UFC 4-023-03). Department of Defense Washington, DC, USA.

Duan K, Keerthi SS, Chu W, et al. (2003) *Multi-category Classification by Soft-Max Combination of Binary Classifiers,* Berlin, Heidelberg: Springer Berlin Heidelberg.

Eberhart RC and Shi Y. (2000) Comparing inertia weights and constriction factors in particle swarm optimization. *Proceedings of the 2000 Congress on Evolutionary Computation. CEC00 (Cat. No.00TH8512).* 84-88

Esfandiari M and Urgessa G. (2018) A Pull-down Dynamic Analysis of Two-Span Steel Frames Subjected to Progressive Collapse.

Esfandiari MJ, Urgessa GS, Sheikholarefin S, et al. (2018a) Optimization of reinforced concrete frames subjected to historical time-history loadings using DMPSO algorithm. *Structural and Multidisciplinary Optimization* 58: 2119-2134.

Esfandiari MJ, Urgessa GS, Sheikholarefin S, et al. (2018b) Optimum design of 3D reinforced concrete frames using DMPSO algorithm. *Advances in Engineering Software* 115: 149-160.

Gsa U. (2003) Progressive collapse analysis and design guidelines for new federal office buildings and major modernization projects. *Washington, DC*.

Jeon J-S, Shafieezadeh A and DesRoches R. (2014) Statistical models for shear strength of RC beam-column joints using machine-learning techniques. *Earthquake Engineering & Structural Dynamics* 43: 2075-2095.

Kennedy J and Eberhart R. (1995) Particle swarm optimization. *Proceedings of ICNN'95 - International Conference on Neural Networks.* Perth, WA, Australia: IEEE, 1942-1948

Marchand KA and Stevens DJ. (2015) Progressive Collapse Criteria and Design Approaches Improvement. *Journal of Performance of Constructed Facilities* 29: B4015004.

Mosavi A and Varkonyi-Koczy AR. (2017) Integration of Machine Learning and Optimization for Robot Learning. *Advances in Intelligent Systems and Computing Recent Global Research and Education: Technological Challenges,* 519: 349-355.

Ni H-G and Wang J-Z. (2000) Prediction of compressive strength of concrete by neural networks. *Cement and Concrete Research* 30: 1245-1250.

Nick W, Asamene K, Bullock G, et al. (2015) A study of machine learning techniques for detecting and classifying structural damage. *International Journal of Machine Learning and Computing* 5: 313.

Paya I, Yepes V, González-Vidosa F, et al. (2008) Multiobjective Optimization of Concrete Frames by Simulated Annealing. *Computer-Aided Civil and Infrastructure Engineering* 23: 596-610.

Qian K and Li B. (2015) Research Advances in Design of Structures to Resist Progressive Collapse. *Journal of Performance of Constructed Facilities* 29: B4014007.

Randall W. Poston and Basile G. Rabbat. (2011) *Building Code Requirements for Structural Concrete (ACI 318-11)*: American Concrete Institute.

Safavian SR and Landgrebe D. (1991) A survey of decision tree classifier methodology. *IEEE Transactions on Systems, Man, and Cybernetics* 21: 660-674.

Sra S, Nowozin S and Wright SJ. (2012) *Optimization for machine learning,* Cambridge, Massachusetts, London, England: Mit Press.

Tahmouresi, A., Robati, A. et al. (2021) A Combined Genetic Algorithm-Artificial Neural Network Optimization Method for Mix Design of Self Consolidating Concrete, *International Journal of Structural and Civil Engineering Research*, Vol. 10, No. 3, doi: 10.18178/ijscer.10.3.106-112.

Talaat M and Mosalam KM. (2007) Towards Modeling Progressive Collapse in Reinforced Concrete Buildings. *Research Frontiers at Structures Congress* Long Beach, California, United States: American Society of Civil Engineers, 1-16.

Wang H, Zhang A, Li Y, et al. (2014) A review on progressive collapse of building structures. *The Open Civil Engineering Journal* 8: 183-192.

Zhu J-Y, Park T, Isola P, et al. (2017) Unpaired Image-to-Image Translation using Cycle-Consistent Adversarial Networks. (Accessed March 01, 2017).

Appendix

Table 2. Results of optimum systems based on LS; ND compared to the system without considering progressive collapse.

	LS								ND								DMPSO							
	Sectional dimensions		Reinforcements						Sectional dimensions		Reinforcements						Sectional dimensions		Reinforcements					
Type	Height	Width	Top-rebar			Bot-rebar			Height	Width	Top -rebar			Bot -rebar			Height	Width	Top -rebar			Bot -rebar		
T1	350	350	5-D16 3-D12	3-D14	6-D16 4-D12	6-D16 4-D12	3-D12 1-D16	5-D16 3-D12	350	350	5-D12 4-D12	3-D14	5-D12 3-D14	3-D12 3-D14	4-D14 4-D16	3-D12 3-D14	300	300	3-D12 3-D14	3-D12	3-D12 3-D14	3-D12 3-D14	3-D12 1-D16	3-D12 3-D14
T2	400	350	3-D16 3-D16	3-D14	5-D16 5-D16	3-D16 3-D16	6-D14	4-D16 4-D16	350	350	5-D12 5-D12	3-D14	5-D12 5-D12	5-D14	4-D12 4-D14	5-D14	350	350	3-D14 3-D14	3-D14	3-D14 3-D14	3-D14	3-D14	3-D14
T3	350	350	4-D14 4-D12	3-D12	4-D14 4-D12	5-D14 4-D12	3-D12 1-D16	6-D14 4-D12	350	300	4-D16 2-D14	3-D12	3-D16 3-D14	3-D12	2-D12 2-D12	3-D12	300	300	3-D12 4-D16	3-D12	3-D12 4-D16	3-D12	3-D12 1-D16	3-D12
T4	350	350	5-D16 4-D14	3-D14	4-D16 3-D14	2-D16 2-D14	5-D14	2-D16 3-D14	350	350	4-D14 4-D14	3-D14	3-D14 3-D14	5-D14	5-D14 5-D12	4-D14	350	350	3-D14 2-D22	3-D14	3-D14 2-D22	4-D14	4-D14	4-D14
T5	400	300	5-D16 4-D14	3-D12	5-D16 4-D14	3-D16 1-D14	3-D12 1-D16	2-D16 2-D14	350	350	5-D14 4-D12	3-D12	5-D14 4-D12	3-D12 2-D16	4-D12 3-D12	3-D12 3-D14	300	300	3-D12 3-D20	3-D12	3-D12 3-D20	3-D12 1-D14	3-D12 1-D16	3-D12 1-D14
T6	400	350	4-D16 5-D12	3-D14	5-D16 3-D12	3-D16 2-D12	4-D14	3-D16 4-D12	400	350	5-D14 5-D14	3-D14	4-D14 4-D14	5-D16 3-D12	4-D14 2-D12	6-D16	350	350	3-D14 2-D22	3-D14	3-D14 2-D22	4-D14	4-D14	4-D14
T7	450	350	9-D14 9-D14	3-D14	5-D14 5-D14	5-D14 3-D12	3-D12 1-D16	4-D14 4-D12	400	300	4-D16 3-D14	3-D12	3-D16 3-D14	6-D12	4-D16 4-D16	5-D12	300	300	3-D12 2-D22	3-D12	3-D12 2-D22	3-D12	3-D12 1-D16	3-D12
T8	400	300	4-D12 5-D14	3-D14	5-D12 6-D14	5-D12 2-D14	3-D12 4-D16	5-D12 2-D14	350	300	5-D12 5-D12	3-D12	4-D12 4-D12	3-D12 1-D14	2-D14 3-D14	4-D14	300	300	3-D12 1-D16	3-D12	3-D12 1-D16	3-D12 1-D10	3-D12 4-D16	3-D12 1-D10
T9	300	300	3-D16 2-D12	3-D14	3-D16 2-D12	3-D16 2-D12	3-D14 1-D12	3-D16 2-D12	300	300	3-D14 2-D12	3-D14	3-D14 2-D12	3-D14	3-D16 3-D14	3-D14	300	300	3-D14 3-D22	3-D14	3-D14 3-D22	3-D14	3-D14 1-D12	3-D14
T10	350	300	3-D16 2-D14	3-D12	4-D16 4-D14	2-D16 2-D14	3-D12 3-D18	4-D16 3-D14	300	300	2-D12 3-D16	3-D12	2-D12 3-D16	3-D12 2-D14	2-D16 2-D12	3-D12 2-D14	300	300	3-D12 3-D24	3-D12	3-D12 3-D24	3-D12 3-D12	3-D12 3-D18	3-D12 3-D12
T11	300	300	3-D16 3-D14	3-D12	3-D16 3-D14	3-D16 2-D14	3-D12 3-D18	2-D16 2-D14	300	300	4-D14 3-D12	3-D12	4-D14 3-D12	3-D12 2-D20	2-D12 2-D14	3-D12 2-D10	300	300	3-D12 3-D25	3-D12	3-D12 3-D25	3-D12 2-D18	3-D12 3-D18	3-D12 2-D18
T12	350	350	4-D16 4-D14	3-D12	5-D16 4-D14	4-D16 3-D14	3-D12 3-D18	5-D16 4-D14	300	300	2-D16 2-D16	3-D12	2-D16 2-D16	3-D12 3-D16	3-D12 3-D12	3-D12 3-D16	300	300	3-D12 4-D22	3-D12	3-D12 4-D22	3-D12 3-D16	3-D12 3-D18	3-D12 3-D16
T13	350	350	3-D14 4-D16	3-D12	4-D14 4-D16	3-D14 3-D16	3-D14 3-D16	2-D14 3-D16	350	350	4-D12 4-D14	3-D14	4-D12 5-D14	3-D14 2-D12	4-D14 4-D16	3-D14 2-D12	350	350	3-D14 3-D25	3-D14	3-D14 3-D20	3-D14 2-D12	3-D14 3-D16	3-D14 2-D12
T14	400	350	5-D16 3-D12	3-D12	8-D16 5-D12	6-D16 4-D12	3-D12 3-D18	5-D16 3-D12	350	300	5-D12 5-D12	3-D12	4-D12 4-D12	3-D12 2-D12	3-D14 3-D14	3-D12 2-D12	300	300	3-D12 3-D24	3-D12	3-D12 3-D24	3-D12 2-D12	3-D12 3-D18	3-D12 2-D12
T15	350	350	3-D12 5-D16	3-D12	4-D12 6-D16	2-D12 3-D16	3-D12 1-D16	3-D12 4-D16	350	350	5-D12 5-D12	3-D12	5-D12 5-D12	3-D12	3-D12 3-D14	3-D12	300	300	3-D12 2-D16	3-D12	3-D12 2-D16	3-D12	3-D12 1-D16	3-D12
T16	400	350	5-D16 5-D16	3-D14	3-D16 3-D16	2-D16 1-D16	3-D12 1-D16	2-D16 1-D16	350	350	4-D12 5-D14	3-D12	3-D12 4-D14	5-D12	5-D12 4-D12	6-D12	300	300	3-D12 3-D16	3-D12	3-D12 3-D16	3-D12	3-D12 1-D16	3-D12
T17	350	350	7-D16 4-D12	3-D12	4-D16 3-D12	5-D16 3-D12	3-D12 1-D12	4-D16 3-D12	350	300	3-D14 3-D14	3-D12	3-D14 3-D14	3-D14	2-D14 3-D14	3-D12 1-D14	350	300	3-D12 4-D16	3-D12	3-D12 4-D16	3-D12	3-D12 1-D12	3-D12
T18	350	350	3-D16 3-D16	3-D12	3-D16 3-D16	3-D16 3-D16	3-D12 2-D16	3-D16 3-D16	350	350	5-D14 4-D12	3-D12	5-D14 4-D12	3-D12 1-D16	4-D14 4-D14	3-D12 1-D16	350	300	3-D12 3-D20	3-D12	3-D12 3-D20	3-D12 1-D16	3-D12 2-D16	3-D12 1-D16
T19	450	300	4-D14 4-D14	3-D14	6-D14 6-D14	3-D14 3-D14	3-D14 1-D12	4-D14 4-D14	450	350	5-D12 6-D14	3-D14	4-D12 6-D14	3-D14 3-D16	6-D14 2-D14	3-D14 2-D16	400	300	3-D14 3-D20	3-D14	3-D14 3-D20	3-D14 2-D16	3-D14 1-D12	3-D14 2-D16
T20	400	350	5-D14 6-D16	3-D14	4-D14 4-D16	3-D14 4-D16	3-D12 1-D16	2-D14 5-D16	400	350	4-D14 4-D14	3-D12	4-D14 4-D14	3-D14 3-D12	3-D12 3-D12	6-D12	300	300	3-D12 2-D25	3-D12	3-D12 2-D25	3-D12 1-D16	3-D12 1-D16	3-D12 1-D16
T21	450	350	5-D14 3-D16	2-D16	5-D14 3-D14	3-D14 7-D14	2-D16 3-D14	5-D14 5-D14	400	300	5-D14 4-D12	2-D16	5-D14 4-D12	2-D16 2-D14	5-D12 5-D12	2-D16 2-D14	350	300	2-D16 2-D22	2-D16	2-D16 2-D22	2-D16 3-D14	2-D16 3-D14	2-D16 3-D14
T22	500	400	5-D14 1-D16	3-D20	5-D14 1-D16	5-D14 2-D14	3-D20	5-D14 5-D14	500	350	4-D16 4-D16	2-D20	4-D16 4-D16	3-D14 2-D12	5-D12 1-D12	2-D20	450	300	2-D20	2-D20	2-D20	2-D20	2-D20	2-D20
T23	300	300	3-D16 3-D14	3-D12	3-D16 3-D14	2-D16 2-D14	3-D12 2-D24	2-D16 2-D14	300	300	2-D14 3-D16	3-D12	2-D14 3-D16	3-D12	2-D12 3-D14	3-D12	300	300	3-D12 4-D20	3-D12	3-D12 4-D20	3-D12	3-D12 2-D24	3-D12
T24	350	300	4-D12 5-D14	3-D12	4-D12 5-D14	3-D12 3-D14	3-D12 2-D24	3-D12 4-D14	300	300	3-D12 3-D14	3-D12	3-D12 3-D14	3-D12 1-D16	3-D12 2-D14	3-D12 2-D16	300	300	3-D12 3-D25	3-D12	3-D12 3-D25	3-D12 3-D14	3-D12 2-D24	3-D12 3-D14
T25	450	350	6-D16 4-D12	3-D14	8-D16 5-D12	8-D16 5-D12	3-D12 2-D24	7-D16 5-D12	400	300	5-D16 3-D12	3-D12	4-D16 3-D12	3-D12 2-D20	4-D12 3-D14	3-D12 2-D20	300	300	3-D12 5-D20	3-D12	3-D12 5-D20	3-D12 2-D20	3-D12 2-D24	3-D12 2-D20
T26	350	350	6-D12 3-D14	3-D12	5-D12 3-D14	3-D12 4-D14	3-D12 2-D24	5-D12 7-D14	300	300	2-D12 3-D16	3-D12	2-D12 3-D16	3-D12 2-D20	2-D14 2-D14	3-D12 2-D20	300	300	3-D12 5-D20	3-D12	3-D12 4-D20	3-D12 2-D20	3-D12 2-D24	3-D12 2-D20
T27	350	350	6-D16 5-D14	3-D12	4-D16 4-D14	3-D16 2-D14	3-D12 2-D24	4-D16 3-D14	350	350	4-D16 3-D12	3-D12	4-D16 3-D12	3-D12 2-D20	3-D12 4-D16	3-D12 2-D20	300	300	3-D12 5-D20	3-D12	3-D12 5-D20	3-D12 2-D20	3-D12 2-D24	3-D12 2-D20
T28	400	350	6-D12 6-D12	3-D14	7-D12 7-D12	7-D12 7-D12	3-D12 2-D20	7-D12 7-D12	350	300	4-D16 3-D12	3-D12	3-D16 2-D12	3-D12 2-D16	3-D12 3-D14	3-D12 2-D16	300	300	3-D12 3-D20	3-D12	3-D12 3-D20	3-D12 2-D16	3-D12 2-D20	3-D12 2-D16
T29	350	350		4-D16			4-D16		350	350		3D-14			4D-14		300	350		2D-14			4D-14	

T30	350	350	4-D16	3-D16	350	350	4D-16	3D-16	300	350	2D-20	2D-20
T31	350	350	4-D20	4-D20	350	350	4D-20	4D-20	300	350	2D-25	2D-25
T32	350	350	4-D20	4-D20	350	350	3D-25	2D-25	300	350	3D-25	2D-25
T33	350	400	3-D20	4-D20	350	350	2D-25	2D-25	300	350	2D-25	2D-25
T34	400	400	5-D16	5-D16	350	400	3D-16	3D-16	350	400	3D-16	3D-16
T35	400	400	3-D20	5-D20	350	400	4D-16	4D-16	400	400	2D-16	6D-16
T36	350	400	5-D20	3-D20	350	350	4D-20	3D-20	300	300	4D-20	2D-20
T37	350	400	3-D20	5-D20	350	350	2D-20	2D-20	300	300	2D-20	2D-20
T38	400	400	4-D20	4-D20	400	400	3D-16	5D-16	400	300	2D-16	6D-16
T39	450	400	5-D16	4-D20	450	400	2D-20	4D-20	450	300	2D-16	6D-16
T40	450	400	4-D25	4-D25	450	400	2D-25	2D-25	450	350	2D-25	2D-25
T41	450	450	4-D25	5-D25	450	450	3D-25	3D-25	450	400	2D-25	2D-25
T42	500	500	6-D25	4-D25	500	500	5D-25	5D-25	450	400	2D-25	6D-25

Electronic Journal of Structural Engineering

Original Article

Cite this: DOI:10.56748/ejse.233942

Received Date: 7 December 2022
Accepted Date: 22 February 2023

1443-9255
https://ejsei.com/ejse

Compression and Bond Properties of Fired Clay Brick Masonry with Cocopeat Blended Binding Mortar

Madhuranya Muralitharan [a] and Navaratnarajah Sathiparan [a]
[a] University of Jaffna, Sri Lanka
* Corresponding Author: sakthi@eng.jfn.ac.lk

Abstract

The production of agricultural, industrial, and demolition trash increases along with global population growth and industrial expansion. They endanger the environment when they are not properly recycled, repurposed, or disposed of. Cocopeat is one such agricultural waste. The use of cocopeat in binder cement is urged to support sustainable construction methods. Because it is seen as trash and discarded in landfills. Cocopeat is an environmentally friendly by-product which can be got during the coconut fibre extraction process. The current study investigates the strength properties of masonry built with binding mortar that incorporates cocopeat as opposed to traditional cement-sand mortar. The mortar prepared with four different integrations of cocopeat as sand replacement of 0, 4, 6 and 8% by weight was used for masonry. Fresh properties of cocopeat binding mortar and their effect on the mechanical characteristics of masonry were investigated. The test results revealed that the mechanical characteristics of masonry were enhanced with increased cocopeat content in the mortar.

Keywords

Masonry, Cocopeat, Binding mortar, Sustainability

1. Introduction

The production of agricultural, industrial, and demolition waste increases along with global population growth and industrial expansion. They endanger the environment when they are not properly recycled, reused, or disposed of. Since cocopeat is a byproduct of the extraction of coconut fiber, it is frequently regarded as waste and disposed of in landfills. Typically, coco husk pieces, coir, and cocopeat are produced when fiber is extracted from coco husk. Although coco husk pieces and coco coir may be utilized to make a variety of goods with added value as shown in Figure 1, coco peat is only employed as a plant-growing medium and the majority of it is disposed of or mixed with nearby water sources. By contaminating the water and the air, these acts put the environment at hazard (Erdogmus 2015).

Cementitious composite materials, such as mortar, are being used more frequently for a variety of construction activities, including masonry blocks, wall finishes, binding mortar, and more. To increase cementitious composite material's ability to provide improved efficiency in construction, there is a growing need for their utilization. Microcracks start to show up along planes that suffer tensile stresses when mortar is subjected to different types of loading. Applying additional loads causes cracks to expand out of control (Chandramouli et al. 2010).

Most of the masonry failure is initiated by the binding mortar itself or the intersection between brick and binding mortar. A good bond between brick and binding mortar has a significant effect on the mechanical characteristic of the masonry wall. This is influenced by many factors such as moisture content, initial water absorption rate, the surface roughness of brick unit and sand grading, composition, consistency, and water retention capacity of the binding mortar. So, improving the performance of binding mortar is one of the optimum ways to im-prove the strength of masonry structures. Generally, by incorporating by industrial waste or fibres are used to improve the performance of binding mortar (Sundaralingam et al. 2021, Thanushan & Sathiparan 2022). Fibers in the mortar mixture serve to counter-act the hydraulic shrinkage, preventing the development of cracks and fissures on the surface of the plaster that has been applied. Also, it was improving the direct tensile strength of the mortar as well as due to roughness, it was improving the bond be-tween the masonry unit and the binding mortar.

Although coconut coir has been continually utilized in cementitious composites such as concrete (Ali et al. 2022), cement mortar (Sathiparan et al. 2017), stabilized earth blocks (Thanushan et al. 2019), surface plaster (Sathiparan & Rupasinghe 2019), etc., the use of cocopeat in cementitious materials is very limited. Priyadarshini et al. (2021) investigate the strength of concrete featuring cocopeat as a partial replacement for sand. Results show that treated cocopeat improved the compressive strength and bonding characteristic of concrete. The strength and durability properties of cement mortar including cocopeat as a substitute for river sand were evaluated by Sathiparan et al. (2022). The findings demonstrated that adding up to 4% of cocopeat content to cement-sand mortar enhances its physical and mechanical characteristics without negatively affecting crucial durability factors. Furthermore, both studies show that using cocopeat as raw materials in construction materials reduces the usage of river sand, so it is a cost-effective and sustainable option. Although these studies show that cocopeat is one sustainable option to reduce sand consumption and value added to cocopeat, still the usage of cocopeat in binding mortar for masonry is one of the areas to explore.

The emphasis of the present study is to investigate the effects of cocopeat-incorporated binding mortar on the mechanical properties of masonry. For that fresh mortar properties, characteristics of hardened binding mortar, and strength characteristics of masonry were investigated through an experimental program.

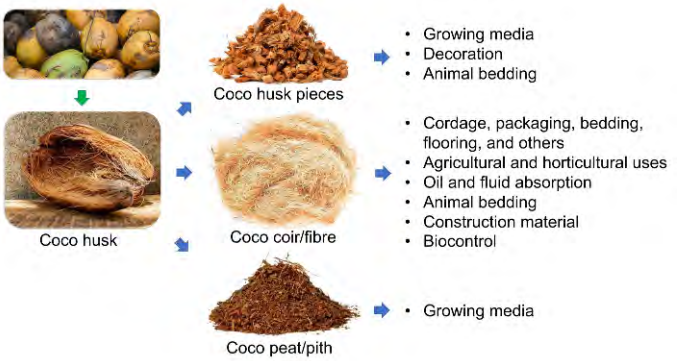

Fig 1. Derivation of by-products of the Coconut extraction process and its commercial use

2. Methodology

2.1 Materials used

The details about raw materials used for the present experimental program are described below.

- Cement: In this investigation, OPC (Ordinary Portland cement) was used as a binder. OPC was found to have a bulk density of 1,280 kg/m3 and a specific gravity of 3.15.
- Fine aggregate: The river sand had a bulk density and specific gravity of 1,680 kg/m3 and 2.41, respectively. Figure 2a displays the grain size distributions of river sand. According to the grain size distribution, fine aggregate contains 3.8% gravel, 95.6% sand, silt, and

0.6% clay particles, respectively. The uniformity coefficient (Cu), gradation coefficient (Cc) and fineness of fine aggregates were found to be 4.01, 1.10 and 2.89, respectively. Accordingly, according to the unified soil classification system, the fine aggregate may be classified as SP - Poorly graded Sand (SP).

- Cocopeat: The cocopeat was gathered from a coconut coir extraction facility. Cocopeat has a bulk density of 306 kg/m3 and a specific gravity of 1.34, respectively. It is less dense than river sand and can be utilized as a lightweight material. Additionally, a cocopeat with a higher water retention capacity helps shorten the curing process (Shenbaga kumar et al. 2019). To define the particle size distribution for husk particles, a sieve ex-amination was conducted. The particle size distribution of cocopeat is represented in Figure 2a. By weight, the cocopeat is made up of around 60% fiber and 40% tiny husk fragments. The average particle size of the cocopeat was approximately 0.78 mm. Figure 2b illustrates the discrepancy of the frequency with the length of the cocopeat, and Figure 2c shows the discrepancy of the frequency with the diameter of the cocopeat. The fiber found in cocopeat had an average length and diameter of 16.7 mm and 20.2 µm, respectively.
- Brick: Bricks with the dimension of 200×85×60 mm3, which are available in the local market were used. The bricks had a compressive strength of 5.88 MPa and a water absorption rate of 8.3%.

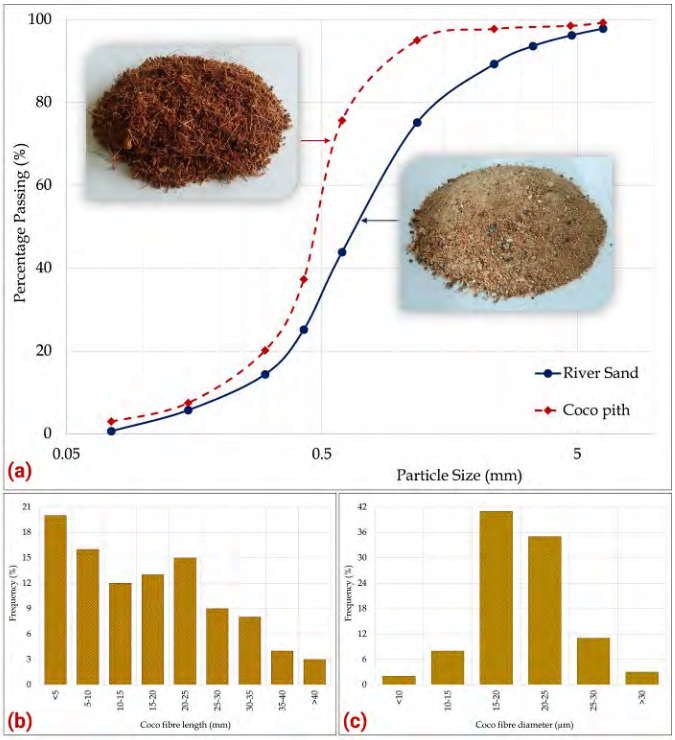

Fig 2. (a) Particle size distribution of cocopeat and river sand, (b) variation of frequency percentage of cocopeat length, and (c) variation of frequency percentage with cocopeat diameter

2.2 Mix design

The objective of this research was to establish whether cocopeat could be used to binding mortar, and it was decided that the mix proportion used on local construction sites was appropriate. As a result, 1:6 by volume of cement to fine aggregates was used to produce mortar. As previously noted, four ratios of cocopeat to cement: 0, 4, 6, and 8% by weight were set. It is not acceptable to replace river sand with cocopeat by weight because cocopeat has a density that is considerably lower than that of river sand. It was so chosen to substitute an equal volume of solid for it. Since the amount of cocopeat in the mix was already determined by the ratio of cocopeat to cement, river sand volume was lowered from the dry mix to make room for the cocopeat.

The quantity of raw materials utilized in each mortar mixture is listed in Table 1. Water requirement was greater for cocopeat due to its hydrophilic nature. The required amount of water needed was decided according to the predetermined slump value of 25-35mm. With the addition of cocopeat to the binding mortar, the amount of required water was increased for the fixed slump.

Table 1. Mix proportion used for binding mortar (for one m^3)

Mix ID	Cocopeat/Cement (%)	Cement (kg)	Sand (kg)	Cocopeat (kg)	Water (l)
C0	0	208.8	1780.0	0.0	281.9
C4	4	208.8	1766.0	8.4	292.3
C6	6	208.8	1758.5	12.5	302.8
C8	8	208.8	1751.0	16.7	313.2

3. Testing

To carry out tests for masonry six masonry prisms, eight masonry triplets, and 8 couplets were prepared to conduct compressive, shear and bond tests respectively as shown in Figure 3. Bricks with the dimension of 200×85×55 mm^3 were used in specimen preparation with the 10mm mortar joint.

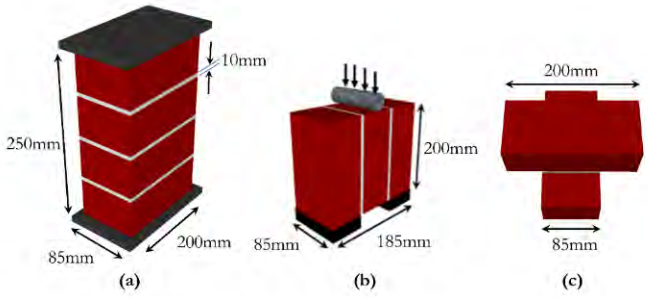

Fig 3. Outline of specimens used for testing; (a) compression test, (b) shear test and (c) bond test

Test on Fresh Mortar

For fresh mortar, slump, slump flow, initial setting time, final setting time and moisture retention capacity were measured. Slump and setting time were measured following ASTM C143 (2020) and ASTM C403 (2016), respectively.

To check the water retention characteristics of fresh mortar, a drying test was done according to CSN EN 16322 (2013). The fresh mortar was filled in the aluminium cylinder (100 mm diameter and 25 mm height) and it was kept in the laboratory environment (humidity of 80% and temperature of 30 °C) to dry out. The weight of the specimen was measured at certain time intervals. The moisture content per unit area at a particular time was given by the function of the mass of the mortar with container after a certain time (mt) and mass of dry mortar with container (md) and area of the aluminium cylinder (A) as Eq. (1).

$$Moisture\ content\ (\%) = (mt - md) \times 100/md \quad (1)$$

The gradient of the preliminary linear section of the moisture content vs. time is defined as the initial drying rate (D1, expressed in %/h). The gradient of the linear section of the moisture content vs. the square root of time is defined as the second phase drying rate (D2, expressed as %/h$^{0.5}$) (Sundaralingam et al. 2022).

Test on Brick and Binding Mortar

Bricks with the dimension of 200×85×55 mm^3 were used to conduct tests on bricks and to carry out tests on mortar 100×100×100 mm^3 cubes, and 200×100×60mm^3 beams were prepared. Compression test flexural tests were done for brick and binding mortar respectively according to ASTM C109 (2020) and ASTM C348 (2020).

Tests on Masonry

A compressive strength test was carried out for masonry prisms made up of 4 blocks and 3 joints of mortar as shown in Figure 3a, according to BS EN 1052-1 (1999). For each composition, the test was performed for six specimens. Spec-miens were cured for 28 days.

The direct shear test is used to test the shear strength of prepared masonry according to BS EN 1052-3 (2002). Eq. (2) was used to calculate the shear strength of the specimens.

$$Shear\ strength = (S + W)/2A \quad (2)$$

Here, S is the maximum shear load, A is the failure surface area and W is the weight of a brick.

Brick couplets cast following ASTM C952 (2012) were used to assess the bond strength. Couplets with distinct mortar designations were manufactured as crosses while maintaining a 10 mm binding mortar thickness and the couplet was created as illustrated in Figure 3c. Specimens were examined on the universal testing machine with a displacement

control method with a loading rate of 0.3 mm/min. The failure load and bond area were used to determine the couplet's bond strength. Using Eq. (3), the bonding strength was determined.

$$Bond\ strength\ =\ (B + Wc + W)/A \quad (3)$$

Here, B is the maximum load before bond failure, A is the area of the brick-mortar contact surface, W is the weight of a brick and Wc is the weight of the cap.

4. Results and discussion

4.1 Fresh mortar properties

To find the influence of cocopeat on fresh mortar characteristics, the slump is one of the indicators. Water was added gradually to find the suitable mix design by increasing the w/c ratio by 0.5. Variations of w/c ratio and corresponding slump values for the mixes are presented in Figure 4, which presents the clear identification about, the addition of cocopeat to the mortar, reduced the workability of the mortar mix. During the experiment, when adding cocopeat to the mix the mortar enhanced stiffer. Therefore, the workability of the mortar mix was reduced. These results were similar to the results found by Wongsa et al. (2020) when using coconut and sisal fibre with geo polymers mortar. Rough surfaces, porous structures and irregular stripes of fibre are the reason for the decrease in workability (Lertwattanaruk & Suntijitto 2015). In the present study, water to cement ratio was selected by fixing the slump value as 30±5mm. To achieve that slump, the water-cement ratio requirement was 1.35, 1.40, 1.45 and 1.50 for 0, 4, 6 and 8% cocopeat blended mortar, respectively.

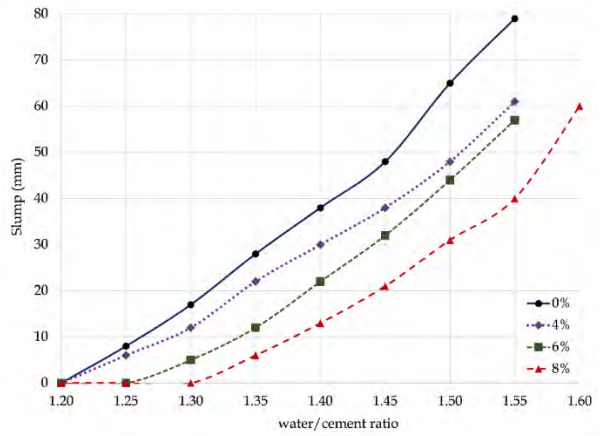

Fig 4. Variation of slump along with water/cement ratio for various mortar mix

Figure 5 depicts the variation of initial and final setting times with the addition of cocopeat to the binding mortar. Fresh mortar can be longer workable with the longer setting time. As per the result, both the initial and the final setting time was increased when adding cocopeat to the mortar, which facilitates the workability of the biding mortar.

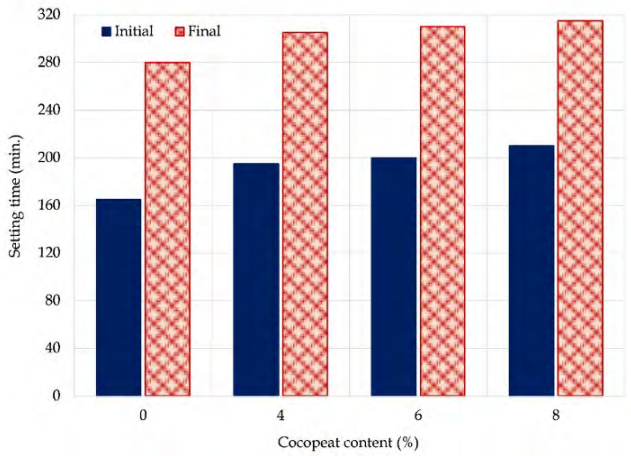

Fig 5. (a) Variation of fresh mortar density for various mortar mix; (b) Initial and final setting time of the various mortar mix

Figure 6 depicts the moisture content variation of mortar with a square root of time. Initial moisture content was observed to be 11.9, 12.1, 12.3 and 12.4% for 0, 4, 6 and 8% cocopeat blended mortar, respectively. It clearly shows that when adding cocopeat to the binding mortar, it keeps the water more. It is necessary to know about the variation of the water retention capacity of mortar with the cocopeat content, as it affects the hydration of cement and the workability of binding mortar.

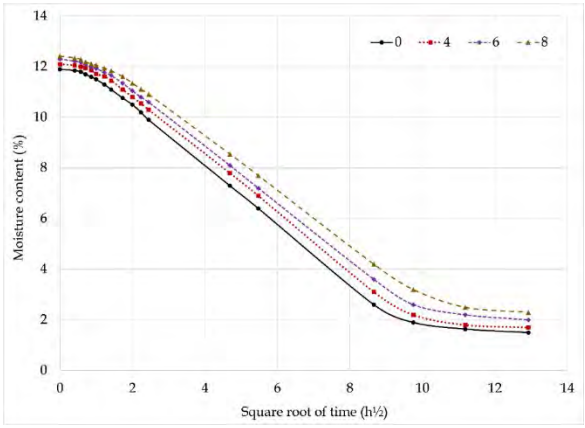

Fig 6. Moisture content variation with elapsed time

The results revealed that the initial evaporation rate reduced with cocopeat in the mortar mix. The initial evaporation rate was 0.40, 0.39, 0.37 and 0.35 % per hour for 0, 4, 6 and 8% cocopeat blended mortar, respectively. A similar trend was witnessed for the second stage as the secondary evaporation rate was 1.18, 1.16, 1.12 and 1.1 %/$h^{0.5}$ for 0, 4, 6 and 8% cocopeat blended mortar, respectively. These results revealed that the incorporation of cocopeat in the fresh mortar improves the water retention capacity.

4.2 Properties of hardened mortar

Table 2 summarizes the density, water absorption rate, compressive strength and flexural strength of brick and binding mortar with different cocopeat content. For all the binding mortar types, the compressive strength of the binding mortar was lesser than brick. But flexural strength of mortars with cocopeat showed higher flexural strength than brick.

The supplement of cocopeat to the mortar affects compressive strength both favorably and unfavorably. On the plus side, the cocopeat's fiber content offers increased tensile strength, which prevents mortar from breaking (Leppänen 2006, Hamidi & Koohdaragh 2011). Thus, improving the mortar's compressive strength as a result. On the other hand, a lower compressive strength was caused by the in-creased porosity that was present in the cocopeat blended mortar (Zhao et al. 2014). When com-pared to the control mortar, the compressive strength of the mortar was raised by 8% when 4% cocopeat was added to it. But cocopeat concentration increased more, and compressive strength declined. Strength decreased by 3 and 25%, for cocopeat contents of 6 and 8%, respectively. The existence of cocopeat in mortar appeared to harm wet compressive strength since there was a drop in compressive strength for the wet condition with a rise in cocopeat content.

When 4% cocopeat was replaced with mortar, the flexural tensile strength increased, but as the cocopeat percentage increased, the strength began to decline. Even when using mortar with an 8% cocopeat content, the flexural tensile strength was higher than that of the control mortar. The connections that the fibers create across the cracks may be responsible for the increase in flexural strength. The force applied to the mortar must be greater than the stress necessary to separate the cement gel-aggregate connection and the friction bond between the fiber and mortar matrix for failure to occur (Donkor & Obonyo 2016). As a result, fibers provide a greater load-bearing capability. Strength decreased after a key threshold (4% cocopeat concentration) because cocopeat is soft and the mortar matrix has more pores.

Table 2. Characteristics of binding mortar with the addition of cocopeat

Properties	Unit (%)	Brick	Mortar			
			0%	4%	6%	8%
Density	kg/m^3	1680	2043	1989	1910	1879
Water absorption rate	kg/m^3	138	196	205	242	255
Dry compressive strength	MPa	5.88	3.94	4.27	3.82	2.94
Wet compressive strength	MPa	4.98	2.79	2.80	2.53	1.77
Flexural strength	MPa	1.75	1.55	2.25	2.09	1.84

4.3 Effect of cocopeat reinforced mortar on mechanical properties of masonry

Compression strength

Figure 7a illustrates the typical compressive failure types of masonry prisms. There is a vertical tensile spitting failure that occurred along the axial loading direction. The crack originated from mortar and it spread through brick.

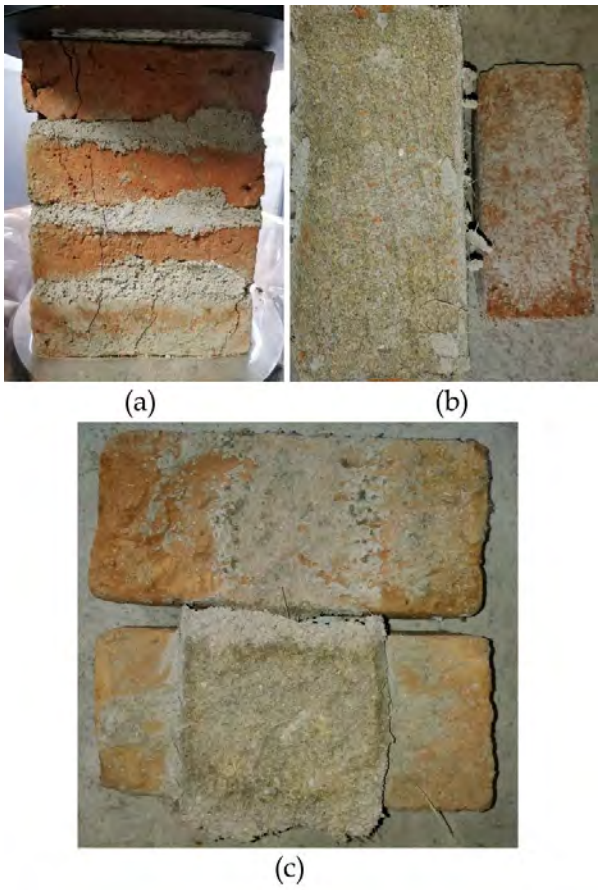

Fig 7. Typical failure modes of masonry prisms under (a) Compression strength; (b) Shear strength; (c) Bond strength

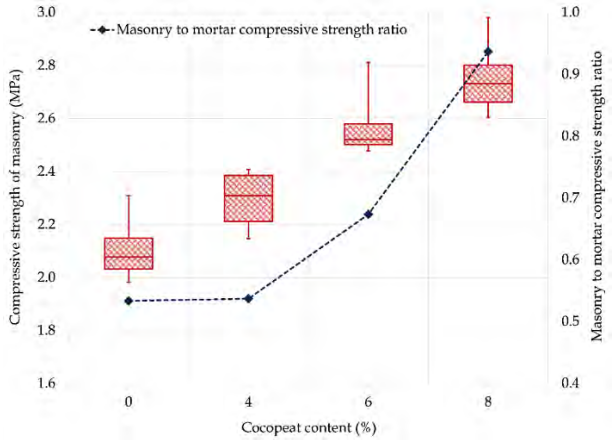

Fig 8. Variation of compressive strength with different binding mortar

Figure 8 illustrates the compressive strength variation of masonry prisms among various types of binding mortar. Results indicated that an increase in the replacement of cocopeat contributed to the higher compressive strength of masonry. Compared with control mortar, the rise in compressive strength was 8.9, 22.1 and 30.7%, respectively for masonry prism with 4, 6 and 8% cocopeat incorporated mortar. The compressive strength of the mortar itself and rough interface surface due to the irregular shape and texture of the cocopeat may attribute to improvement in the overall compressive strength of the masonry. When comparing the masonry strength to mortar strength ratio, the increase rate proportionally increases with mortar strength. The ratio is equal to 0.53, 0.54, 0.67 and 0.94 for 0, 4, 6 and 8% cocopeat blended mortar, respectively.

Shear strength

Figure 7b presents the failure pattern of the interface surface of the masonry triplet observed in shear tests. All the specimens were failing along the interface between brick and mortar. This mainly occurred when bond strength amongst brick and mortar was lesser than the tensile splitting strength of brick and mortar.

Figure 9 illustrates the shear strength variation of masonry triplets with a different type of binding mortar. When stronger brick and weaker mortar are used in masonry, the shear strength depends on mortar strength itself, the water absorption characteristic of the brick and the water retention characteristic of the mortar.

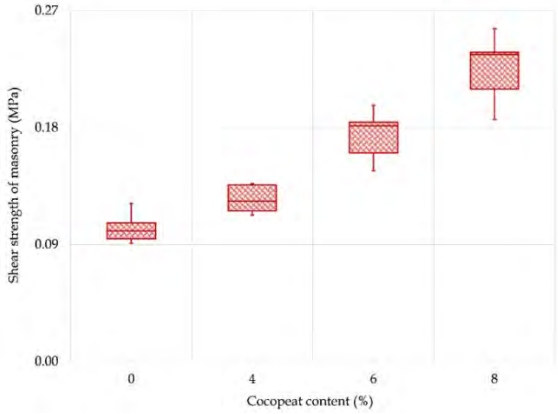

Fig 9. Variation of shear strength with different binding mortar

Since mortars are often spread over absorptive fired-clay bricks, the water retention capability of the fresh mix is very important (Sébaïbi et al. 2003). Namely, these materials readily absorb mixed water from the mortar and this may lead to irregular hardening. In this case, designed properties of the mortar are not achieved. Only by retaining enough water, mortar can preserve adequate plasticity and reach designed properties. Since cocopeat incorporated mortar can absorb more water at the fresh stage, which might be released back to when desiccation occurs and thus affect positively the hydration process of the mortar. It makes a better bond between brick and mortar. In the present study, the same type of bricks was used, therefore shear strength improves with cocopeat quantity. Compared with control mortar, the increase in compressive strength was 22.7, 69.9 and 118.1% for masonry triplet with 4, 6 and 8% cocopeat incorporated mortar, respectively.

Bond strength

All the masonry couplets failed in the brick-mortar interface during the bond test as shown in Figure 7c. This kind of failure happens due to the weak bond strength of the brick-mortar interface compared to the tensile strength of brick-and-mortar.

Figure 10 presents the bond strength variation with masonry cross-couplets with different binding mortar. Similar to shear strength, bond strength also increased with cocopeat content in the mortar. Compared with control mortar, the increase in compressive strength was 24.9, 47.9 and 89.1%, respectively for masonry triplet with 4, 6 and 8% cocopeat incorporated mortar.

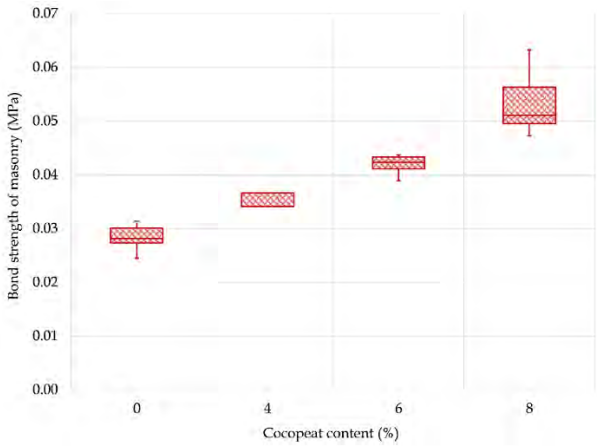

Fig 10. Variation of bond strength with the different binding mortar mix

Relationship between properties

Figure 11 illustrates the relationship between the shear and bond strength of masonry and with compressive strength of masonry. From the research, we have obtained a linear graph for the relationship. The below equations are derived from the test results which give the relationship of characteristic shear strength with characteristic compressive strength as Eq. (4) and characteristic bond strength with characteristic compressive strength as Eq. (5) respectively.

$$fvm = 0.1641fcm - 0.2353 \quad (4)$$

$$fbm = 0.0314fcm - 0.0346 \quad (5)$$

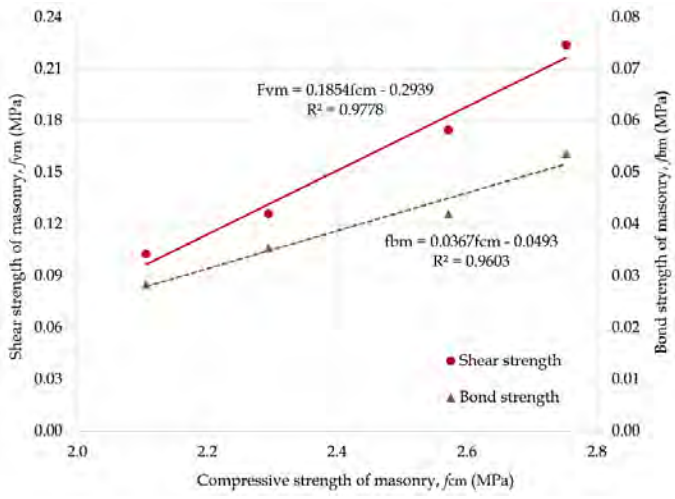

Fig 11. The relationship between characteristic shear, bond and compressive strength of the masonry.

5. Conclusion

The compressive, shear and bond strength of the brick masonry with cocopeat-incorporated binding mortar was studied. The following conclusions are drawn from the current study:

- For mortar mixes including cocopeat, a higher quantity of water is required to obtain the desired slump. However, for a specific slump, adding cocopeat to binding mortar while still fresh demonstrated increased water retention capacity and setting times.
- Mortar containing 4% cocopeat exhibits better compressive and flexural strength after being hardened.
- The compressive, shear, and bond strengths of masonry were increased with binding mortar incorporating greater cocopeat content. Shear, bond, and compressive strength of the brickwork were generally noted to be the sequence in which the influence of cocopeat integrated mortar on masonry strength was noticed.

These findings suggest that cocopeat may be effectively used to create more environmentally friendly binding mortar for masonry. The use of cocopeat as a masonry binder mortar lowers the need for river sand and the environmental damage brought on by the disposal of groundnut shell waste.

References

Ali, B., Hawreen, A., Ben Kahla, N., Talha Amir, M., Azab, M., and Raza, A., "A critical review on the utilization of coir (coconut fiber) in cementitious materials", *Construction and Building Materials*, Vol. 351, 2022, ID 128957.

ASTM-C109, 2020. Standard test method for compressive strength of hydraulic cement mortars (using 2-in. or [50-mm] cube specimens). ASTM International, West Conshohocken, PA.

ASTM-C143/C143M, 2020. Standard test method for slump of hydraulic-cement concrete. ASTM International, West Conshohocken, PA.

ASTM-C348, 2020. Standard test method for flexural strength of hydraulic-cement mortars. ASTM International, West Conshohocken, PA.

ASTM-C403/C403M, 2016. Standard test method for time of setting of concrete mixtures by penetration resistance. ASTM International, West Conshohocken, PA.

ASTM-C952, 2012. Standard test method for bond strength of mortar to masonry units (withdrawn 2018). ASTM International, West Conshohocken, PA.

BS-EN-1052-1, 1999. Methods of test for masonry. Determination of compressive strength. British Standards Institution (BSI), London.

BS-EN-1052-3, 2002. Methods of test for masonry. Determination of initial shear strength. British Standards Institution (BSI), London.

Chandramouli, K., Rao, P.S., Pannirselvam, N., Sekhar, T.V.S., and Sravana, P., "Strength properties of glass fibre concrete", *ARPN Journal of Engineering and Applied Sciences,* Vol. 5, No. 4, 2010, pp. 1-6.

CSN-EN-16322, 2013. Conservation of Cultural Heritage - Test methods - Determination of drying properties. British Standards Institution (BSI), London.

Donkor, P., and Obonyo, E., "Compressed soil blocks: Influence of fibers on flexural properties and failure mechanism", *Construction and Building Materials,* Vol. 121, 2016, pp 25-33.

Erdogmus, E., "Use of fiber-reinforced cements in masonry construction and structural rehabilitation", *Fibers*, 2015, Vol. 3, No. 1, pp. 41-63.

Hamidi, B., and Koohdaragh, M., "Effect of application of microsilis, steel fibers and different type bars and aggregate size on concrete compressive force", *Australian Journal of Basic and Applied Sciences,* 2011, Vol. 5, No. 12, pp 2600-2605.

Leppänen, J., "Concrete subjected to projectile and fragment impacts: Modelling of crack softening and strain rate dependency in tension", *International Journal of Impact Engineering*, 2005, Vol. 32, No. 11, pp 1828-1841.

Lertwattanaruk, P., and Suntijitto, A., "Properties of natural fiber cement materials containing coconut coir and oil palm fibers for residential building applications", *Construction and Building Materials*, 2015, Vol. 94, pp 664-669.

Priyadarshini, V., Felixkala, T., Depaa, R.A.B., Hemamalinie, A., Francis Xavier, J., Surendra Babu, K., and Jeya Arthi, A.J., "Experimental investigation on properties of coir pith and its influence as partial replacement of fine aggregate in concrete", *Materials Today: Proceedings*, 2021, Vol. 45, pp 6903-6906.

Sathiparan, N., Anburuvel, A., Muralitharan, M., and Isura Kothalawala, D.A., "Sustainable use of coco pith in cement-sand mortar for masonry block production: Mechanical characteristics, durability and environmental benefit", *Journal of Cleaner Production*, 2022, Vol. 360, ID 132243.

Sathiparan, N., and Rupasinghe, M.N., "Mechanical behavior of masonry strengthened with coir fiber reinforced hydraulic cement mortar as surface plaster", *Journal of Structural Engineering & Applied Mechanics*, 2019, Vol. 2, No. 1, pp 12-24.

Sathiparan, N., Rupasinghe, M.N., and Pavithra, B., "Performance of coconut coir reinforced hydraulic cement mortar for surface plastering application", *Construction and Building Materials, 2017*, Vol. 142, pp 23-30.

Sébaïbi, Y., Dheilly, R.M., and Quéneudec, M., "Study of the water-retention capacity of a lime–sand mortar: Influence of the physicochemical characteristics of the lime", *Cement and Concrete Research*, 2003, Vol. 33, No. 5, pp 689-696.

Shenbaga kumar, V., Udhaya kumar, K., Ramesh, R., Ram kumar, R., and Venkateshwari, N., "An experimental study on behaviour of concrete with coco-peat", *International Research Journal of Engineering and Technology*, 2019, Vol. 6, No. 3, pp 2452-2457.

Sundaralingam, K., Peiris, A., Anburuvel, A., and Sathiparan, N., "Quarry dust as river sand replacement in cement masonry blocks: Effect on mechanical and durability characteristics", *Materialia*, 2022, Vol. 21, ID 101324.

Sundaralingam, K., Peiris, A., and Sathiparan, N., "Manufactured sand as river sand replacement for masonry binding mortar", *2021 Moratuwa Engineering Research Conference (MERCon)*, 2021, pp. 403-408.

Thanushan, K., and Sathiparan, N., "Mechanical performance and durability of banana fibre and coconut coir reinforced cement stabilized soil blocks", *Materialia*, 2022, Vol. 21, ID 101309.

Thanushan, K., Yogananth, Y., Sangeeth, P., Coonghe, J.G., and Sathiparan, N., "Strength and durability characteristics of coconut fibre reinforced earth cement blocks", *Journal of Natural Fibers*, 2021, Vol. 18, No. 6, pp 773-788.

Wongsa, A., Kunthawatwong, R., Naenudon, S., Sata, V., and Chindaprasirt, P., "Natural fiber reinforced high calcium fly ash geopolymer mortar", *Construction and Building Materials*, 2020, Vol. 241, ID 118143.

Zhao, H., Xiao, Q., Huang, D., and Zhang, S., "Influence of pore structure on compressive strength of cement mortar", *The Scientific World Journal*, 2014, ID 247058.

Electronic Journal of Structural Engineering

Original Article

Cite this: DOI:10.56748/ejse.234022

Received Date: 19 December 2022
Accepted Date: 03 March 2023

1443-9255
https://ejsei.com/ejse

System of Integrated Management Platform for Smart Park： Design and Project Case

Jianwen Zhang [a]*, Jingchao Zhang [b] , Lu yang [a] , Ang Li [a] and Yan Zong [a]
[a] College of Civil Engineering, Henan University of Engineering, Zhengzhou, China
[b] Chinese Sixth Design and Research Institute of Machinery Industry Company Limited, Zhengzhou, China
*Corresponding author: 511017988@qq.com

Abstract

With the continuous development and transformation of 5G, big data, the Internet of Things and other technologies, data sharing and information processing means are becoming more efficient, making smart parks a reality. There are some problems such as unclear design dimensions, poor interactivity of subsystems and high expansion costs in the development of smart park. In the face of these problems, an application-oriented comprehensive management platform system of intelligent park is designed. It is built on a digital twin software-defined campus which is scalability and flexibility with wisdom in the cloud and application at the end as the core service concept. The overall system architecture and management platform module composition are introduced in which the software defined network (SDN) technology is used to separate the control plane and da-ta plane and the four dimensions of people, things, affairs and space are digitalization in the smart Park. One application carries a variety of park services such as production, official business handling, property administration and so on to realize the effective application of the underlying network facilities. The project of high-tech information intelligent park of the Chinese Sixth Design and Research Institute of Machinery Industry Company Limited has been implemented. As an engineering case the platform system can provide personalized design for the park and carry out multi-professional and multi-terminal integrated management, application and display so as to improve the intelligent management level and the service experience to create greater economic and social value.

Keywords

Smart Park; Internet of Things; Integration Management; Digital Twin; Software Defined Network

1. INTRODUCTION

The development of smart parks has experienced the process from large-scale industrial parks, high-tech parks, high-tech and capital-intensive parks to smart parks. With the development of the Internet of Things (IOT), artificial intelligence, 5G technology and the arrival of the industry 4.0 era, the research and establishment of smart cities and smart parks are increasing and bringing great convenience and benefits to human society (Chen, 2022; Bokolo, 2021; Kahkashan, 2022). Smart Park is the guide and demonstration of smart city that integrates the new generation of information and communication technology and has the ability of rapid information collection, high-speed information transmission, highly centralized computing, intelligent transaction processing and omnipresent service provision. Timely perception, transmission and processing of information as well as interaction within the park can improve the industrial agglomeration ability of the park and the economic competitiveness of enterprises and drive the development of related industrial chains in the smart city (He and Liu et al, 2021; Guo and Wang et al. 2015; Emir and Ejub et al, 2020; Amir and Mohammad et al, 2022).

Park economy has gradually become an important part of regional economy that has been developing continuously. The smart park faces the following difficulties in the process of construction (Chen, 2015; Nicos and Christina et al, 2022): (1) The dimensions of the design system are not clear; (2) The linkage between the internal subsystems is poor, and the degree of intelligence is not high; (3) High expansion costs and high management costs. In order to solve the above problems and establish a safe, sophisticated and efficient intelligent park, it is necessary to design a comprehensive management system platform assembling integrated office, life services, energy consumption supervision, emergency command and management decision-making (Ari and Pekka, 2014). This platform can realize one application to carry a variety of park services promoting the development of intelligent parks, and improving the park's operation, service and management capabilities (Liu, 2017; Zhang and Wang et al, 2021).

2. SMART PARK CONSTRUCTION OBJECTIVE

The traditional physical devices such as firewalls and switches are used to deploy a complete IT (internet technology) system platform in smart park, and virtual private network (VPN) are used to realize the effective link and communication between branches. However, laying the IT system platform requires a large amount of investment, professionals and time, resulting in excessive costs and affecting the capital turnover. With the development of advanced information technology and virtual reality technology, the software defined network (SDN) can be used to realize information reconstruction (Peng, 2022), which can solve the problems in the construction process of traditional smart park. SDN technology can effectively separate the control plane from the data plane, and centrally control the network state by using advanced information technology to manage the network hierarchically according to different network operating states and realize effective application of the underlying network facilities (Van and Truong et al, 2015). At the same time, SDN technology can carry out global deployment from the whole point of view to effectively improve the use efficiency of resources and quickly obtain the global information of network resources. By using SDN technology, network functions, virtualization technology and big data technology, the IT system of the park is completely virtualized, as well as the layout management of the park is simplified, and the enterprise environmental management is strengthened so as to truly realize the development goal of the smart park.

The needs of different groups should be met in the construction and planning process of smart park (Wang and Huang, 2015). From the operator's point of view, the efficient intelligent management, green and energy-saving facilities are needed. From the perspective of enterprises, its long-term development needs all kinds of enterprise service resources. From the perspective of employees, a good office environment and perfect life services are the primary needs. Centering on the development requirements of enterprises and the spiritual needs of talents, the resources of the government, enterprises and other parties must be coordinated to realize the intelligence of management, work and life which build a smart park in a trinity. We want to build the park into a software-defined park based on the digital twinning to provide the operators and users with services for wisdom in the cloud and application at the end, so as to maintain the balance between sustainable development and high-quality services of the park as shown in Figure 1.

A software-defined park means that the park can be defined and changed according to operation and maintenance requirements to ensure that the park can continuously adapt to the changes of the era. Wisdom in the cloud and service at the end means that data analysis and computing run on the cloud leaving difficulties to the platform. The applications will be connected to various terminals to provide more convenient and efficient services for employees' work and life.

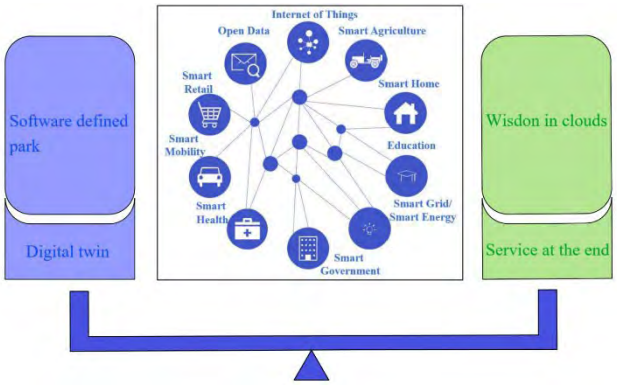

Fig 1. Smart Park construction balance relationship

3. DIMENSIONS OF SMART PARK

The dimensions of smart city are smart economy, smart transportation, smart environment, smart people, smart life and smart management according to relevant literature (Gifnger and Gudrun, 2010; Mohanty and Choppali et al, 2016). These aspects are independent and intersecting which are the main content of smart city construction. The literature (Wang and Sheng et al, 2020) specifically studies the construction of smart e-commerce logistics park in Beijing from the perspective of smart management, in which synergy among the three subjects of city management, park management and enterprise management is considered. Smart Park is an important form of smart city. It not only reflects the main system mode and development characteristics of smart city, but also has the uniqueness that is different from the development mode of smart city. Smart parks have gradually become an important way to attract investment and reserve talents. The smart park uses various intelligent and information applications to help the park to realize the transformation of industrial structure and management mode, improve the market competitiveness of enterprises in the park, and promote industrial aggregation with the park in favor of creating economic and brand benefits for the park and its enterprises. The digitization of dimensions is the foundation of building a smart park. According to the dimensions of smart city and the characteristics of smart park, four dimensions of the park are given, namely people, things, affairs and space. The expansion and connection of the relevant chain can be further realized for these four dimensions. The core of the construction of smart park is the digitization of the park. Digitalized people, digitalized things, digitalized affairs and digitalized space are the four dimensions to realize the digitalized park as shown in Figure 2.

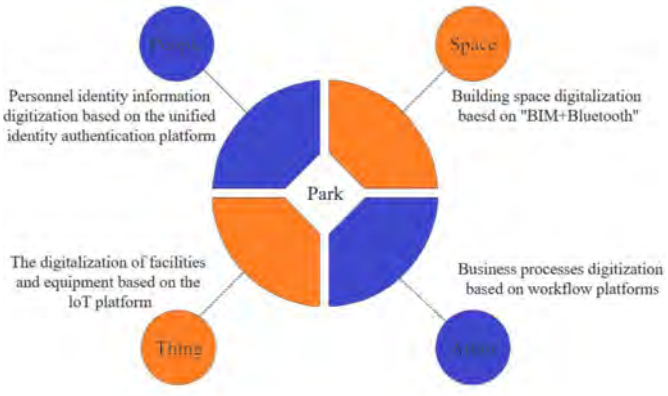

Fig 2. Four dimensions of digital park

4. SMART PARK SYSTEM FRAMEWORK

4.1 Overall Architecture

The main goal in smart park is to realize interconnection among the single systems through the perception system. The multi-dimensional intelligent analysis with the help of cloud computing and the effective integration of IT and other IT technologies can make the park's infrastructure operation more intelligent and greener and make the operation management of the park more standardized and efficient. These can help the park to provide customers with more high-quality and convenient value-added services in order to enhance the park's differentiated competitive advantages.

The network architecture includes cognitive layer, network layer and application layer based on smart city (Jin and Mikail er al, 2019). Literature (Zohreh and Viviana et al, 2020) shows that enterprise architecture layers used for services in smart cities include technology layer, information layer and service layer. Literature (Shwet and Pramod 2022) provides the architecture of IOT including the cognitive layer, network layer, service layer and association layer based on smart city. Literature (Wang and Li, 2020) put forwards an application-oriented cloud platform architecture that includes infrastructure layer, platform service layer and software service layer. The platform architecture in literature (Lin, 2021) is divided into perception communication layer, cloud infrastructure layer, data service layer, application support layer and software service layer. Literature (Ki and Young, 2022) provides the overall architecture of smart factory including physical layer, network layer, analysis layer and application layer.

This intelligent park information architecture of enterprise-oriented consists of the following four layers as shown in Figure 3 which are designed from the equipment layer (including air conditioner, lighting, elevator, etc.), the control layer (including EMS for energy management service, EAM for enterprise asset management, etc.) to the platform of integrated management service (PIMS) and finally to the intelligent operation center (IOC). The hierarchy of the information system architecture of the park is clearly divided. The overall architecture is shown in Figure 4 which includes 1 foundation, 1 platform, N applications and 1 brain.

Fig 3. Enterprise Park information architecture system

4.2 Composition of operation management platform

The composition of the operation management platform is shown in Figure 5. The operation man-agement platform can help enterprises realize effi-cient collaborative office, assist the whole process management, and improve the profitability of enter-prises. According to the needs of enterprises, plat-form modules can be expanded and integrated.

4.3 The main modules of platform

IOT platform

The IOT platform is a cross-industry and cross-field platform that provides equipment access, sys-tem access, data collection, data analysis and other support for smart park and digital twin. The platform has built-in mainstream protocols such as Modbus, BACNET, KNX, OPCUA/DA and MQTT which can meet the requirements of various data acquisition scenarios. With the help of rule engine and AI algo-rithm, the platform has the ability of data cleaning and data governance analysis which can provide strong platform support for application development and operation as shown in Figure 6.

Unified identity authentication platform

The unified identity authentication platform is a secure, flexible, stable and extensible enterprise-level unified identity and access control platform. Based on the unified identity account, the platform pro-vides the unified identity account, unified identity authentication, centralized authorization, application management, security audit and other capabilities to support platform, product, and project software de-velopment, and to realize the mutual sharing of basic data (organizations, accounts, etc.) of all applications in the park, unified authentication and login for all terminal applications (website/mobile APP/ desktop client).

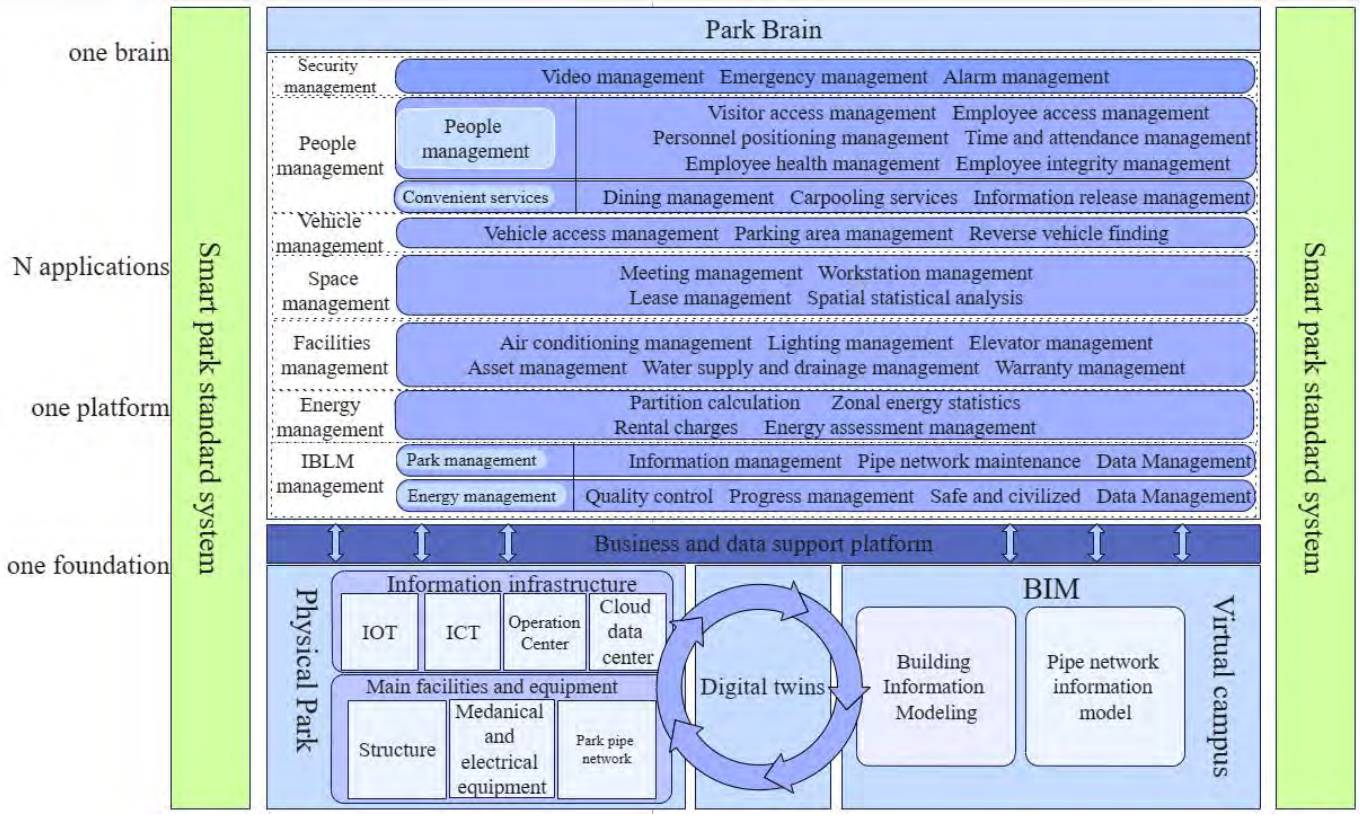

Fig 4. Overall Architecture

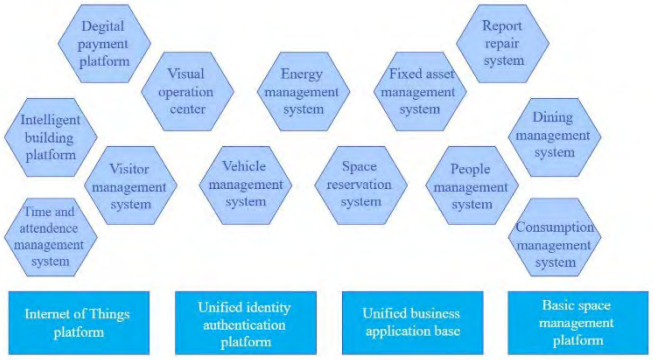

Fig 5. Operation management platform

Fundamentals of unified application

Unified business application base is an enabling platform for efficient collaborative office. It integrates the two essential basic capabilities that are unified collaborative communication and application development for enterprise information construction, thus it can help enterprises to work efficiently and grow rapidly. All kinds of services are distributed and scheduled to users through data bus to complete data collection and summary, thus breaking the information islands of each application system and building the overall big data of the enterprise.

Basic space management platform

In order to meet the spatial location management needs of the park for assets, meeting rooms, exhibition halls, offices, functional rooms and so on, a six-level spatial system of park - building - floor area - room - station to code all the physical spatial locations is used in the smart park .Assets, meeting rooms, exhibition halls, offices and functional rooms can be directly associated with specific spatial locations. Meanwhile, park managers can also grasp the use of each room in the park and their departments based on the spatial system.

Digital delivery platform

These functions such as BIM geometric model management, positioning query, model lightweight, attribute data management, archive data management, IOT integrated management, application scenario release management and the secondary development API (Application Programming Interface) can be provided by the digital delivery platform established on BIM completion model which integrates project design, construction completion information and key parameter information of facilities and equipment based on model lightweight engine and park object coding technology focused on digital asset map service. The organization and management of the model can be supported by the platform according to the relationship of system, partition, space and topology to establish the data collection, sorting and reuse mechanism based on the information model. It can provide model data and development interface data center for park and enterprise operation and maintenance so as to form important data assets for enterprises.

Intelligent building platform

The intelligent building integrated management and control platform is mainly used for the integrated management and control of intelligent building systems to provide system monitoring, alarm management, equipment operation data analysis, calendar configuration, mode configuration, operation log management and other functions. The platform fully embodies the characteristics of intelligent complex and adopts the advanced technology to realize the sharing and management of information resources among the intelligent subsystems in the building complex. The related system can realize mutual operation, fast corresponding and linkage control in order to achieve the goal of automatic monitoring and remote management.

Other modules of the platform

The visual operation center is the BIM comprehensive monitoring system after processing and beautification of the BIM models. The equipment is located and monitored through the system and the fault alarms generated in the management process are collected and pushed to the relevant maintenance personnel in time to confirm the timely maintenance of the equipment and ensure the normal operation of the equipment. Maintenance personnel can improve maintenance efficiency through work order management and task distribution.

According to the user's requirements, the energy management system collects all kinds of data measurement and sensors and completes the main data monitoring, technical analysis, daily report, monthly report, annual statistics and report output functions based on which the operation plan is executed. The collected data is summarized, analyzed and sorted out for energy management which includes energy actual analysis and management, energy quality management, energy cost management, energy balance management, energy forecasting and analysis, etc. to form energy management statements.

The fixed Asset Management system provides functions such as asset information management, asset repair reporting, asset transfer, asset loss reporting, asset scrapping, asset return, and asset information error correction to meet the daily management requirements of the administration department for the park assets. The administrator can effectively perform routine maintenance on assets. Before asset information management the asset type is needed to be configured and assigned to the corresponding information type. The functions of asset

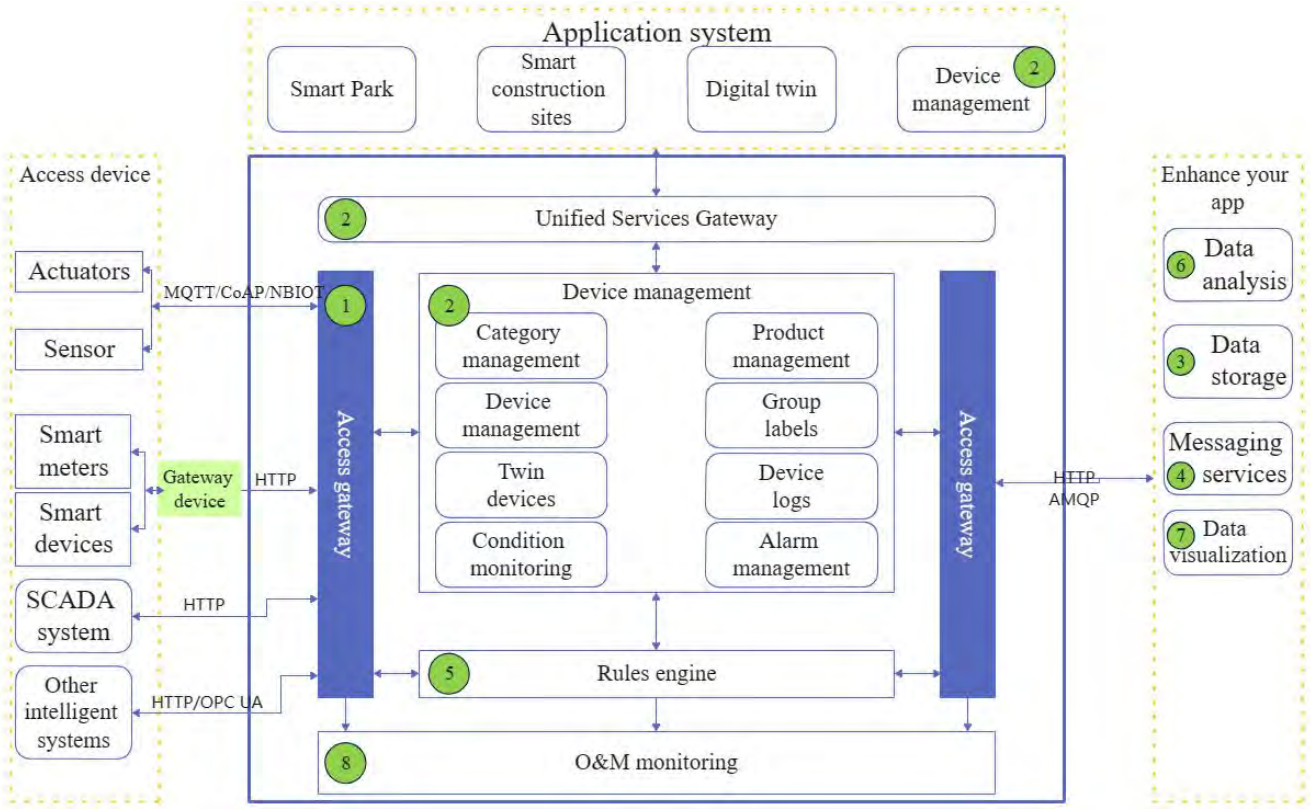

Fig 6. IOT platform

repair, asset transfer, asset loss, asset scrapping, asset return and asset information error correction record the details of asset information status.

The report repair system is a system that can initiate problem record and report anytime and anywhere. Employees use mobile applications to record problems in the form of photos, videos, and text descriptions, locate the problem through Bluetooth, and send the information to maintenance personnel. The administrator can query problem report records and at the same time the event dictionary, the type of on-tap events, and the frequently asked questions can be managed.

Attendance management system is used for staff attendance assessment, including team management, shift management, scheduling management, leave management, card replacement management, daily attendance statistics, monthly attendance summary, etc. The mobile application of attendance management is not only compatible with the face punch card and vehicle punch card of access control system, but also supports various mobile punch cards such as Bluetooth punch card, WIFI punch card, GPS punch card and other mobile punch cards. It also supports the query of personal attendance data, which not only meets the management needs of the company, but also provides more convenience for employees.

The visitor management system collects statistics on visitors' appointments, which facilitates the administrator to query the records of visitors so as to strengthen the security management of visitors. At the same time, it can simplify the visitor registration and verification process to avoid the tedious reception, contact confirmation, access control release process. Visitor management system provides visitor invitation registration, visitor appointment approval and other functions.

Different types of vehicles such as internal employee vehicles, external visiting vehicles, temporary vehicles can be registered, approved and authorized in the vehicle management system to complete the unified management of different types of vehicles. Administrators can view all registered vehicles and owner's information which can be added, deleted, changed, checked. Authorization can be extended for registered vehicles through authorization management. Employees can inquire the number and location of remaining parking spaces through the mobile application and locate their vehicles for easy search.

The conference room and other rooms are endowed with different space locations through the coding of the space location. The space usage is master's in real time through the space management system. Space reservation system can provide functions including space administrator scheduling, space maintenance, space service supplies configuration which can set the cost of service supplies and details and other information. Users can query the unused space through the mobile application and register the space reservation. The administrator receives and reviews the reservation application. The space can be used after the approval.

The number of people in and out of the park and their status are counted in real time in the form of Kanba for different types of people (employees, property, visitors, etc.) in dynamic personnel management system.

Dining management system is a multi-directional management system including menu management, window management, menu calendar, evaluation management, system configuration. The operation of adding, deleting and modifying dishes, dining window and window administrator configuration, daily menu display can be performed for dining personnel to view the menu. The evaluation function collects improvement suggestions for the restaurant, and the administrator can also make evaluation and reply through the background. Employees can query the current staff flow information of the restaurant and the information of today's dishes and can evaluate and give a like to the dishes.

The consumption management system is integrated with the consumption system to meet the needs of mobile terminal online recharge, wallet balance, subsidy and consumption record inquiry. The administrator can view the charging record, circled record and consumption record from the background, and the user-defined query can be conducted according to the time range.

One-code/face-pass can provide digital service for entrance guard management, catering consumption, visitor management and other scenarios through identity identification of enterprise employees, third party personnel and external visitors to realize intelligent management of the park.

5. PROJECT CASE

A system of the high-tech information park operation and maintenance management platform is designed for the Chinese Sixth Design and Research Institute of Machinery Industry Company Limited. Figure 7 is the scene of the intelligent operation center of the high-tech information park.Data are collected and distributed uniformly meanwhile multi-specialty, multi-terminal can be integrated to realize comprehensive application and display by the intelligent park platform established on the emerging IT technologies of BIM, IOT and networking.

The smart park project platform is developed and constructed in accordance with the principles of platformization, unification and servitization. Platformization refers to the integration data of people, things, affairs, space on the same platform. The basic platform framework of "BIM+IOT+ network " has been built first to consolidate the foundation of digital operation and management of the park. Unification refers to the realization of application of platform framework and micro-service. Employees only need to install an APP to use a variety of park applications such as production, office, property etc. The platform supports application expansion of requirements. Servitization means that the intelligent system of the park provides services for both managers and ordinary employees, so that employees can have a better sense of experience and participation in the construction of the smart park.

Fig 7. Smart operation center scenario

6. CONCLUSIONS

Since the concept of smart park was put forward, the development of smart park has been limited by the high cost and technical bottleneck. In recent years, with the development of communication technology, the construction of smart parks has opened a new development path and entered a stage of rapid development. According to the development goal of the smart park, the core concept of four dimentions of digital people, digital things, digital affairs and digital space is put forward. This paper gives the enterprise park information architecture system and the overall structure, that describes the operation management platform components. Finally, a smart park case is given. There is no universal software network architecture for smart parks in different fields (Nebojša and Alok, 2021; Liu and Wang et al, 2022; Yan, 2021), and the proposed design system can be adjusted according to users' requirements with flexibility and expansibility. SDN technology is used to separate the control function from the network equipment, and the function and type of the network equipment are all defined by the software which can obtain a faster response. At the same time, better interaction between architectural elements improves the convenience and functionality of the system and avoids information silos. The intelligent operation center (IOC) is the brain of park management, which is visible, controllable and manageable and supports a large number of business applications.

Despite the rapid development of smart parks, they still face many challenges, such as scientific planning, security issues, experience issues, cost issues, etc. (Ge and Chen et al, 2022; Guo and Wang et al, 2022; Zhu and Xu et al, 2022). In the process of continuous upgrading and development of the smart park, the future operation requirements of the park are needed to be discovered through industry analysis and practice. The functional modules of the design system are gradually optimized, improved and expanded in the direction of integration, networking and green development.

REFERENCES

Amir S, Mohammad R E D, Mohammad A A. An intelligent parking management system using RFID technology based on user preference. Application of Soft Computing, 26, 2022, PP 13869-13884.

Ari-Veikko A, Pekka V, Stephen J B. Smart cities in the new service economy: building platforms for smart services. AI & Society. 29, 2014, PP 323-334.

Bokolo A J. A case-based reasoning recommender system for sustainable smart city development. AI & SOCIETY. 36, 2021, PP 159-183.

Chen H L. Research and Application of new intelligent park based on the internet of things. Telecom Power Technology. 39(8), 2022, pp 122-125.

Chen X. Assessment of the transformation of smart in china's industrial park. Science & Technology Progress and Policy. 32(10), 2015, PP 114-118.

Emir U, Ejub K, Zakaria M et al. Immersing citizens and things into smart cities: a social machine-based and data artifact-driven approach. Computing. 102, 2020, PP 1567-1586.

Ge J P, Chen W, Wu J C et al. Security perception system of modern smart logistics warehousing park based on artificial intelligence technology. Electrical Automation. 44(2), 2022, PP 68-71.

Gifnger R, Gudrun H. Smart cities ranking: an effective instrument for the positioning of the cities? ACE Archit City Environ. 4(12), 2010, PP 7-26.

Guo H, Wang W X, Li X M et al. The smart park evaluation method that takes into account common ground and individual characteristics. Journal of Geo-information Science. 24(6), 2022, PP 1061-1072.

Guo J H, Wang H X, Shi B S et al. Design of an integrated park management system based on smart city concept. Computer Technology & Applications. 37(3), 2015, PP 30-36.

Kahkashan T. An intelligent metro tracking system for Riyadh Smart City. Internet Journal of Information Technology. 12(4), 2022, PP 1103-1109.

He Y Z, Liu Y Z, Yang P et al. Key technologies and prospects of smart parks in the era of 5G. Journal of Smart Agriculture. 1(1), 2021, PP 26-32.

Jin C P, Mikail M S, Jeong H J et al. CIoT-Net: a scalable cognitive IoT based smart city network architecture. Human-centric Computing and Information Sciences. 2019, PP 9-29.

Ki J Y, Young S J. Smart factory: security issues, challenges, and solutions. Journal of Ambient Intelligence and Humanized Computing 13, 2022, PP 4625-4638.

Lin B R. Exploration and practice of smart park construction. China's New Technology and New Products. 6, 2021, PP 130-131.

Liu L W. Analysis and discussion of intelligent cloud service platform for industrial parks. Chinese Business Theory. 2, 2017, PP 8-9.

Liu Y, Wang J Y, Hu S G. Research on the system framework of automotive intelligence detection industrial park. Intelligent Building and Smart City. 7, 2022, PP 91-93.

Mohanty S P, Choppali U, Kougianos E. Everything you wanted to know about smart cities: the internet of things is the backbone. IEEE Consum Electron Mag. 5(3), 2016, PP 60-70.

Nebojša G, Alok M. Software architecture of the internet of things (IoT) for smart city, healthcare and agriculture: analysis and improvement directions. Journal of Ambient Intelligence and Humanized Computing 12, 2021, PP 1315–1336.

Nicos K, Christina K, Luca M et al. Towards high impact smart cities: a universal architecture based on connected intelligence spaces. Journal of the Knowledge Economy 13, 2022, P 1169-1197.

Peng Y H. The cloud network fusion scheme analysis of "internet intelligent park" based on SDN. World of Communication. 3, 2022, PP 172-174.

Shwet K, Pramod K M. A contemporary survey on IoT based smart cities: architecture, applications, and open issues. Wireless Personal Communications. 125, 2022, PP 2319–2367.

Van G N, Truong X D, Young H K. SDN and virtualization-based LTE mobile network architectures: a comprehensive survey. Wireless Pers Commun. 86, 2016, PP 1401-1438.

Wang C H, Li S N, Cheng T. A construction of smart city evaluation system based on cloud computing platform. Evolutionary Intelligence. 13, 2020, PP 119-129.

Wang C L, Sheng Y F, Wang W J et al. Thoughts on building smart e-commerce logistics park in Beijing. Logistics Technology. 39(3), 2020, PP 25-28.

Wang L F, Huang H A. Discussion on overall planning and consultation of intelligent park. Mobile Communication. 19, 2015, PP 45-49.

Yan Y. Application research of intelligent park security system based on GIS technology. The Journal of New Industrialization. 11(1), 2021, 34-35.

Zhang X L, Wang D, Zhu Q et al. Yixing smart cloud platform development. Intelligent Building. 6, 2021,PP 91-93.

Zhu Z F, Xu Y, Cen H F et al. Optimal configuration of park-level integrated energy system considering demand response. New Energy. 50(1), 2022, 37-44.

Zohreh P, Viviana B, Markus H. Standardisation of enterprise architecture development for smart cities. Journal of the Knowledge Economy 11, 2020, PP 1336-1357.

Electronic Journal of Structural Engineering

Original Article

Cite this: DOI:10.56748/ejse.233832

Received Date: 01 November 2022
Accepted Date: 18 January 2022

1443-9255
https://ejsei.com/ejse

Developing a Compression-moulded Composite Partitioning Panel from Banana Fibres and Polylactic acid (PLA)

Dumindu Dassanayaka [a], Dilshan Hedigalla[a] , Dakshitha Weerasinghe [b]*, Nandula Wanasekara [a], Ujithe Gunasekera [a] and Damith Mohotti [b]

[a] Department of Textile and Apparel Engineering, Faculty of Engineering, University of Moratuwa, Moratuwa 10600, Sri Lanka
[b] School of Engineering & IT, The University of New South Wales, Campbell 2600, ACT, Australia
* Corresponding author: dakshitha92@gmail.com

Abstract

Green construction materials developed using renewable resources have become the focus of concurrent research owing to increasing environmental considerations and legislations. However, most of the available literature focus only on load-bearing construction elements. Consequently, little attention has been paid towards non-load-bearing construction elements such as partitioning materials. The present work aims to address this gap by investigating the viability of using the biodegradable bioplastic PLA in combination with yarns spun using banana fibres to manufacture a composite panel intended for temporary partitioning materials used in the construction industry. Pre-tensioned banana yarns were used as the reinforcement while PLA was used as the matrix. The composite panels were manufactured using the compression moulding technique. The effect of process parameters such as moulding temperature and pressure, the effects of the degree of pre-tension and the amount of reinforcing yarn on the performance of the panels were investigated. The optimum moulding conditions were found to be 180oC moulding temperature and 15 tons of moulding pressure. Yarn pre-tensioning exhibited a positive effect on the performance of the composite panels. However, increasing the reinforcing yarn percentage caused a degradation of flexural performance of the composite. Finally, the performance was compared against the most widely used partitioning material currently, medium-density fibreboard (MDF). The novel composite panel manufactured at optimum conditions exhibited 52% higher impact strength and 55% higher flexural strength when compared to MDF. The composite panel presented herein has the potential to replace MDF as a better performing material manufactured using renewable resources.

Keywords

Construction material, PLA, banana yarn/fibre, composite panel, partitioning material

1. Introduction

With the rapid growth of world population and overall improvement of living standards during last two decades, the demand for construction materials and energy consumption have also seen a steep rise (Gavali & Ralegaonkar, 2020). The construction sector is considered as one of the most energy-consuming, greenhouse gas-emitting and solid waste generating industries (Tiskatine et al., 2018). It has been shown that construction activities are responsible for consuming about 40% of natural resources such as stone, sand, wood and water (Mateus et al., 2013). 50% of total waste accumulated in landfills, as well as 30% of total carbon emissions (Vasconcelos et al., 2013). In attempts to alleviate these negative impacts to the environment, numerous strategies have been introduced to the construction industry (Commission, n.d.). where 'green buildings' is a new basic requirement in the Construction Products Regulation (CPR) (Marques et al., 2017). Consequently, novel material development for the construction industry using renewable resources has been the focus of numerous contemporary research (Kim et al., 2019, Marques et al., 2020, Darwish et al., 2019, Dissanayake et al., 2021a, Dissanayake & Weerasinghe, 2021, Dissanayake & Weerasinghe, 2021).

However, it can be observed that the main focus of concurrent research has been more towards load-bearing construction materials than their counterparts, even though the amount of non-load-bearing construction materials is significant (Passer et al., 2012). It has also been shown that non-load bearing construction materials such as internal partitioning walls account for 41% of the environmental impacts, from the usage of the raw material (Passer et al., 2012). Medium-density fibreboards (MDFs) is the most commonly used partitioning material currently. MDF is a composite made of wood and formaldehyde and is cheaper than most of the other conventional partitioning materials. However, MDFs have inherent disadvantages. MDFs are made out of trees. MDF exhibits high water absorption which results in swelling of the material at affected areas, and tend to crack or split under extreme stress. Moreover, the use of urea formaldehyde in its production could cause irritation to lungs and eyes. MDF dust has also been reported as a health concern (Thetkathuek et al., 2016). Therefore, a better class of substitutive materials is required in place of MDFs. However, the reported literature in this niche research area is relatively scarce and constitutes the premise of the present study. The means of developing a composite panel intended to be used as a partitioning material is presented.

Application of fibres in construction and building materials receives great attention due to their inherent properties such as, strength, lightweight, physical performance and less thermal conductivity (Binici et al., 2012, Barbero-Barrera et al., 2016). In particular, natural fibres such as jute, sisal, flax, hemp and banana have been used as substitutive materials replacing synthetic fibres (Komal et al., 2020, Kiruthika, 2017, Asumani and Paskaramoorthy, 2020, Takagi, 2019, Cho et al., 2007). The present work aims to develop a composite material using fully renewable resources; PLA and banana fibres. Banana fibre is a commonly used natural fibre and PLA is a biodegradable, thermoplastic material produced from starch-rich plants such as corn and sugar cane. PLA is renewable material that is widely used in composite applications (Katogi et al., 2012, Ben et al., 2007). However, PLA inherently possesses weak mechanical properties, especially, low impact strength (Komal et al., 2020). This hinders the potential of renewable PLA being used in commercial applications such as construction and building materials which demand superior mechanical properties from raw materials. This can be overcome by using banana yarns/fibres as a reinforcing material in combination with PLA as the matrix material, in a composite system.

Dissanayake et al. (Dissanayake et al., 2018) used the compression moulding technique to produce a thermal insulation composite panel using post-industrial textile waste intended to be used as a construction material. Nylon/Spandex fabric and polyurethane shreds were used to produce the panels where the nylon polymer acted as a binding agent upon being melted. Dissanayake et al. (Dissanayake et al., 2021) produced an environmentally friendly sound insulation material for the construction and building sector, also from post-industrial textile waste where natural rubber was used as a binding material. The compression moulding technique was used to manufacture the composite panel. Compression moulding is known to be less complicated and is relatively a fast method of manufacturing a rigid composite panel, which is advantageous in manufacturing a construction material required in bulk quantities. Therefore, compression moulding technique is selected as the method of manufacturing the composite panels in the present work. Moreover, banana

fibres/yarns in particular are selected as the reinforcing material due to the abundant availability, ease of manufacturing and most importantly, renewability. Banana is the most planted tree in Sri Lanka (469 842 tons/year, 49,168 hectare) and its fibres have been used in yarn manufacturing (Mumthas et al., 2019, Balakrishnan et al., 2019).

Dissanayake et al. (Dissanayake et al., 2021) and Dissanayake et al. (Dissanayake et al., 2018) reported that the compression moulding parameters such as moulding temperature and moulding pressure are critical parameters in developing a suitable compression-moulded panel. Therefore, the effects of varying moulding conditions on the performance of the panel were investigated in detail in the present study. Moreover, the effects of degree of pre-tension of the reinforcing banana yarns and the amount of banana yarns present in the composite on the performance of the panel were also investigated. The performance of the panels was determined by testing the composite panels for their impact strength (ASTM D256) and flexural strength (ASTM D790). The optimum moulding conditions, reinforcement yarn pre-tension and amount of reinforcement yarns are presented.

2. Materials and Methods

2.1 Materials

Banana yarns were used as the reinforcement while PLA was used as the matrix material for all the composite panels prepared in the present study. Yarns were manufactured using Cavendish AAA banana tree ('*Musa acuminata*') stems.

As the matrix of the composite, Poly-Lactic Acid (PLA) was used. PLA filaments were sourced from Unitech Trading (Pvt) Ltd, Colombo, Sri Lanka in the filament form with a diameter of 1.75 mm. A general-purpose silicon emulsion was used as the mould release agent. A pre-tensioning apparatus was manufactured using metal rods to hold and tension the reinforcing yarns.

2.2 Methods

Preparation of banana yarns

The pseudo stems of the banana trees were initially cut approximately one metre pieces. These pseudo stems were fed to a decorticator in order to extract banana fibres with an approximate length of one metre. This is shown in Fig 2 (a) and (b).

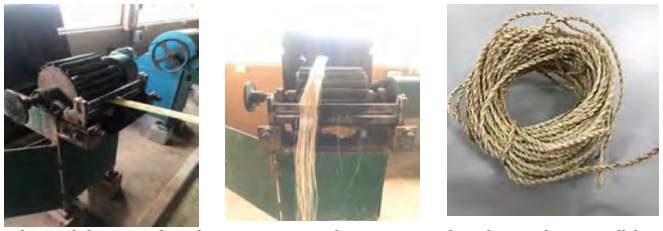

Fig 2. (a) Inserting banana pseudo stem to the decorticator, (b) extracted banana fibers and (c) hand-spun banana yarns

Subsequently, these fibres were hand-spun in order to produce 100% banana yarns as shown in Fig 2 (c). These yarns were subsequently used for the manufacture of the composite panels. The composition of the banana yarns were investigated using a Fourier-transform infrared spectroscopy (FTIR) test. The strength was also characterised in accordance with ASTM D2256 (Standard Test Method for Tensile Properties of Yarns by the Single-Strand Method) standard. A thermal analysis of the banana yarns was also carried out using a thermogravimetric analysis (TGA). The yarn count was measured according to ISO 2060 standard.

Composite Fabrication

Two types of composite panels were prepared in the present study, unidirectional and bidirectional. In the unidirectional panels, pre-tensioned banana yarns were laid unidirectionally, while pre-tensioned banana yarns were laid bidirectionally for the bidirectional panels. For bidirectional panels, the two yarn sets were laid orthogonal to each other. The metal frame with unidirectional and bidirectional yarn lays are shown in Fig 1.

Tensioning of the yarns was achieved by a custom-made metal frame and known weights as shown in Fig 3.

A square-shaped mould with dimensions 101 mm x 101 mm x 4mm was used and is shown in Fig 4 (c). Mould parameters were selected such that 100 mm x 10 mm x 4mm specimens could be prepared in order to perform flexural and impact strength tests. Banana yarns were laid with different tensions using the metal frame and known weights. PLA filaments were crushed into pieces of approximately 2 mm in length and placed inside a mould as shown in Fig 4 (a) and (b).

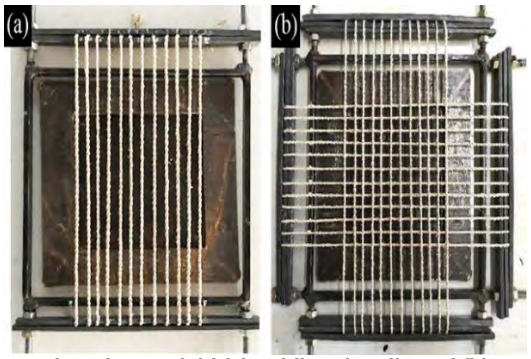

Fig 1. Tensioned yarns laid (a) unidirectionally and (b) bidirectionally

Fig 3. Yarn tensioning frame

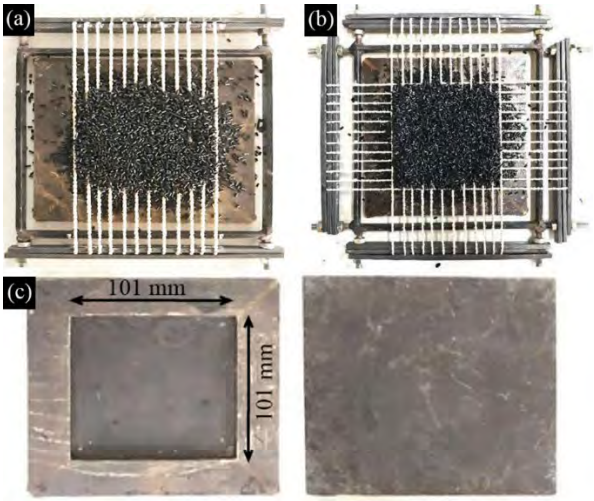

Fig 4. Crushed PLA placed inside the mould with (a) unidirectional yarn lay-up and (b) bidirectional yarn lay-up and (c) the empty mould.

Before placing the PLA, the releasing agent was applied on the inner surface of the mould. Here, the yarn reinforcements were placed in-line with the mould such that the reinforcements lie in the mid-plane of the composite panel and the composite panels were then prepared under a range of different moulding temperatures and pressures. Reinforcement yarn weight percentage, moulding pressure, moulding temperature, and pre-tensioning force were varied to prepare a total of fourteen different samples as summarised in Table 1.

Table 1. Sample matrix

Yarn lay-up	Controlled parameter	Value
Unidirectional	Yarn weight percentage (%)	2, 4, 6
	Moulding pressure (ton)	5, 10, 15, 20
	Moulding temperature (°C)	180, 190, 200
	Pre-tension of reinforcing yarn (N)	5, 7.5, 10, 12.5, 15
Bidirectional	Yarn weight percentage (%)	3, 6, 9
	Moulding pressure (ton)	5, 10, 15, 20
	Moulding temperature (°C)	180, 190, 200
	Pre-tension of reinforcing yarn (N)	5, 7.5, 10, 12.5, 15

The employed value ranges were selected by considering the available resources and the required quality of the final product. Weight percentage of the yarn was calculated according to Eq. 1.

$$W = \frac{W_1}{W_2} \times 100 \quad (1)$$

Here, 'W' is the yarn weight percentage, 'W_1' is the weight of the composite after manufacturing (g) and 'W_2' is the weight of yarns laid in the cavity of the mould (g). 'W_2' was calculated according to Eq. 2.

$$W_2 = L \times \lambda \quad (2)$$

Here, 'L' is the length of yarn laid in mould cavity (cm) and 'λ' is the linear density of the yarn (gcm^{-1}).

Testing composite panels

Each of the samples was tested for flexural and impact strength. All the results were taken after averaging four values of impact strength or flexural strength. Flexural strength was calculated in accordance with the ASTM D790 (Standard Test Methods for Flexural Properties of Unreinforced and Reinforced Plastics and Electrical Insulating Materials) standard, using Eq. 3.

$$\sigma = \frac{3PL}{2bd^2} \quad (3)$$

Where, 'σ' is the stress of outer fibres at mid-point (MPa), 'P' is the load at a given point of the load-deflection curve (N), 'L' is the support span (mm), 'b' is the width of the beam tested (mm) and 'd' is the depth of the beam tested (mm). Moreover, impact strength of the samples was calculated in accordance with ASTM D256 (Standard Test Methods for Determining the Izod Pendulum Impact Resistance of Plastics) standard, Izod Impact Testing (Notched Izod).

3. Results and discussion

3.1 Chemical and mechanical properties of the banana yarns

The TGA test results of the banana yarn are shown in Fig 5. The blue curve of the TGA of banana yarn indicates the mass of a banana yarn as a function of temperature as the temperature of the sample is increased in a controlled atmosphere. The green curve of the TGA of banana yarn indicates the first derivative of the weight loss curve (blue curve) and the red curve indicates the heat flow during testing. It can be observed that 5.5% weight percentage of banana yarn is lost, when sample is heating from around 25 ^{0}C to 120 ^{0}C due to the vaporisation of water. Another 1.5% weight percentage of banana yarn is lost, when the yarn is further heated from 125 ^{0}C to 200 ^{0}C due to loss of low molecular weight compounds. Moreover, the results also reveal that banana yarn starts to thermally decompose around 125^{0}C.

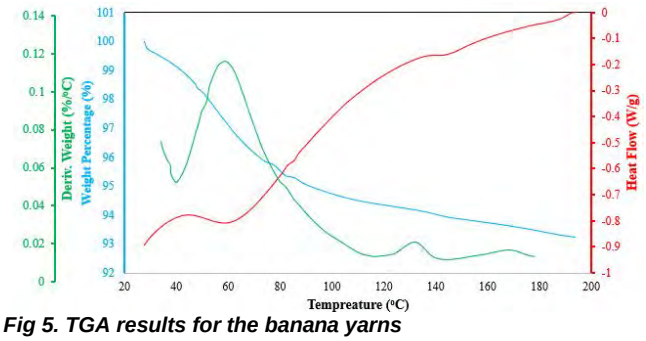

Fig 5. TGA results for the banana yarns

The produced banana yarns were also tested for their strength in accordance with ASTM D2256. The yarn count was measured (in accordance with ISO 2060) to be 1175 Tex. Fig 7 shows the typical force-elongation behaviour of a banana yarn. The ultimate tensile strength of the banana yarn was observed to be 102.5N. Therefore, the pre-tension used for reinforcing yarns was varied from 5N to 15N, which is approximately 5% and 15% of the average ultimate tensile strength of the banana yarn. The yarn showed approximately 16% strain at failure. Therefore, it can be assumed that the banana yarns could provide sufficient reinforcement for a non-load bearing application such as a partitioning panel.

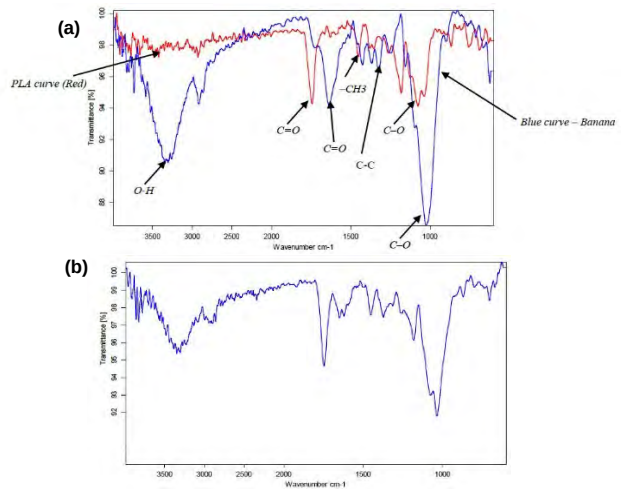

Fig 6. (a) FTIR curves of banana and PLA and (b) the composite panel

The FTRI spectra of banana yarns and PLA and the composite panel are given in Fig 6 (a) and (b), respectively. PLA usually shows characteristic stretching frequencies for C=O, –CH3 asymmetric, –CH3 symmetric, and C–O, at 1746, 2995, 2946 and 1080 cm^{-1} wavenumbers, respectively. Bending frequencies for –CH3 asymmetric and –CH3 symmetric have been identified at 1452 and 1361 cm^{-1}, respectively (Ramachandran et al., 2016). Banana yarns shows the relative intensities of bands at 3400 cm^{-1} (O-H stretching), 2900 cm^{-1} (C-H stretching), 1036 cm^{-1} (C-O stretching), 1725 cm^{-1} (C=O stretching), 1150 cm^{-1} (C–O–C and C–O stretch) and 1500–1600 cm^{-1} (C-C aromatic skeletal vibrations) (Milani et al., 2016). Sharp peaks around the abovementioned wavenumbers can be observed in Fig 6 (a). Moreover, it can also be observed in Fig 6 (b) that the same sharp peaks are available approximately around the same wavenumbers. This implies that the chemical composition of PLA/Banana yarns remained unchanged upon manufacturing of the composite panel.

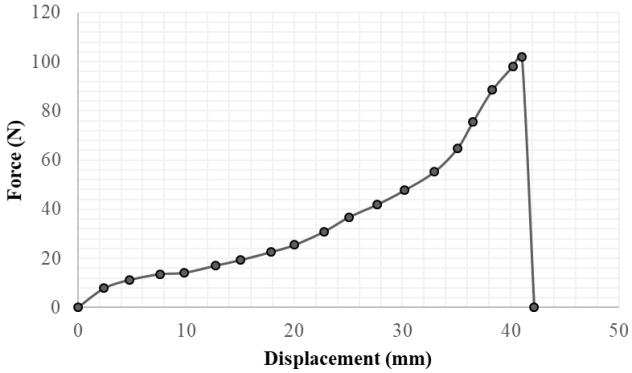

Fig 7. Force-elongation curve for the banana yarn

3.2 Effects of moulding conditions on the impact strength

As discussed in Section 2.2.2, a series of composite panels were prepared under different moulding conditions: moulding temperatures and pressures. Each sample was tested for its impact and flexural strengths and was compared to those of MDF boards. The MDF boards exhibited an impact strength of 5.62 kJ/m^2 and a flexural strength of 34.92 MPa.

The variation of impact strength of the unidirectional and bidirectional panels with moulding temperature is illustrated in Fig 8 (a) and (b), respectively. Moreover, the variation of flexural strength of the unidirectional and bidirectional panels with moulding temperature is illustrated in Fig 8 (c) and (d), respectively. The impact tests were carried out both along and across the reinforcement yarns for the unidirectional panels, in order to evaluate any anisotropic properties. It was observed that the impact strength properties of the unidirectional panels is highly anisotropic. The impact strength is far superior along the reinforcement yarn direction than across it. This is anticipated since the impact strength along the reinforcement yarn is supported by the reinforcing yarns in contrast to the impact strength across the reinforcing yarns where the strength is governed by the strength of the PLA matrix. However, the directional effect is absent on the bidirectional panels since the composite panel is reinforced in both directions. It was observed that the impact strength decreased with moulding temperature for both unidirectional and bidirectional composite panels. The reduction is approximately the same

for both composite panels and stands at ca. 20%, when the moulding temperature was increased from 180°C to 200 °C. However, it was also observed that the across-yarn impact strength of the unidirectional composites remained approximately constant when the moulding temperature was increased. The flexural strength of the panels also followed a similar trend. Moreover, it is observed that both the impact and flexural strengths are superior to the MDF boards at all temperatures, with the exception of impact strength across reinforcing yarns (unidirectional panels). It was observed that the lowest moulding temperature yielded the highest flexural strength. Therefore, the optimum moulding temperature was selected to be 180°C, considering both the impact and flexural strengths of the materials. At a moulding temperature of 180°C, both the impact and flexural strengths are well above the strengths of the MDF boards (except across yarn unidirectional panel).

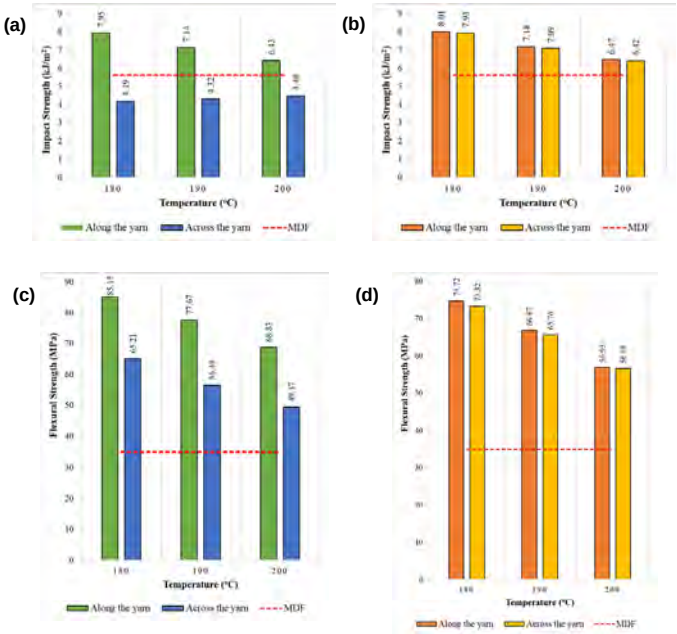

Fig 8. The effect of moulding temperature on the impact strength of (a) unidirectional composite panels, (b) bidirectional composite panels and the flexural strength of (c) unidirectional composite panels and (d) bidirectional composite panels

Similarly, the variation of impact strength of the unidirectional and bidirectional panels with moulding pressure is illustrated in Fig 9 (a) and (b), respectively. A strong material anisotropy can be observed when the moulding pressure is varied in the unidirectional composite panel, similar to the anisotropy observed when the moulding temperature was varied. However, instead of a strictly decreasing trend, a parabolic distribution of impact strength variation can be observed. The impact strength exhibited a maximum at a moulding pressure of 15 tonnes for both unidirectional and bidirectional composites. Moreover, the impact strength of the unidirectional panels remained approximately the same when tested across the reinforcing yarns. This is anticipated and occurs due to the reinforcement being present only along one direction as explained above. The impact strengths of the bidirectional panels were observed to be approximately the same in both perpendicular directions. Similar to the impact strength, the flexural strength followed a similar parabolic trend. However, the flexural strength of the unidirectional panels also exhibited a parabolic fluctuation in contrast to the impact strength distribution. It was also observed that the maximum flexural strength was approximately 6% higher in the unidirectional composite at 15-ton moulding pressure. This difference is apparent for all the different moulding pressures. This is due to the premature failure of the bidirectional panel due to the presence of yarn intersections. For bidirectional panels, due to the overlapping of orthogonal reinforcing yarns, yarn intersections are present. Matrix cracking initiated from such intersections thereby causing failure. Since unidirectional composites did not have such intersections, they exhibited a higher flexural strength.

It is also observed that the impact and flexural strengths are superior to the MDF boards at almost all the moulding pressures, with the exception of across yarn impact strengths of unidirectional panels. It can be concluded that the optimum moulding pressure is approximately 15 tonnes for both unidirectional and bidirectional panels, considering both the impact and flexural strengths of the composite panels. At a moulding pressure of 15 tonnes, both the impact and flexural strengths are well above the strengths of the MDF boards (except across yarn unidirectional panel).

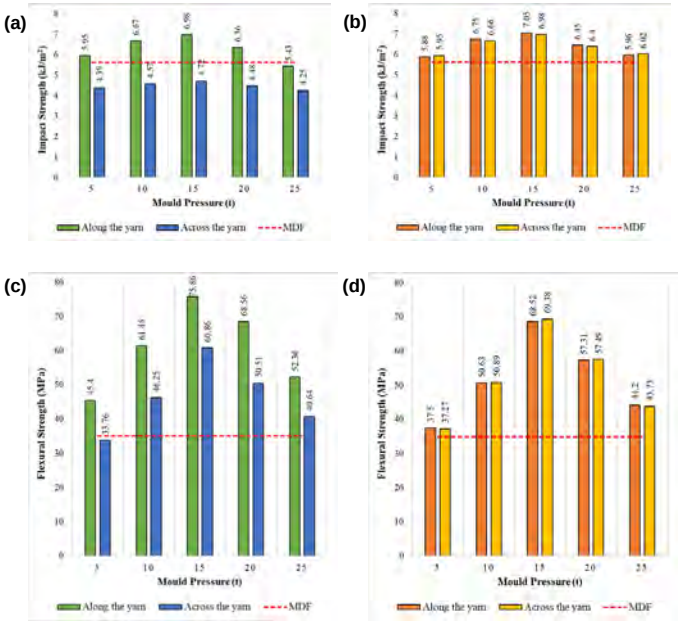

Fig 9. The effect of moulding pressure on the impact strength of (a) unidirectional composite panels, (b) bidirectional composite panels and the flexural strength of (c) unidirectional composite panels and (d) bidirectional composite panels

4. Effects of reinforcement yarn conditions on the impact strength

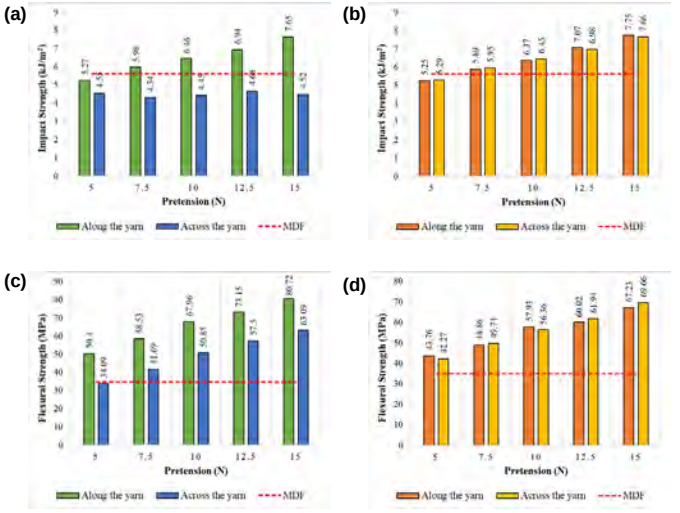

Fig 10. The effect of reinforcing yarn pre-tension on the impact strength of (a) unidirectional composite panels, (b) bidirectional composite panels and the flexural strength of (c) unidirectional composite panels and (d) bidirectional composite panels

The variation of impact strength of the unidirectional and bidirectional panels with reinforcing yarn pre-tension is illustrated in Fig 10 (a) and (b), respectively. Material anisotropy continues to appear in the unidirectional panels. When the reinforcing yarn pre-tension is increased up to 15N, the impact strength difference between the along and across yarn directions is approximately 41%. The impact strength across the yarns in unidirectional composites remains approximately the same, similar to the earlier occurrences, since the strength is governed only by the strength of the PLA matrix. However, the bidirectional panels exhibit approximately the same impact strength regardless of the direction. Both the panels exhibit a strictly increasing trend in impact strength when the reinforcement yarn pre-tension was increased from 5N to 15N. It was observed that the impact strength was increased by more than 30% when the pre-tension was increased up to 30%. Furthermore, the flexural strength also followed the increasing trend when the reinforcing yarn pre-tension was increased. Similar to the cases of moulding conditions, it can be observed that the flexural strength across the reinforcement yarns in unidirectional composites also followed an increasing trend. For the unidirectional composite panels, the flexural strength was increased by 38% along the reinforcement yarn and 46% across the reinforcement yarn. For the

bidirectional composite panels, the flexural strength was improved by approximately 40%, considering both directions. Therefore, the optimum reinforcement yarn pre-tension was concluded to be 15N. Even though the strictly increasing trend suggests using a higher pre-tension would yield better results, it should be noted that the maximum yarn pre-tension possible was limited by the designed frame used in the present work. Moreover, the higher the pre-tension, the higher the strain the reinforcing yarns undergo. Since the banana yarns used exhibited a limited strain of 16% to failure, using a pre-tension of approximately 15N is justified, which occurs at less than 5% strain.

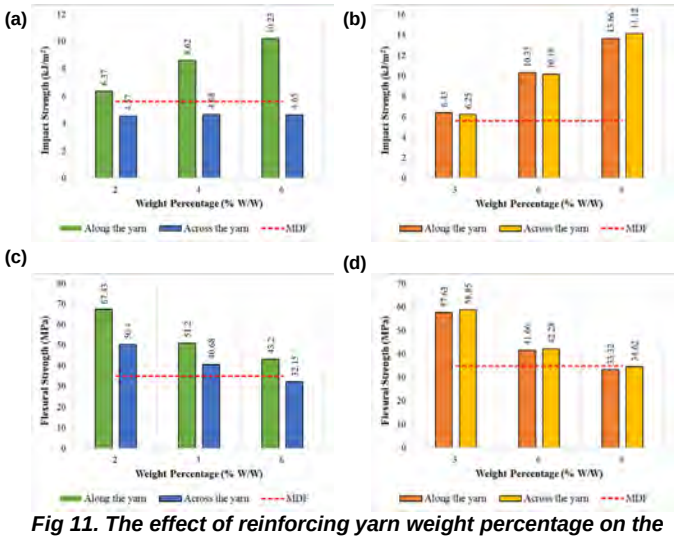

Fig 11. The effect of reinforcing yarn weight percentage on the impact strength of (a) unidirectional composite panels, (b) bidirectional composite panels and the flexural strength of (c) unidirectional composite panels and (d) bidirectional composite panels

In contrast to all the other variables, the reinforcement yarn percentage exhibited opposing trends in impact and flexural strengths. It was observed that the impact strength of both types of composite panels showed an increasing trend whereas the flexural strength showed a decreasing trend, when the yarn weight percentage was increased. The impact strength exhibited a similar strictly increasing trend when the reinforcing yarn weight percentage was increased, for both unidirectional and bidirectional composite panels. While the across yarn impact strength did not exhibit an increasing trend, the along yarn impact strength exhibited an increase of approximately 38%. However, it was observed that the impact strength of the bidirectional composite panels was increased by approximately 56% when the yarn weight percentage was increased to 6%. Similar to the other cases, the bidirectional panels did not exhibit noticeable material anisotropy in terms of both impact and flexural strength. However, the flexural strength exhibited a strictly decreasing trend when the reinforcing yarn weight percentage was increased for both types of panels. The flexural strength was reduced by 36% for unidirectional composites while the strength was reduced by 40% for the bidirectional composites. This is also explained by the nature of failure of the panels explained above.

Consequently, when choosing the optimum weight percentage of reinforcing banana yarns, it is a tradeoff between the impact strength and flexural strength. For instances where high flexural strengths are required, a lower reinforcing yarn weight percentage can be used. Similarly, for instances where the impact strength is a concern, a higher weight percentage of reinforcing yarns can be used. The optimum weight percentage in this case is taken as 6% (4% for unidirectional panels) considering both impact and flexural strengths.

In summary, the optimum process parameters can be tabulated as given in Table 2, to produce a composite partitioning material by the compression moulding technique. The unidirectional panels cannot be recommended for commercial use given their inferior performance when tested across the reinforcing yarns. On the other hand, bidirectional panels exhibit far superior performance than MDF boards.

Table 2. Optimum process parameters to manufacture the composite panel.

Variable	Optimum value
Reinforcement yarn lay-up	Bidirectional
Moulding temperature	180°C
Moulding pressure	15 tonnes
Pre-tension of the reinforcing banana yarns	15 N
Weight percentage of the reinforcing banana yarns	6%

A bidirectional composite panel was moulded as per the conditions given in Table 3. The composite panel was then tested for its impact and flexural strengths. This composite panel exhibited an impact strength of 11.56 kJ/m^2 and a flexural strength of 76.81 MPa. When compared to MDF, the impact strength is 51.5% higher while the flexral strength is 54.6% higher in the composite panel.

5. Conclusions

Based on the experimental work carried out in the present work, the following conclusions can be drawn.

1. A composite partitioning material can be manufactured using banana yarns/fibres and the bioplastic PLA, which are renewable resources, using the compression moulding technique. The optimum moulding conditions are 180°C moulding temperature and 15 tonnes of moulding pressure.
2. Bidirectional reinforcement yarn layup better reinforces the composite panels than unidirectional layup. Flexural strength is higher for unidirectional composite panels along the reinforcing yarn. However, the impact strength is poor when tested across the reinforcing yarns.
3. Pre-tensioning of the reinforcing yarns show an improvement of both flexural and impact strengths. The higher the pre-tension, the better the properties.
4. With increasing weight percentage of reinforcing yarns the impact strength improved while the flexural strength deteriorated. A weight percentage of 6% (bidirectional panel) yielded desirable properties. With 6% reinforcing yarns, the impact strength was 45% more and flexural strength was 17% more than MDF.
5. At the optimum production conditions, the PLA-banana yarn composite panel exhibits 52% higher impact strength and 55% higher flexural strength than MDF.

References

Gavali, H.R., & Ralegaonkar, R.V. (2020). Design development of sustainable alkali-activated bricks. Journal of Building Engineering, 30, 101302.

Tiskatine, R., Bougdour, N., Oaddi, R., et al. (2018). Thermo-physical analysis of low-cost ecological composites for building construction. Journal of Building Engineering, 20, 762–775.

Mateus, R., Neiva, S., Bragança, L., et al. (2013). Sustainability assessment of an innovative lightweight building technology for partition walls – Comparison with conventional technologies. Building and Environment, 67, 147–159.

Vasconcelos, G., Lourenço, P.B., Mendonça, P., et al. (2013). Proposal of an innovative solution for partition walls: Mechanical, thermal and acoustic validation. Construction and Building Materials, 48, 961–979.

Commission, E. (n.d.). The European construction sector: A global partner.

Marques, B., Tadeu, A., De Brito, J., et al. (2017). A Perspective on the Development of Sustainable Construction Products: An Eco-Design Approach. International Journal of Sustainable Development and Planning, 12, 304–314.

Kim, B., Wisniewski, J., Baker, T., et al. (2019). Behaviour of sand-filled plastic bottled clay panels for sustainable homes. Journal of Building Engineering, 26, 100895.

Marques, B., Tadeu, A., Almeida, J., et al. (2020). Characterisation of sustainable building walls made from rice straw bales. Journal of Building Engineering, 28.

Darwish, E.A., Mansour, Y., Elmously, H., et al. (2019). Development of sustainable building components utilizing date palm midribs for light wide-span multi-purpose structures for rural communities in Egypt. Journal of Building Engineering, 24, 100770.

Dissanayake DGK, Weerasinghe D, Perera TDR, et al. (2021) A Sustainable Transparent Packaging Material from the Arecanut Leaf Sheath. Waste and Biomass Valorization, 12:5725–5742. https://doi.org/10.1007/s12649-021-01382-5.

Dissanayake DGK, Weerasinghe DU. (2021) Fabric Waste Recycling: a Systematic Review of Methods, Applications, and Challenges. Materials Circular Economy, 3.

Dissanayake DGK, Weerasinghe D. (2021) Towards Circular Economy in Fashion: Review of Strategies, Barriers and Enablers. Circular Economy and Sustainability.

Passer A, Kreiner H, Maydl P. (2012) Assessment of the environmental performance of buildings: A critical evaluation of the influence of technical building equipment on residential buildings. The International Journal of Life Cycle Assessment, 17:1116–1130.

Thetkathuek A, Yingratanasuk T, Ekburanawat W. (2016) Respiratory Symptoms due to Occupational Exposure to Formaldehyde and MDF Dust

in a MDF Furniture Factory in Eastern Thailand. Advances in Preventive Medicine, 2016:1–11.

Binici H, Gemci R, Kucukonder A, et al. (2012) Investigating sound insulation, thermal conductivity and radioactivity of chipboards produced with cotton waste, fly ash and barite. Construction and Building Materials, 30:826–832.

Barbero-Barrera MDM, Pombo O, Navacerrada MDLÁ. (2016) Textile fibre waste bindered with natural hydraulic lime. Composites Part B: Engineering, 94:26–33.

Komal UK, Lila MK, Singh I. (2020) PLA/banana fiber based sustainable biocomposites: A manufacturing perspective. Composites Part B: Engineering, 180:107535.

Kiruthika A V (2017) A review on physico-mechanical properties of bast fibre reinforced polymer composites. Journal of Building Engineering 9:91–99.

Asumani O, Paskaramoorthy R (2020) Fatigue and impact strengths of kenaf fibre reinforced polypropylene composites: effects of fibre treatments. Advanced Composite Materials 1–13.

Takagi H (2019) Review of Functional Properties of Natural Fiber-Reinforced Polymer Composites: Thermal Insulation, Biodegradation and Vibration Damping Properties. Advanced Composite Materials 28:525–543.

Cho D, Seo JM, Lee HS, et al. (2007) Property improvement of natural fiber-reinforced green composites by water treatment. Advanced Composite Materials 16:299–314.

Katogi H, Shimamura Y, Tohgo K, et al. (2012) Fatigue Behavior of Unidirectional Jute Spun Yarn Reinforced PLA. Advanced Composite Materials 21:1–10.

Ben G, Kihara Y, Nakamori K, et al. (2007) Examination of heat resistant tensile properties and molding conditions of green composites composed of kenaf fibers and PLA resin. Advanced Composite Materials 16:361–376.

Dissanayake DGK, Weerasinghe DU, Wijesinghe KAP, et al. (2018) Developing a compression moulded thermal insulation panel using postindustrial textile waste. Waste Management 79:356–361.

Dissanayake DGK, Weerasinghe DU, Thebuwanage LM, et al. (2021) An environmentally friendly sound insulation material from post-industrial textile waste and natural rubber. Journal of Building Engineering 33:101606.

Mumthas ACSI, Wickramasinghe GLD, Gunasekera US (2019) Effect of physical, chemical and biological extraction methods on the physical behaviour of banana pseudo-stem fibres: Based on fibres extracted from five common Sri Lankan cultivars. Journal of Engineered Fibers and Fabrics 14:155892501986569.

Balakrishnan S, Wickramasinghe G, Wijayapala US (2019) Investigation on improving banana fiber fineness for textile application. Textile Research Journal 89:4398–4409.

Ramachandran M, Bansal S, Raichurkar P (2016) Scrutiny of jute fiber poly-lactic acid (PLA) resin reinforced polymeric composite. Journal of the Textile Association 76:372–375.

Milani MDY, Samarawickrama DS, Dharmasiri GPCA, et al. (2016) Study the Structure, Morphology, and Thermal Behavior of Banana Fiber and Its Charcoal Derivative from Selected Banana Varieties. Journal of Natural Fibers 13:332–34

Electronic Journal of Structural Engineering

Review Article

Cite this: DOI:10.56748/ejse.234142

Received Date: 19 January 2023
Accepted Date: 10 March 2023

1443-9255
https://ejsei.com/ejse

Stability Consideration in Design of Steel Structures: A Review

Fatimah De'nan [a]*, Jia Shen Lau [a], Adham Mohamade Ounahe [a], Mohamed Inas Kamel [a] and Nor Salwani Hashim [a]
[a] School of Civil Engineering, Universiti Sains Malaysia, 14300 Nibong Tebal, Pulau Pinang, Malaysia
* Corresponding Author: cefatimah@usm.my

Abstract

The adoption of steel in the construction industry will consistently grow due to rapid urbanisation and the demand of more structures and infrastructures. The main reasons of steel adaptation in construction industry are due to steel attributes that are flexible, sustainable, cost effective and a versatile material. The significant characteristics of steel provide the suitability for the construction of structures such as tall buildings and bridges all around the world. Along with the constant development of technology, the steel industry also aims to increase the sustainability of steel structure construction through constructing low carbon neutral and energy efficient building with steels. Moreover, steels are also considered as one of the most recycled materials in the world which allows the enhancement of the overall environmental performance of a structure's life cycle. With the increasing utilisation of steel in the design of structures, the stability consideration of the steel structures has become the most crucial concern during the structural designing phase. Stability of structures is vital for every building as the structure instability may lead to catastrophe such as structural collapse that may threatens the safety of occupants inside the building as well as the well -being of the community around the area.

Keywords

Steel, Stability, Beam, Frames, H-section

1. Introduction

Steel is a popular material used in the field of civil engineering and construction industry. According to the World Steel Association, steels used in the construction industry for buildings and infrastructures accounts to 50% and more of the world steel demand (World Steel Association, 2020). Steel adaptation in construction industry is able to significantly reduce the concrete usage where it concurrently reduces the overall carbon dioxide emission as well as mitigate climate change through construction project (Nidheesh & Kumar, 2019). Hence, steels are recommended materials for the design of structures as it possesses great advantages in terms of its functionality as well as towards the environment.

In addition, stability of structure is also part of fundamental issues in solid and structural mechanics which are relatively important in ensuring the integrity of the structure. The stability theory plays a key role in various civil engineering fields and structures including tall structures, geotechnical structures, space frame structures and material sciences. According to the structural collapse history, it is observed that the collapse of structure is mainly caused by the misinterpretation or neglection of stability aspect during the process of structural design. Evident of collapsed structures due to instability includes the Tacoma Narrow Bridge collapsed in 1940 and the cause of instability of steel structure Matukituki Suspension Footbridge collapsed in 1977 (Arioli & Gazzola, 2017). These disastrous events have also raised interest of engineers and designers to take stability and structural fundamental concerns seriously in the future designs.

2. Stability of beam-columns

Instability of a steel structure are caused by several reasons which includes neglecting of stability design, human error during construction phase, degradation of steel due to fire and failures due to seismic event (Alpsten, 2017; Bravo-Haro et al., 2020; Xu et al., 2018). To avoid these issues as mentioned, the consideration of stability should be improved to ensure better structural integrity. Analysis of structural stability and integrity can be studied using the Euler's theory in accordance with the fundamental of solid and structural mechanics. Both linear and non-linear behaviour analysis should also be considered during the structural designing phase for better and more accurate design results. The structural element that will directly affect the stability of the structure consists of structural beam-columns, frames, and joints. In this paper, each structural element will be comprehensively discussed for the understanding of the consideration between the stability of structure with regards to the structural elements of beam-columns, frames, and joints.

1. A formulas of interpolation (Nidheesh & Kumar, 2019) concerning Eurocode 3, Part 1–1 clauses 6.2.9, which represents the cross-sectional resistance, and Eurocode 3, Part 1–1 clauses 6.3.3, which describes the member buckling resistance, for the moment load effect Mz,Ed =0.
2. The so-called general method of clause 6.3.4 c.

The member buckling resistance by its linear compound of two stability utilization ratio components can be determined by the interpolation formulas presented in Eurocode 3, Part 1–1 clause 6.3.3(Nidheesh & Kumar, 2019):

a) axial compression buckling resistance utilization ratio, and
b) Lateral–torsional buckling (LTB) utilization ratio for moment about the y-y axis multiplied by the interaction coefficients *kij* for *ij=yy* or zy that consider the nonlinear character and complexity of the behaviour of steel-beam column elements of actual structural systems

The general second-order relation produced the *kij* coefficient and presented in (Nidheesh & Kumar, 2019) throughout two methods. Method 1 which is presented in Annex A and is considered the more accurate method, but it requires very complicated hand calculation. Whereas method 2 is presented in Annex B is considered for quick verification of the resistance. These coefficients, which are named the equivalent uniform bending moment factors, are dependent on many other parameters. The parameters are defined by a sensitivity analysis as the most critical factors that play an important role in affecting the accuracy of the design interpolation criteria. Boissonnade et al., 2004 and Greiner, 2006 have reported the degree of the verification accuracy of this kind of design methods.

The behaviour of the in-plane beam-columns is considered a crucial engineering practice especially in the design of the steel structures, such as planar portal and multi-storey frames. The behaviour of the beam-columns with ideal geometry was described by Chen and Atsuta, 2007. Moreover, Trahair et al., 2017 and Ziemian, 2010 stated the guidelines of the stability and design of imperfect segments. Columns and beam-columns are susceptible to flexural buckling (FB) especially, in the case of in-plane behaviour. Bjorhovde, 2010 was stated in his review study the development criteria of the column stability included in studies and design codes.

An experimental and numerical study of stocky beam-columns manufactured of hot-rolled steel I-sections under combined compression and bending moment was reported by Yun et al., 2018. Experimental and numerical studies of laterally restrained steel columns with variable web-tapered I cross-section were reported in Tankova et al., 2018, Cristutiu et al., 2012. The buckling behaviour of high-strength compression steel columns was experimentally investigated by Ban et al., 2018; Ban et al., 2012.

Goncalves and Camotim, 2004 conducted a study about the utilization of so-called Level 1 (Greiner, 2001) and Level 2 (Muzeau et al., 2002) beam-column interaction formulae to isolated members with arbitrary loading and end support conditions. They conducted a comparison between the

analytical in-plane resistance of members and the values of finite element analyses under second-order plastic zone beside the application of initial bow imperfection and residual stress distributions. In their analysis, focus was directed to problems relating to the proper collection and decision of the equivalent moment factor used in formulas of analytical interaction.

The evaluation of the rules of safety stated in EN 1993-1-1 (Gardner and Nethercot, 2005) for flexural buckling of the columns manufactured by hot-rolled I-shaped cross-sections was illustrated by Silva et al., 2017. The assessment revealed that the imperfection factors for flexural buckling about the minor axis of steel-columns produced of S460 steel, which are described in Eurocode (Gardner and Nethercot, 2005), are unsuitable, and a new suggestion was made and recommended that the use of buckling curves were more proper and adequate. In the recent version of the EN 1993-1-1 (Gardner and Nethercot, 2005), flexural buckling curves for hot-rolled I-shaped cross-sections with height-to-width ratios h/b_f> 1.2 and flange thicknesses t_f> 100 mm are not available. Snijder et al., 2014 and Spoorenberg et al., 2014 were detailed these kinds of heavy I-shaped cross-sections which are formed by mild and high-strength steel beside the use of European buckling curves (Gardner and Nethercot, 2005). It was reported by Taras and Greiner, 2008 that the "torsional and flexural–torsional buckling phenomena of laterally restrained columns" could not be represented by the European buckling curves obtained from Gardner and Nethercot, 2005. It was formulated a new flexural–torsional buckling (FTB) curve for columns subjected to uniform compression, which is fully compatible with the background and methodology of the European column buckling curves, by Greiner and Taras, 2010.

According to EN 1993-1-1 (Gardner and Nethercot, 2005), the resistance of steel columns and beam-columns can be determined by second-order analysis considering equivalent initial bow imperfections. Checking the flexural buckling in accordance with (Gardner and Nethercot, 2005) using bow imperfections was produced by Lindner et al., 2016. Whereas it may be conservative to use the equivalent imperfections based on (Gardner and Nethercot, 2005) where this was reported by Lindner et al., 2016 and Jönsson et al., 2017. In (Chladný and Štujberová, 2013) it was proposed that by applying the Ayrton–Perry formulation, the structural analysis could be performed with equivalent column bow imperfections." It was performed by Chladny and Stujberova, 2013 the procedure by using the equivalent unusual global and local imperfection in the form of the elastic buckling mode. A design example of a planar steel multi-storey frame was considered. It was remarked that the shape of the imperfection, which is given by the higher mode, could be considered (Agüero et al., 2015). Papp, 2016 was stated a suggestion for the generalization of an overall imperfection method employing linear buckling analysis for beams, columns, and beam-columns. Lechner, 2006 reported the application of the Eurocode design methods in (Gardner and Nethercot, 2005) to determine the FB resistance of a steel planar portal frame. Effects of geometric imperfections on flexural buckling resistance of laterally braced columns can be found in (Dou & Pi, 2016).

In-plane resistance of structural steel elements can be verified with the use of both stiffness reduction (Kucukler et al., 2014, Kucukler et al., 2016) and direct strength (Taras, 2016) methods. Recently, Tankova et al., 2018 reported a novel general formulation that is based on stress utilization, with the buckling mode as the shape of the initial imperfection that can be used to check in-plane resistance of beam-columns.

The application of the general method approach proposed in (Gardner and Nethercot, 2005) relates to the out-of-plane buckling resistance. The background of this method was explained in detail by Bijlaard et al., 2009, Simoes da Silva et al., 2010, and in the ECCS design manual (Simoes da Silva et al., 2010).

Recently, research efforts for establishing design criteria for beam-column resistance have been focused on the Ayrton-Perry approach to stability problems. Tankova et al., 2017 presented a simplification of the exact solution yielded from the differential equilibrium state of crooked beam–column elements for their use in the codification of FTB resistance of beam-columns. The method proposed in (Tankova et al., 2017) is closely based on the theoretical derivation of the generalization of the Ayrton-Perry formula reported by Szalai and Papp, 2010 and referenced to LTB problems of beams and beam-columns. A complete closed-form universal Ayrton-Perry format-type solution for all types of buckling modes of steel beam-columns was derived by Szalai, 2017. Simple concepts of the Ayrton-Perry analytical formulation were developed in (Gizejowski et al., 2018) for FB of columns and in (Gizejowski et al., 2016) for FTB resistance of beam-columns. These concepts were further investigated by Gizejowski et al., 2019 and presented in two parts as a unified approach to predicting the resistance of beam-columns with regard to their in-plane and out-of-plane failure modes. As a result of Gizejowski et al., 2019 study, the in-plane interaction curve, expressed in dimensionless coordinates, that describes the beam-column in-plane flexural buckling resistance without considering lateral-torsional buckling effects, is obtained. The results of nonlinear finite element simulations are used for the verification of the developed analytical formulation. It was concluded that this proposal yields fewer conservative predictions than those based on the interaction relationships of clause 6.3.3 of Eurocode 3, Part 1–1.

3. Stability of frames

Frames in steel structures are commonly seen in tall buildings. Tall buildings with frames consist of various height and width that may significantly affect the stability of structures. Hence, tall buildings are the most vital structures that require the consideration of stability to avoid any structural issues in the near future. It is evident that the failure of most structures is mainly due to the frame instability with regards to the P-delta effect where the global or element of structure observes imperfection and deformations (Walport et al., 2018). P-delta analysis is crucial for structures significantly affected by wind loads, seismic events or even natural catastrophe. Structural frames should be rigid to withstand the lateral forces that will be acting on the structures to avoid structural instability. Instability of structures often occurs when the structure is close to failures which include swaying of structure frames or even buckling due to external loading.

P-delta effect is caused by the horizontal movement or loads where the second order overturning moment is generated which will lead to the deformation of structure. This deformation can be calculated by the total summation of "P" each vertical axial load multiply with the "Delta" lateral displacement of the structure to obtain the structure overturning moment. Tall buildings that possess great stiffness with regards to weight ratios which are seismically strong and well strengthen can neglect the P-Delta consideration as the changes of structural displacement is relatively low and less than 10% of the internal force in first order theory (Abhishek & Sumit, 2019). However, the imperfection of construction work and human error may not provide a perfect structure which might eventually affect the stability of structure. Hence, P-delta analysis is crucial in the design of tall steel buildings. To accurately obtain the collapse load of the structure, the P-delta effect should be also considered as the P-delta analysis provides the true moment rotation relationship of the structure over a period of time. Consideration of the relationship between the P-delta effect and the storey stability should also be studied to understand the overall structural stability. The stability assessment of steel frame structure as well as the needs of the P-delta effect consideration are also listed in the standards of steel design EN 1993-1-1 (Walport et al., 2018).

Moreover, the frame stability is also closely related to the yielding of material as well as the amount of plastic hinges formation on frames. These two factors play an important role in avoiding frame structure deterioration as well as the instability of structure. The yielding of material can be determined using tensile test for the purpose of understanding the material strength as well as the elastic modulus of the material. The stress-strain model of the material will also be generated through the tensile test technique for identifying the internal forces and its yielding point of the material prior to structural design (Gardner, 2018). In addition, the plastic hinge formation that will also significantly affect the stability of steel frame structure can be studied through the global sway behaviour model. The global sway behaviour model can be elucidated by plotting the graph of load factor against the lateral displacement (Fig. 1) swayed by the structure. Through the graph, it is observed that the increasing number of plastic hinges reduces the required loading condition of the elastic buckling load which also indicates the loss of stiffness in the steel structure frames.

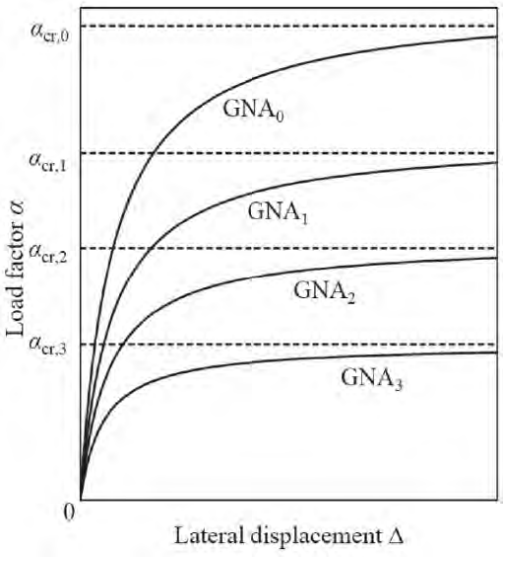

Fig 1. Second order elastic frame response with plastic hinges (Walport et al., 2018).

Meanwhile, as load acting on the frame structure starts deflecting, the load induces second order forces as well as moments which cause the response diverges from the linear graph. This response is also known as the second order elastic analysis as shown in the figure above. During this process, loads acting on the frame structure increases which eventually leads to the increase of frame internal forces as well as the moment until it reaches a turning point on the straight linear line where it indicates the formation of plastic hinge. Furthermore, to identify the stiffness degradation degree of structural frame more accurately and consistently, the consideration of modified elastic buckling load factor (αcr,mods) can be adopted. This consideration takes into account the stiffness reduction of the frame structure as well as its plasticity in accordance with the provided design load and its material. This technique implies the structure's first order plastic analysis where the initial stiffness, (K) relates to the secant stiffness (Ks) as shown in the figure below. The modified elastic buckling load factor (αcr,mods) can also be obtained by using the equation shown below. With this technique, the treatment of second order effect for both plastic and elastic analysis can be identified accurately as well as consistently. Hence, by determining the accurate load factor allows the engineers as well as designers to design the steel frame structure more efficient, stable, and able to withstand more lateral loading. The analysis of frame stability is fairly important and can be conducted using computational methods or advance structural software. By identifying the suitable structural material used as well as the ultimate elastic buckling load of structure for design may efficiently ensure the stability of structure and avoid any catastrophe such as failure and collapse of structure.

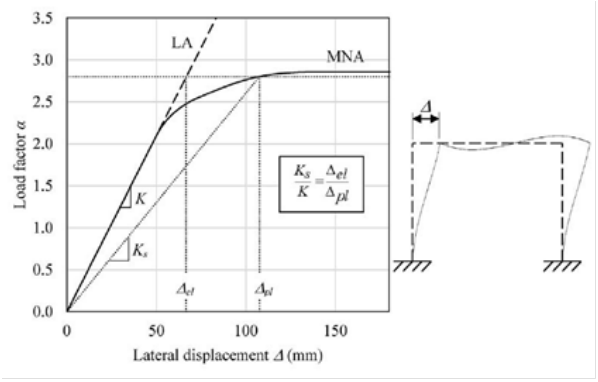

Fig 2. Material nonlinearity results based on reduction of global sway stiffness (Gardner, 2019).

$$\alpha cr, mods = 0.8\, KsK\, \alpha cr \quad (1)$$

Subsequently, to enhance the stability of steel frame structure the adoption of bracing on structure should also be considered. The utilisation of bracing increases the structural strength which allows the structure ability to withstand more lateral load especially during seismic events. Moreover, the additional use of bracing can effectively reduce the horizontal storey drift as well as observes a significant increase in stiffness, energy dissipation and strength (Setyowulan et al., 2020). However, the drawback of eccentrically brace frame system is the connection between the ends of bracing as well as structural element should be rigid to ensure the bracing efficiency at its maximum capability. Therefore, the use of bracing should be adopted by tall steel frame structures with huge lateral drift for the structural stability enhancement.

3.1 Bracing systems

Bracing systems are typically currently three types, namely Moment resisting frames (MRFS), Concentric braced system (CBFS) and Eccentric braced frame (EBFS). For MRFS it is the frames with longitudinal beam and column assemblies, with beams strongly linked to the columns while CBFS is effective and economical lateral load-resistant devices in seismic regions worldwide to withstand seismic loads (Dawood, 2019). For EBFS it is to reduce the total material specifications and contribute to an intense seismic architecture feature that remains in moderate loads and ductile (Dawood, 2019).

The seismic reaction of steel frameworks is influenced primarily by the behaviour. Many experiments have been performed by various scholars who could not come up with any conclusions on which types of bracings should be used (Kumar, 2014). Comparative analyses by separate authors were obtained from the analysis of the joint by Jagadeesh, Anitha and Dhiman. The seismically reaction of the steel framework with concentrated bracing method has been tested by Jagadeesh, 2016. Two configurations were used: the irregular vertical (VIRM) and vertical irregular model with mega bracing (VIRM MB). The stainless-steel frame versions comprised of five bays with five stories with and without bracing. In addition, the analysis involved the use of ETABS (Jagadeesh, 2016). A variety of criteria were compared such as storey drift, storey displacements and base shear. Analysis of inelastic properties found that mega bracing was more successful than VIRM with no bracing frame to survive earthquakes, owing to decreased drifts, storey displaced erratic verticals were 77.64% and the highest base shear was 23.42% (Jagadeesh, 2016).

A distinction has been made between the seismic impact on knee braced steel frame and other forms of bracings by Anitha & Divya, 2015. The modelling was conducted with the assistance of finite element programme, ANSYS 14.5, under non-linear time history analysis and non-linear static analysis. For non-linear static studies, dynamic loading of 10kN was allocated and El-Centro earthquake data were assigned for the study of time history (Anitha & Divya, 2015). For the required seismic refitting process, knee bracing can be used. Double knee bracings demonstrated outstanding results during seismic activity in non-linear static study, as ultimate loads were very strong and lateral rigidity. The overall displacement observed during historical research was 90.5% more than without bracing and 50% greater than the eccentric bracing system (Anitha & Divya, 2015).

The response from braced and unbraced systems subject to seismic loads was evaluated by Dhiman et al., 2015. Different types of braces were used for dead and live loads such as cross brace, braced chevron, diagonal k-braced and dead load, X and Z seismic load respective (Dhiman et al., 2015). Structure displacement decreased as the bracing system was applied and lateral displacement was maximally diminished when the cross-bracing system had been used. The inclination and shear forces in columns were also diminished (Dhiman et al., 2015).

4. STABILITY OF JOINTS

Connections or joints shall be used for the transition to other parts of the structure or supports of the forces provided by a structural member. The braces and other members that provide the structural component with constraints are also used as connection. Eurocode 3 have different meaning for the connections and joints where connection consists of fasteners such as bolts, pins, rivets, or welds, fastener that is connected to the local member elements and might consist of external plates or cleats (Trahair et al., 2017). While joint consists of the region in which the members are linked, and involves the connection, along with the portions of the member or members required to facilitate the transition of action at the joint. The structure of a joint is normally selected to suit the type of motion (force or moment) that is being transmitted and to link the variety of member (tension or compression member, beam, or beam-column). The structure should be preferred to prevent unnecessary costs because it is typically time-consuming to plan, detail, construct and assemble a joint because it could cause increase in cost and impact. Such that, a heavier part is often best used instead of stiffeners because this decreases the amount of manufacturing processes needed (Trahair et al., 2017). A joint is first constructed by defining transfers of force from the member to the other part of the system via the components of the joint. Each part is then proportioned such that the force to be conveyed can be resisted adequately.

4.1 Stability Issues Between Joint and Steel Structure

Steel moment-resisting frames become a common seismic-resistant method because steel is a well-established with high strength to mass ratio with the ductile material. Brittle fracture of connection is not the cause of damage but associated with local buckling and yielding (Kumar, 2014). The development of plastic bends in beam-column joints and column bases is one of the characteristics of an inelastic action that resists the frame for steel moment (Kalyana Chakravarthy et al., 2018). The connections between cyclic loading and failure modes have been varied in several experimental works but show mainly ductile behaviour based on several mechanisms, characterised by bolt slip, yielding of steel, elongation of bolt holes, etc.

The use of bolted connections between the dissipative areas and the remaining structures to replace the damage incurred by dissipating elements on eccentrically braced frames will minimise lateral movement. An additional brace at the end of the RBS will necessarily decrease beam flanges and column twist transverse rotation, which can induce to cyclic degradation (Kalyana Chakravarthy et al., 2018).

The analysis of braced system subjected to join shows that the bracings minimise floor lateral movement, in columns, axial forces rise from unbraced to brace, less horizontal movement in cross-bracing than diagonal bracing, cross braced stories would have a higher peak than unbraced and diagonal braced frames, shear forces decline in the column from unbraced to braced. shear strength is stronger in diagonal braced columns than in cross-braced, the cross bracing is subject to more simple shear than diagonal bracing and the steel brace frame is with more base shear than unbraced frames (Coelho and Bijlaard, 2010). Moreover, the structure with higher heights or more stories would have baser shear under the same

bracing system and loading than the smaller one and the bending moment decreases in column from unbraced to brace. The braced diagonal column is more twisting than the braced diagonal column.

When transmitting force by in-plan motion, plates are relatively strong and rigid but relatively weak and flexible when the force is transmitted by external bending. The angle cleat and the seat are therefore flexible and permit the attachment members to rotate comparatively, while flanges and web stiffeners are rigid and limit their relative rotation. The simplicity and comparative rigidity of the welded connections have also contributed to the failure of stiffening plates when it is not needed for force purposes. Thus, by welding the beam directly to the column flanges and by excluding the web stiffeners column, the rigid connection can be greatly simplified (Shin & Park, 2014). This neglect would, however, make the connection much more versatile because local column flange and web distortions are no longer preventable.

4.2 Beam-to-Column Connection

For the beam- to- column connection, the failure mode takes different forms because of the diversity within connection type configurations such as fracture around welds, fractures in highly tight fracture material, welding access holes fractures in the net section of bolts, bolt failure due to shearing and tensile, bolt bearing and bolt shear failures.

4.3 Column Splices

Column splice at the failure modes is similar to the connection of beam to column modes. In the case of column splices failure, the bending and tension resistance is not only reduced or eliminated, but also the shear force transfer column is reduced or removed.

4.4 Column Bases

Column bases mode of failure depends on the column-foundation connection. They involve anchorage or pulling off, fracturing in plates of the base or in connections between columns and base plate, and extreme local and lateral torsional buckling if the area above the base connection has inelastic deformations localised.

4.5 Connections in Braced Frame

A Braced Frame is a structural structure designed mainly to withstand the effects of wind and earthquake. Members of the braced frame act like a truss system where it is designed to function in stress and compression. The braced frames consist of steel components only. The benefit of the bracing system is that it is ideal for all kinds of systems, such as bridges, ships, grids, homes, and electric transmission towers, simple to install with lack of experience or know-how, and no difficulties in linking the connections if the bolted connections are used.

Bracing connections entail bolting of flat, angle, channel, I-section, and hollow section members to a gusset plate under which the column or other members are supported. The bracing component can operate either in equilibrium or in tension and compression alone and stabilise the main components by load distribution. The choice of a bracing configuration depends on a variety of considerations. This includes the proportions of height to width of the bay and the scale and position of the required open areas in the structure height. These requirements will substitute design parameters with structural optimisation (Kalyana Chakravarthy et al., 2018). The implementation of the e/L parameter leads to a widespread framing device definition.

4.6 Bolted Double Angle Cleats

Typical dual-angle bolted cleat links all along the column's main and minor axis. Any basic study of equilibrium can be used when constructing such a relation. The course of motion that the shear transition between the beam and the column is recommended for this publication suggests that the column is on its face (Soltani & Kerdal, 2011). The bolt group that attaches the cleats to the beam web must be optimised for the shear force of the end shear product and for the time generated by the column face to the eccentricities of the bolt group. For the applied shear alone, the connections linking the cleats of the bolt to the column face should be designed. The cleats to the column are never crucial in operation, and the arrangement is almost always guided by the bolt bearing to the network of the beam (Soltani & Kerdal, 2011). The rotary capability of this relation is primarily determined by the angles and slip distortion capacity between the attached components. The rotation of the links is mostly due to angle deformation, while the connection deformation is very minimal.

4.7 Fin plates

The implementation of the fin plate relation was a more modern invention that follows Australian and American standard. This form of link is used mainly for beam end reactions and is cost efficient in construction and easy to install (Kalyana Chakravarthy et al., 2018). It is necessary to identify the proper course of action for the shears when designing a fin plate connection. The shear operates on the column face, or the shear works alongside the middle of the bolt group and links the end plate to a beam web (Shin & Park, 2014). For this purpose, the vertical shear product and distance between the face of the column (or a beam web) and the middle of the bolt group should be tested at a minimum moment. The resulting moment is regulated in accordance with the vertical shear for each of the critical sections. The fin plate is welds to their maximum strength due to the unknown moment added to the fin plate (Coelho & Bijlaard, 2010). Fin plate connections derive them in-plane rotational capacity is determined by bolt distortion in shear, distortion of the bearing bolt holes, and the out-of-plane bending of the fin plate. Be aware of the possibility failing in lateral torsional due to buckle fin plates with long projection. In the construction protocols for fin plate connections, extra monitoring for this activity is used.

5. CONCLUSIONS

A three-dimensional frame structure may be analysed as the group of a number of independent two-dimensional frames, while individual members are usually considered as one-dimensional and the joints as points. It can be believed that the joints are frictionless hinges or that they are semi-rigid or rigid. In some cases, comparisons are made on an idealized model which approximates part, or all of the structure may substitute or complement the analysis. For beams and columns, structural steel members can be one-dimensional (whose lengths are far wider than their transverse dimensions) or two-dimensional as for frames (whose lengths and widths are much greater than their thicknesses). Thus, according to the mechanism by which they distribute the forces in the structure, structural members may be categorized as stress or compression members, beams, beam-columns, torsion members, or plates. A person member's real behaviour will depend on the powers working on it. Thus, before their material non-linearity becomes essential, tension members, laterally supported beams, and torsion members remain linear, until they reach the maximum plastic state. However, geometric non-linearity is demonstrated by compression members and laterally unsupported beams as they reach the buckling loads. Beam-columns are members that relay transverse and axial loads, such that both material and geometric non-linearity are reflected. The structural steel members can also be joined together in a range of ways at joints, and by using a variety of connectors. This includes pins, rivets, bolts, and welds. Beam-columns are structural members which combine the beam function of transmitting transverse forces or moments with the function of transmitting axial forces of the compression (or tension) component. In skeletal arrangements, structural frames are composed of one-dimensional members joined together that transfer the applied loads to the supports. Thus, the function of beam-column, joint and frame in column plays important rule for the stability of the structure and maintaining the stability of the material is important to provide strong and durable steel structure.

ACKNOWLEDGEMENTS

The author conveys heartfelt gratitude and highest appreciation to University Sains Malaysia for the financial support.

REFERENCESS

World Steel Association, “2020 World Steel in Figures,” 2020 World steel Fig., no. 30 April, 2020, [Online]. Available: http://www.worldsteel.org/wsif.php.

P. V. Nidheesh and M. S. Kumar, “An overview of environ-mental sustainability in cement and steel production,” J. Clean. Prod., vol. 231, pp. 856–871, 2019, doi: 10.1016/j.jclepro.2019.05.251.

G. Arioli and F. Gazzola, “Torsional instability in suspension bridges: The Tacoma Narrows Bridge case,” Commun. Nonlinear Sci. Numer. Simul., vol. 42, pp. 342–357, 2017, doi: 10.1016/j.cnsns.2016.05.028.

G. Alpsten, “Causes of structural failures with steel struc-tures,” IABSE Work. 2017 Ignorance, Uncertain. Hum. Errors Struct. Eng., pp. 100–108, 2017.

M. A. Bravo-Haro, M. Liapopoulou, and A. Y. Elghazouli, Seismic collapse capacity assessment of SDOF systems incorporating duration and instability effects, vol. 18, no. 7. Springer Netherlands, 2020.

L. Xu, T. Ma, and Y. Zhuang, “Storey-based stability of un-braced structural steel frames subjected to variable fire loading,” J. Constr. Steel Res., vol. 147, pp. 145–153, 2018, doi: 10.1016/j.jcsr.2018.04.003.

J. P. W.E. Ayrton, “On struts, Engineer 62 (1886) 464–465.”

L. Gardner and D. Nethercot, “Designers’ Guide to EN 1993-1-1 Eurocode 3: Design of Steel Structures: General Rules and Rules for Buildings,” 2005.

N. Boissonnade, J. –P. Jaspart, and J. Muzeau, “New interac-tion formulae for beam-columns in Eurocode 3: The French–Belgian

approach," J. Constr. Steel Res., vol. 60, pp. 421-431, 2004, doi:10.1016/S0143-974X(03)00121-4.

R. Greiner, J. L.-J. of C. S. Research, and undefined 2006, "Interaction formulae for members subjected to bending and axial compression in EUROCODE 3—the Method 2 approach," Elsevier.

W. Chen and T. Atsuta, Theory of beam-columns, volume 2: space behavior and design. 2007.

N. Trahair, M. Bradford, D. Nethercot, and L. Gardner, The behaviour and design of steel structures to EC3. 2017.

R. Ziemian, Guide to stability design criteria for metal struc-tures. 2010.

R. Bjorhovde, "Evolution and state-of-the-art of column stability criteria," J. Civ. Eng. Manag., vol. 16, no. 2, pp. 159–165, May 2010, doi: 10.3846/jcem.2010.16.

X. Yun, L. Gardner, N. B.-J. of C. Steel, and undefined 2018, "Ultimate capacity of I-sections under combined loading–Part 1: Experiments and FE model validation," Elsevier.

T. Tankova, J. P. Martins, L. S. da Silva, R. A. Duarte Simoes and H. D. Craveiro. "Experimental buckling behaviour of web tapered I-section steel columns," J. Const. Steel Res., vol. 147(c), August 2018, doi:10.1016/j.jcsr.2018.04.015

I.-M. Cristutiu, D. L. Nunes, and A. I. Dogariu, "Experimental study on laterally restrained steel columns with variable I cross sections." Steel and Composite Structures, vol. 13, no. 3, September 2012, pp. 225-238. DOI: https://doi.org/10.12989/scs.2012.13.3.225

H. Ban and G. S. Research, "Overall buckling behaviour and design of high-strength steel welded section columns," J. Constr. Steel Res., 2018.

H. Ban, G. Shi, Y. Shi, and Y. W. Research, "Overall buckling behavior of 460 MPa high strength steel columns: Exper-imental investigation and design method," - J. Constr. Steel 2012, Undefined, 2012.

R. Gonçalves, D. C.-J. of C. S. Research, and undefined 2004, "On the application of beam-column interaction formulae to steel members with arbitrary loading and support conditions," Elsevier.

R. Greiner, "Background Information on the Beam-Column Interaction Formulae at Level 1, Report TC8–2001-002, ECCS Technical Committee 8," 2001.

P. Muzeau, N. Boissonnade, J.-P. Jaspart, J.-P. Muzeau, and M. Villette, "A. Boissonnade, J.-P. Jaspart, J.-P. Muzeau, M. Villette, Improvement of the interac-tion formulae for beam columns in Eurocode 3, Comput. Struct. vol. 80, pp. 2375–2385, 2002.

L. Simões Da Silva, T. Tankova, and C. Rebelo, "Safety as-sessment of eurocode 3 stability design rules for the flex-ural buckling of columns International Symposium on Risk analysis and Safety of Large Structures and Compo-nents (ISRAS2017) View project HILONG High Strength Long Span Structures View project," researchgate.net, doi: 10.18057/IJASC.2016.12.3.7.

H. Snijder, L. Cajot, … N. P.-R. J. of, and undefined 2014, "Buckling curves for heavy wide flange steel columns," purl.tue.nl.

R. Spoorenberg, H. Snijder, L. C.-J. of C., and undefined 2014, "Buckling curves for heavy wide flange QST col-umns based on statistical evaluation," vol. 101, pp. 280-289, Oct. 2014.

A. Taras, R. G.-J. of constructional steel research, and unde-fined 2008, "Torsional and flexural torsional buckling—A study on laterally restrained I-sections," vol. 64, no. 7–8, pp. 725-731, July–August 2008.

R. Greiner and A. Taras, "New design curves for LT and TF buckling with consistent derivation and code-conform formulation," Steel Constr., vol. 3, no. 3, pp. 176–186, Sep. 2010, doi: 10.1002/stco.201010025.

J. Lindner, U. Kuhlmann, and A. Just, "Verification of flex-ural buckling according to Eurocode 3 part 1-1 using bow imperfections," Steel Constr., vol. 9, no. 4, pp. 349–362, Nov. 2016, doi: 10.1002/stco.201600004.

J. Jönsson, T. S.-J. of C. S. Research, and undefined 2017, "European column buckling curves and finite element modelling including high strength steels," vol. 128, pp. 136-151, Jan. 2017.

E. Chladný and M. Štujberová, "Frames with unique global and local imperfection in the shape of the elastic buckling mode (Part 1)," Stahlbau, vol. 82, no. 8, pp. 609–617, Aug. 2013, doi: 10.1002/stab.201310080.

A. Agüero, L. Pallarés, and F. P., "Equivalent geometric im-perfection definition in steel structures sensitive to flexur-al and/or torsional buckling due to compression," Eng. Strct., vol. 96, pp. 160-177, August 2015.

F. P.-E., "Buckling assessment of steel members through overall imperfection method," Eng. Strct., vol. 106, pp. 124-136, January 2016.

A. L.-P. of the I. colloquium on and undefined 2006, "Flex-ural buckling of frames according to the new EC3 rules–a comparative, parametric study," graz.pure.elsevier.com.

C. Dou and Y.-L. Pi, "Effects of Geometric Imperfections on Flexural Buckling Resistance of Laterally Braced Col-umns," J. Struct. Eng., vol. 142, no. 9, pp. 04016048, Sep. 2016, doi: 10.1061/(asce)st.1943-541x.0001508.

M. Kucukler, L. Gardner, L. M.-E. "A stiffness reduction method for the in-plane design of structural steel ele-ments," Eng. Strct., vol. 73, pp. 72-84, August 2014.

M. Kucukler, L. Gardner, L. M.-J. "Development and as-sessment of a practical stiffness reduction method for the in-plane design of steel frames," J. Const. Steel Res., vol. 126, pp. 187-200, November 2016.

A. T.-J., "Derivation of DSM-type resistance functions for in-plane global buckling of steel beam-columns," J. Const. Steel Res., vol. 125, pp. 95-113, October 2016.

T. Tankova, L. da Silva, L. M.-J., "Buckling resistance of non-uniform steel members based on stress utilization: General formulation," J. Const. Steel Res., vol. 149, pp. 239-256, October 2018.

F. S. K. Bijlaard, M. Feldmann, J. Naumes, and O. Sedlacek, "The 'general method' for assessing the out- of-plane sta-bility of structural members and frames and comparison with alternative rules in en 1993 - Euro code 3-part 1-1," in ICASS '09/IJSSD - Proceedings of Sixth International Conference on Advances in Steel Structures and Progress in Structural Stability and Dynamics, 2009, pp. 1167–1185, doi: 10.1002/stco.201010004.

L. da Silva, L. Marques, C. R. "Numerical validation of the general method in EC3-1-1 for prismatic members," J. Const. Steel Res., vol. 66, no. 4, pp. 575-590, April 2010.

L. Da Silva, R. Simões, and H. Gervásio, Design of Steel Structures: Eurocode 3: Design of Steel Structures, Part 1-1: General Rules and Rules for Buildings. 2012.

T. Tankova, L. Marques, … A. A.-J. "A consistent methodol-ogy for the out-of-plane buckling resistance of prismatic steel beam-columns," J. Const. Steel Res., vol. 128, pp. 839-852, January 2017.

J. Szalai, F. P.-J. "On the theoretical background of the gen-eralization of Ayrton–Perry type resistance formulas," J. Const. Steel Res., vol. 66, no. 5, pp. 670-679, May 2010.

J. S.-E. "Complete generalization of the Ayrton-Perry formu-la for beam-column buckling problems," J. Const. Steel Res., vol. 153, pp. 205-223, 15 December 2017.

M. Gizejowski et al., "A new method of buckling resistance evaluation of laterally restrained beam-columns," In book: Metal Structures 2016, pp.197-205, doi: 10.1201/b21417-27.

G. A.-P. M.A. Gizejowski, Z. Stachura, "Approach for the evaluation of beam-column resistance, in: A. Zingoni (Ed.), Insights and Innovations in Struc-tural Engineering, Mechanics and Computation, Taylor & Francis Group, London 2016, pp. 25."

M. Gizejowski, Z. Stachura, R. Szczerba and M. Gajewski, "Buckling resistance of steel H-section beam–columns: In-plane buckling resistance," J. of Constr. Steel Re-search, vol. 157, pp. 347-358, March 2019, doi:10.1016/j.jcsr.2019.03.002

F. Walport, L. Gardner, and D. A. Nethercot, "A method for the treatment of second order effects in plastically-designed steel frames," Eng. Struct., vol. 200, no. Decem-ber 2018, pp. 109516, 2019, doi: 10.1016/j.engstruct.2019.109516.

V. Abhishek and V. Sumit, "Seismic Analysis of Building Frame Using P-Delta Analysis and Static & Dynamic Analysis: a Comparative Study," i-manager's J. Struct. Eng., vol. 8, no. 2, pp. 52, 2019, doi: 10.26634/jste.8.2.15462.

L. Gardner, "Stability and design of stainless steel structures – Review and outlook," Thin-Walled Struct., vol. 141, no. December 2018, pp. 208–216, 2019, doi: 10.1016/j.tws.2019.04.019.

D. Setyowulan, L. Susanti, and M. Wijaya, "Study on the behavior of a one-way eccentric braced frame under lat-eral load," Asian J. Civ. Eng., vol. 21, Jun. 2020, doi: 10.1007/s42107-020-00234-2.

R. Kumar, "Seismic Analysis of Braced Steel," Seism. Anal. Braced Steel, no. 110, 2014.

P. R. Kalyana Chakravarthy, R. Janani, S. Durgalakshmi, T. Ilango, and S. Sivaganesan, "Connections in structural steel joints," Int. J. Civ. Eng. Technol., vol. 9, no. 3, pp. 323–331, 2018.

R. Soltani and D. E. Kerdal, "Behaviour of elementary bolted steel T-stub connections: An evaluation of EC3 design procedure," Turkish J. Eng. Environ. Sci., vol. 35, no. 1, 2011, doi: 10.3906/muh-1005-32.

A. O. Dawood, "Analysis of Rigid Steel Frames with and Without Bracing Systems under the Effect of Wind Loads in Maysan Province.," vol. 1, December, 2019.

B. N. Jagadeesh, "Seismic Response of Steel Structure with Mega Bracing System," Int. J. Eng. Sci. Reseacrh Tech-nol., vol. 5, no. 9, 2016.

M. Anitha and K. K. Divya, "Study on Seismic Behavior of Knee Braced Steel Frames," pp. 40–45, 2015.

S. Dhiman, M. Nauman, and N. Islam, "Behaviour of Multi-story Steel Structure with Different Types of Bracing Sys-tems (A Software Approach)," Int. Ref. J. Eng. Sci. ISSN, vol. 4, no. 1, pp. 2319–183, 2015.

S. M. Shin and H. J. Park, "Analysis of the behaviour of beam-to-column connection with the newly reformed T-stub connections by exponential function," Int. J. Softw. Eng. its Appl., vol. 8, no. 1, 2014, doi: 10.14257/ijseia.2014.8.1.24.

A. M. G. Coelho and F. S. K. Bijlaard, "Behaviour of high strength steel moment joints," Heron, vol. 55, no. 1, pp. 1–32, 2010.